

Renormalized Unruh-DeWitt particle detector models for boson and fermion fields

Daniel Hümmer,^{1,2} Eduardo Martín-Martínez,^{2,3,4} and Achim Kempf^{2,3,4}

¹*Institut für Theoretische Physik, Ruprecht-Karls-Universität Heidelberg, Philosophenweg 16, 69120 Heidelberg, Germany*

²*Department of Applied Mathematics, University of Waterloo,*

200 University Avenue West, Waterloo, Ontario, N2L 3G1, Canada

³*Institute for Quantum Computing, University of Waterloo, Waterloo, Ontario, N2L 3G1, Canada*

⁴*Perimeter Institute for Theoretical Physics, 31 Caroline Street North, Waterloo, Ontario, N2L 2Y5, Canada*

(Dated: January 26, 2016)

Since quantum field theories do not possess proper position observables, Unruh-DeWitt detector models serve as a key theoretical tool for extracting localized spatiotemporal information from quantum fields. Most studies have been limited, however, to Unruh-DeWitt (UDW) detectors that are coupled linearly to a scalar bosonic field. Here, we investigate UDW detector models that probe fermionic as well as bosonic fields through both linear and quadratic couplings. In particular, we present a renormalization method that cures persistent divergencies of prior models. We then show how perturbative calculations with UDW detectors can be streamlined through the use of extended Feynman rules that include localized detector-field interactions. Our findings pave the way for the extension of previous studies of the Unruh and Hawking effects with UDW detectors, and provide new tools for studies in relativistic quantum information, for example, regarding relativistic quantum communication and studies of the entanglement structure of the fermionic vacuum.

I. INTRODUCTION

While the spatial and temporal meaning of wave functions in first quantization is straightforward, it is notoriously difficult to extract spatiotemporal information from the quantum fields of second quantization. This is in large part due to the fact that there are no position observables in quantum field theory (QFT) [1]. As a consequence, one often works with nonlocal field modes instead, for example, in order to calculate S -matrix elements in the case of particle physics or Bogolubov transforms in the case of QFT on curved space.

Actual experiments, of course, probe quantum fields on finite patches of spacetime. A technique which does allow one to model the extraction of localized spatiotemporal information from quantum fields was pioneered by Unruh and DeWitt [2, 3]. The key idea is to probe quantum fields by coupling the quantum field in question to a localized first quantized system, called a detector. An excitation of the detector system is then interpreted as the absorption and therefore detection of a particle from the quantum field.

For example, a hydrogen atom, first quantized, can serve as such a detector system for the photons of the second quantized electromagnetic field. The technique of probing quantum fields by coupling them (at least in gedanken experiments) to so-called Unruh-DeWitt (UDW) detectors has been used successfully, in particular, to analyze the Hawking and Unruh effects. One of the key insights gained from these studies has been the finding that and why the very notion of particle is observer dependent.

More recently, UDW detectors have been used extensively in studies on quantum communication via field quanta [4, 5] and, more generally, in studies on a host of effects related to the presence of spatially distributed entanglement in the quantum field theoretical vacuum

[6–10]. In spite of these successes, however, most of these studies have been limited in scope to the model of a UDW detector that probes a quantized real scalar boson field through a linear coupling.

Here, our aim is to widen the applicability of the general UDW detector approach. To this end, we investigate Unruh-DeWitt detector models that probe bosonic as well as fermionic, nonscalar fields through both linear and quadratic couplings. We show how certain persistent divergencies can be overcome through renormalization and we show how perturbative calculations with UDW detectors can be streamlined through the use of extended Feynman rules that include the scattering of detector excitations.

Historically, idealized particle detector models were first introduced by Unruh [2], in an attempt to resolve the well-known ambiguity in defining field states corresponding to physical particles on curved spacetimes or for noninertial observers [2, 11, 12]. This was the finding that different quantization procedures yield incompatible Fock spaces and thus lead to ambiguous definitions of particle number eigenstates [13, 14]. Unruh’s groundbreaking idea is best summarized in his now famous dictum “a particle is what a particle detector detects.” He initially modeled a particle detector for a quantized scalar field as being a quantized scalar field itself, albeit one that is restricted to a cavity so that its excitation events come with spatiotemporal information. Unruh calculated that, when uniformly accelerated through the Minkowski vacuum, this detector will measure a flux of particles that are thermally distributed, which established the famous Unruh effect [2, 14, 15].

A few years later, DeWitt improved and simplified Unruh’s original model by introducing approximations that effectively replace the detecting field with a nonrelativistic two-level quantum system [3], inventing what is now called the Unruh-DeWitt detector. The detector couples

directly to the field Φ through its monopole moment μ :

$$H_{\text{int}} \propto \mu \Phi . \quad (1)$$

This model fixed minor problems with Unruh’s initial suggestion [13]. More importantly, the UDW detector has the advantage of being much easier to work with in calculations, because the detector is described by quantum mechanics rather than quantum field theory. Other detector models for quantized scalar fields followed, using both two-level systems and full fields as detectors, and featuring different ways to couple the detector to the fundamental quantum field (see e.g. [13, 16–18]). In the present paper, we will generally call any model that uses DeWitt’s monopole as the detecting system a (UDW-type) detector, irrespective of the field it probes and the coupling it uses.

UDW particle detector models have proven to be very versatile and useful tools. They were first used to analyze the effects of accelerations, spacetime curvature and horizons on scalar quantum fields (see e.g. [2, 19]). Further, UDW detectors have been used in quantum field theory to quantify vacuum fluctuations and the structure of vacuum states [20, 21]. In relativistic quantum information, pairs of detectors are crucial for measuring and harvesting the entanglement of quantum fields [22–25], and serve as senders and recipients of information in quantum signaling [5, 26]. Moreover, they can be good toy models for light-matter interaction in quantum optics [27, 28].

Because UDW detector models for quantized scalar fields have proven so valuable, the question arises to what extent analogous techniques can be developed and applied to other types of fields, such as quantized spinor or vector fields, which in Nature are of course more common than quantized scalar fields. This question is of fundamental interest by itself and there are also concrete applications where detector models for quantized spinor fields could immediately be useful, such as for analyzing the fermionic Unruh effect [29], and for investigating the related Hawking radiation of Dirac particles [30]. Moreover, it has recently been pointed out that such more general UDW detector models could resolve ambiguities that arise in defining measures for the entanglement between disjoint patches of a fermionic field [31].

A key aim of the present work is, therefore, to find a counterpart of the UDW detector for quantized spinor fields. More precisely, we are interested in a pair of particle detector models, one each for quantized scalar and spinor fields, that is comparable in the sense that differences in the detectors’ reaction to scalar and to spinor fields are due to the probed field alone, not caused by any other feature of the respective detector models. We will focus on only half-integer spin fermions and integer-spin bosons, i.e., we will here not be concerned with nontrivial spin/statistic combinations that may arise in low dimensional systems.

To the best of our knowledge, only two detector models for quantized spinor fields have been suggested so far: the first one by Iyer and Kumar [32] uses a quantized scalar field in a cavity as detecting system, close in spirit to

Unruh’s original suggestion. The second one by Takagi [20, 33] seeks to imitate DeWitt’s simpler model by coupling an UDW-type two-level system to a quantized spinor field Ψ through

$$H_{\text{int}} \propto \mu \bar{\Psi} \Psi , \quad (2)$$

making it a likely candidate for the closest spinor field equivalent to the scalar field UDW detector. While the above interaction may not be immediate from first principles, that is, from the Standard Model of particle physics, we may for example think of it as an attempt at a first-quantized, simplified version of a second-quantized cavity detector: in quantum electrodynamics, a spinor field (electrons) is coupled to a vector field A_μ (photons) through

$$H_{\text{QED}} \propto A_\mu \bar{\Psi} \gamma^\mu \Psi . \quad (3)$$

In this logic, certain modes of the electromagnetic field restricted to a cavity with appropriate boundary conditions (realized, e.g., as superconducting mirrors) could serve as a detector for the electron field. The spatiotemporal profile of the detector is then determined by the extent of the cavity and the time over which the electromagnetic field is observed. It is conceivable that by a series of approximations—e.g., neglecting all but one mode in the cavity and restricting its occupation to at most one quantum—we could arrive at a model of the type of Eq. (2). A two-level system coupled through Eq. (2) may then be thought of as an approximation to a cavity detector, much in the same way that the UDW detector is a simplification of Unruh’s original cavity setup. In the following, however, we will keep with the original idea of such detectors as simple tools to obtain spatiotemporally resolved information about quantum fields, and set aside considerations of how exactly they could arise from first principles. This is justified by the fact that, as discussed above, UDW detectors provide a very useful tool for extracting spatiotemporal information from quantum fields, at least in gedanken experiments.

We begin in Sec. II with an overview of the UDW-type detector models that we will study. In Sec. III, the excitation probability for the different detector models at rest in Minkowski vacuum is calculated for these models, also to test to what extent these models are comparable. We demonstrate that any UDW-type detector featuring an interaction Hamiltonian which is *quadratic* in the field has divergent excitation probabilities. This is true for spinor field models like Eq. (2), but also for quantized (real and complex) scalar field detector models with coupling

$$H_{\text{int}} \propto \mu \Phi^\dagger \Phi . \quad (4)$$

Unlike divergent probabilities reported before [13, 20, 34, 35], it is not possible to regularize these divergencies by considering a detector of finite size and switching it on and off adiabatically. However, the divergencies are readily understood from a field theoretic point of view: In Sec. IV we show that they are closely related to tadpoles

in quantum electrodynamics, and this analogy leads us to a renormalization scheme for quadratically coupled detectors. Sec. V is dedicated to the comparison of the vacuum excitation probabilities of the detector models. We establish that it is indeed justified to compare the two models Eq. (2) (for quantized spinor fields) and Eq. (4) (for quantized complex fields), at least at leading order in the coupling constant. As an example, their response to massless quantum fields in $(1, 1)$ dimensions is studied explicitly, using both a sudden switching of the detector, as well as a Gaussian switching function, in addition to a Gaussian spatial detector profile.

The second part of this work is dedicated to the derivation of fully fledged Feynman rules for all detector models discussed, valid on Minkowski spacetime. The Feynman rules are to facilitate investigating whether the discussed models are finite, or at least renormalizable, and whether they are comparable at higher orders as well. Sec. VI summarizes the required calculation methods, such as the Feynman propagators and Wick's theorem, with the proofs moved to Appendix C for better readability. After applying these methods in Sec. VII to the probability for a detector to remain in its ground state when interacting with a field in the vacuum state (the vacuum no-response probability), the Feynman rules then follow in Sec. VIII.

In Appendix A, we summarize canonical results in classical and quantum field theory to introduce notation as well as for the convenience of the reader. Appendix B explains the origin of the different normalization conditions for scalar and spinor field mode functions, which plays a crucial role in the UV behavior of the theories.

Throughout this work, natural units $c = 1 = \hbar$ are used. The metric of $(n + 1)$ -dimensional Minkowski spacetime has signature $(+, -, \dots, -)$.

II. UNRUH-DEWITT-TYPE PARTICLE DETECTOR MODELS

Unruh-DeWitt particle detectors are two-dimensional quantum systems. We choose the energy levels to be zero and some $\Omega > 0$ so that the detector's Hamiltonian, which generates translations in its proper time τ , reads

$$H_d = \Omega |e\rangle \langle e| = \Omega \sigma^+ \sigma^- . \quad (5)$$

Here, the ladder operators

$$\sigma^+ = |e\rangle \langle g| , \quad \sigma^- = |g\rangle \langle e| \quad (6)$$

are expressed in term of the ground and excited states $|g\rangle$ and $|e\rangle$. We parametrize the detector's trajectory $x(\tau) = (t(\tau), \mathbf{x}(\tau))$ by its proper time. Since the detector's trajectory will be prespecified rather than dynamical, spacetime translational symmetry is broken and overall energy and momentum are not conserved (unless one considers also the agent that keeps the detector on its trajectory). The detector's effective spatial profile, which

may be thought of as the distribution of its charge, centered around \mathbf{x} , will be described by a function

$$p(\mathbf{x}, \cdot) : \mathbb{R}^n \rightarrow \mathbb{R} \quad (7)$$

that is normalized to one unit of charge,

$$\int_{\mathbb{R}^n} p(\mathbf{x}, \mathbf{y}) d\mathbf{y} = 1 , \quad (8)$$

where n is the number of spatial dimensions. For example, for a pointlike detector

$$p(\mathbf{x}, \mathbf{y}) = \delta(\mathbf{x} - \mathbf{y}) , \quad (9)$$

while for a detector with Gaussian profile

$$p(\mathbf{x}, \mathbf{y}) = (2\pi\sigma^2)^{-n/2} \exp\left(-\frac{(\mathbf{y} - \mathbf{x})^2}{2\sigma^2}\right) . \quad (10)$$

It will sometimes be convenient to combine the switching function χ and the spatial profile p into a *spacetime* profile f by defining

$$f(x) = f(t, \mathbf{x}) \equiv \chi(t) p(0, \mathbf{x}) \quad (11)$$

in the detector's rest frame.

An UDW detector is to detect field quanta by becoming excited. To this end, the field must couple to an operator, μ , of the UDW detector that does not commute with the detector's Hamiltonian H_d . Without restricting generality, one can define this so-called *monopole moment* operator of the detector to be

$$\mu = \sigma^+ + \sigma^- . \quad (12)$$

Let us now systematically consider how the monopole moment μ of an UDW detector can be coupled to the various types of fields.

A. Linear coupling

We begin by considering a pointlike UDW-type detector coupled to a quantized real field Φ through the interaction Hamiltonian

$$H_{\text{int}} = \lambda \mu \Phi(\mathbf{x}) , \quad (13)$$

where $\lambda \in \mathbb{R}$ is the coupling strength. This is the particle detector model originally proposed by DeWitt [3]. It can be viewed as an idealization of the two lowest states of an atom interacting with the electromagnetic field.

As is well known, UV divergencies in the excitation probabilities arise in this setup, in particular, if the detector is abruptly switched (i.e. coupled) on or off; see, e.g., [13, 34, 35]. The pointlike structure of this detector also leads to UV divergencies; see, e.g., [13, 20]. The divergencies can be regularized by switching the detector on and off gradually, i.e., by using a sufficiently smooth

switching function $\chi(t)$, and by endowing the detector with a finite spatial profile p :

$$H_{\text{int}}(\tau) = \lambda\chi(\tau) \mu \int_{\mathbb{R}^n} p(\mathbf{x}(\tau), \mathbf{y}) \Phi(\mathbf{y}) d\mathbf{y} . \quad (14)$$

Let us now consider the coupling of an UDW detector to a quantized complex field, Φ . In this case, one cannot couple them as in Eq. (13) because $\Phi^\dagger \neq \Phi$ would imply that the interaction Hamiltonian is not self-adjoint. In principle, one may instead view Φ as composed of two quantized real fields $\Phi = \frac{1}{\sqrt{2}}(\Phi_1 + i\Phi_2)$ and couple any real linear combination of Φ_1 and Φ_2 to the detector. This approach, however, would single out a direction in the complex plane and would therefore make any $U(1)$ symmetry for Φ impossible [20]. The same incompatibility arises with any unitary symmetry if Φ carries higher-dimensional complex group and/or spin representations. We conclude that the coupling of UDW detectors to quantized complex fields should not be linear.

B. Quadratic coupling

Any interaction Hamiltonian between an UDW detector and a field must be a self-adjoint scalar. Since an UDW detector's monopole moment is a self-adjoint Lorentz scalar, UDW detectors always need to couple to an expression in the field which is also both scalar and self-adjoint. In the case of a quantized spinor field, the simplest self-adjoint Lorentz scalar is $\bar{\Psi}\Psi = \Psi^\dagger\gamma^0\Psi$. This suggests the following interaction Hamiltonian:

$$H_{\text{int}}(\tau) = \lambda\chi(\tau) \mu \int_{\mathbb{R}^n} p(\mathbf{x}(\tau), \mathbf{y}) \bar{\Psi}(\mathbf{y})\Psi(\mathbf{y}) d\mathbf{y} . \quad (15)$$

Note that the interaction is now quadratic in the field. This is plausible also because an UDW detector coupled linearly to a fermion field would be able to violate fermion number conservation by creating and annihilating individual fermions. Coupling an UDW detector quadratically to the field ensures that the detector can only pair create or annihilate fermion antifermion pairs. An example of this type of coupling was first considered by Takagi [20, 33] and has been used since; see [36–39].

It is straightforward to couple UDW detectors quadratically not only to quantized spinor fields but also to quantized (real and complex) scalar fields while preserving symmetries:

$$H_{\text{int}}(\tau) = \lambda\chi(\tau) \mu \int_{\mathbb{R}^n} p(\mathbf{x}(\tau), \mathbf{y}) \Phi^\dagger(\mathbf{y})\Phi(\mathbf{y}) d\mathbf{y} . \quad (16)$$

This type of coupling was first suggested by Hinton for quantized real fields [17]. It may be possible to justify interpreting this model as an effective description of some fundamental interaction, for example when the scalar field describes composite particles at sufficiently low energy. However, in the present work, we will use it as a theoretical

		coupling	
		linear	quadratic
field	real	1. $H_{\text{int}} \sim \Phi$	2. $H_{\text{int}} \sim \Phi^2$
	complex	–	3. $H_{\text{int}} \sim \Phi^\dagger\Phi$
	spinor	–	4. $H_{\text{int}} \sim \bar{\Psi}\Psi$

Table I. Overview of the particle detector models discussed in this paper – listed is the power of the field to which the detector (i.e. μ) is coupled.

tool for investigating what difference it makes to an UDW detector's behavior whether it is coupled to a bosonic (scalar) or to a fermionic (spinor) field. This is because to this end we can now compare model Eq. (16) and model Eq. (15) which are both quadratically coupled, i.e., they differ essentially only in the spinor structure but not in the type of coupling. We will separately investigate the impact of quadratic versus linear coupling, such as model Eq. (16) versus model Eq. (14).

In Table I, the four different detector models we will discuss are summarized and numbered for easy reference: model 1 for quantized real fields couples linearly through Eq. (14); model 2 couples quadratically to quantized real fields; model 3 to quantized complex; and model 4 to quantized spinor fields with the Hamiltonians Eq. (16) and Eq. (15), respectively.

III. FIRST ORDER: EXCITATION PROBABILITY IN THE VACUUM

For simplicity, only UDW-type detectors that are at rest in $n+1$ dimensional Minkowski spacetime will be considered in our investigation of the different detector models. In particular, we study vacuum excitation probabilities (VEP), i.e., probabilities $P_{0,g \rightarrow e}$ of the detector evolving from its ground state $|g\rangle$ to its excited state $|e\rangle$ when the field is initially in the vacuum state $|0\rangle$. We calculate the vacuum excitation probability or *vacuum response* for the four different detector models under consideration, up to leading order in perturbation theory. Calculation of the VEP serves a double purpose:(a) to demonstrate the need for renormalization of the models 2, 3 and 4 in Table I and, after successful renormalization, (b) as a means to gauge whether these two models can be viewed as equivalent.

For concrete calculations, we consider both bosonic and fermionic quantum fields F quantized in the cylinder with toroidal spatial sections consisting of the following product of intervals with periodic boundary conditions:

$$B = [-L/2, L/2]^n \subset \mathbb{R}^n . \quad (17)$$

Therefore,

$$F(t, \mathbf{x} + \boldsymbol{\delta}) = F(t, \mathbf{x}) \quad \forall \boldsymbol{\delta} \in L \cdot \mathbb{Z}^n. \quad (18)$$

The zero mode.— In the cylinder quantization, the field boundary conditions allow for constant classical solutions, that is, solutions of vanishing momentum \mathbf{k} and energy $\omega_{\mathbf{k}}$. These degrees of freedom mathematically behave like free particles, rather than harmonic oscillators. They therefore have to be quantized differently from the rest of the field modes. Since there is no canonical vacuum state for such a zero mode, further subtleties appear when we couple the zero mode to particle detectors [40].

One could get rid of all the problems of the presence of a zero mode by using alternative boundary conditions which, unlike the periodic boundary conditions, do not permit solutions of zero momentum. A simple such choice is the use of Dirichlet boundary conditions, $F(t, \mathbf{x}) = 0$ for all $\mathbf{x} \in \partial B$, such that solutions of zero momentum vanish everywhere. These boundary conditions are straightforward to implement for scalar fields, but full Dirichlet boundary conditions are too restrictive for spinor fields in the Dirac representation on \mathbb{C}^4 because the only solution would be $\Psi = 0$. Instead, a weaker variant can be realized: imposing Dirichlet boundary conditions on the upper (or lower) two components of a four component spinor is possible; see for example [41]. However, it is not as clear how to construct a basis of the solution space that consists of eigenfunction of ∂_0 (corresponding to energy eigenfunctions in quantum theory) and σ_3 (corresponding to spin eigenfunctions), which makes quantization of the theory too involved. In this work we will therefore keep to periodic boundary conditions and simply exclude the zero mode from interactions, as described above.

Fortunately, in most cases, it is possible to choose “safe” states for the zero mode that would minimize its impact on the dynamics of the particle detectors [40]. Based on this fact, in this work we will assume *ad hoc* that the detector does not couple to the zero mode of the field, as it is often done in quantum optics. The question in what circumstances dropping the zero mode can be justified is not vital to the discussion here, and is still subject to active research.

Defining the vacuum response.— We assume that both field and detector are in their respective free ground states at time t_0 . The state of the composite system is then characterized by the density operator

$$\rho(t_0) = |0, g; t_0\rangle \langle 0, g; t_0| = |0, g\rangle \langle 0, g|. \quad (19)$$

The coupled system is allowed to evolve unitarily until time $t = t_0 + T$; time-evolution is performed using the time-evolution operator U generated by the total Hamiltonian

$$H = H_F + H_d + H_{\text{int}}, \quad (20)$$

where H_F is the Hamilton operator of the free field, H_d is given by Eq. (5), and H_{int} depends on the model under consideration. The system ends up in the state

$$\rho(t) = U(t, t_0) \rho U^\dagger(t, t_0) \quad (21)$$

and the probability for the detector to be excited is encoded in the corresponding component of the density operator, after tracing out the field:

$$P_{0, g \rightarrow e}(t, t_0) = \langle e | \text{tr}_F \rho(t) | e \rangle. \quad (22)$$

At the end, we take the limit

$$P_{0, g \rightarrow e} = \lim_{\substack{t_0 \rightarrow -\infty \\ t \rightarrow +\infty}} P_{0, g \rightarrow e}(t, t_0) \quad (23)$$

such that the actual duration of the interaction is determined by the switching function $\chi(t)$ alone: at times outside the support of χ , both systems evolve freely.

It is convenient to reformulate Eq. (22) in terms of state vectors in the interaction picture:

$$P_{0, g \rightarrow e}(t, t_0) = \sum_a |\langle a, e; t | U(t, t_0) | 0, g; t_0 \rangle|^2, \quad (24)$$

where $|a\rangle$ is an orthonormal basis of the Hilbert space of states of the free quantum field F . Recall that the interaction picture is related to the Schrödinger picture through the partial inverse time evolution $U_0(t) = e^{iH_0 t}$ which only takes into account the free Hamiltonian $H_0 = H_F + H_d$ [42].

Finally, we set up the usual perturbation theory under the assumption that λ is small. To this end, the time-evolution operator is expanded in the Dyson series

$$U(t, t_0) = \sum_{n=0}^{\infty} \frac{(-i\lambda)^n}{n!} U^{(n)}(t, t_0), \quad (25)$$

where the operator at order n is [43]

$$U^{(n)}(t, t_0) = \frac{1}{\lambda^n} T \prod_{i=1}^n \int_{t_0}^t dt_i H_{\text{int}}(t_i). \quad (26)$$

For $n = 0$ we have $U^{(0)} = \mathbb{1}$ (no change over time at all), but since $\langle e | g \rangle = 0$, order zero does not contribute to $P_{0, g \rightarrow e}$ in Eq. (24). Therefore,

$$\begin{aligned} P_{0, g \rightarrow e}(t, t_0) &\approx \sum_a \left| -i\lambda \langle a, e; t | U^{(1)}(t, t_0) | 0, g; t_0 \rangle \right|^2 \\ &\equiv \sum_a \left| \mathcal{A}_{a, e}^{(1)} \right|^2 \end{aligned} \quad (27)$$

to leading order in λ , where $\mathcal{A}_{a, e}^{(1)}$ is simply the probability amplitude for the system to evolve from $|0, g\rangle$ to $|a, e\rangle$ at leading order.

In the following, we calculate the VEP for quantized scalar fields in linear coupling, as well as for quantized scalar and spinor fields in quadratic coupling (all models in Table I).

A. Linear coupling to quantized scalar fields

1. Vacuum excitation probability

In preparation for the derivation of new results concerning fermionic detector models, we begin by rederiving

the standard case of a quantized real field Φ (see, among others, [34, 35, 44]). In order to work as generally as possible, we will avoid choosing a particular spatial profile and switching function. We couple an UDW-type detector to the quantized scalar field using the interaction Hamiltonian Eq. (14) (model 1 in Table I). We are dealing with a detector at rest, so its trajectory is

$$\mathbf{x}(\tau) = \mathbf{x}_0, \quad t(\tau) = \tau. \quad (28)$$

The time-evolution operator at leading order reads

$$U^{(1)}(t, t_0) = \int_{t_0}^t dt' \chi(t') \mu(t') \int_{\mathbb{R}^n} d\mathbf{y} p(\mathbf{x}_0, \mathbf{y}) \Phi(t', \mathbf{y}) \quad (29)$$

according to Eq. (26). Notice that for a sufficiently localized spatial profile p (as for example a Gaussian profile), if the localization length σ is much smaller than the compactification length L , we can extend the integration region to the full space to a good approximation.

Here, the monopole operator in the interaction picture is

$$\mu(t) = e^{i\Omega t} \sigma^+ + e^{-i\Omega t} \sigma^-. \quad (30)$$

Similarly, the field operator

$$\Phi(t, \mathbf{x}) = \sum_{\mathbf{k}} \frac{1}{\sqrt{2\omega_{\mathbf{k}}}} \left[a_{\mathbf{k}} e^{-i\omega_{\mathbf{k}} t} \varphi_{\mathbf{k}}(\mathbf{x}) + a_{\mathbf{k}}^\dagger e^{i\omega_{\mathbf{k}} t} \varphi_{\mathbf{k}}^*(\mathbf{x}) \right], \quad (31)$$

where $\omega_{\mathbf{k}}$ is the energy of a single mode, the ladder operators $a_{\mathbf{k}}$ satisfy the usual canonical commutation relations Eq. (A14), and the mode functions $\varphi_{\mathbf{k}}$ Eq. (A10) form an orthonormal basis of the solution space of the Klein-Gordon equation. The field is restricted to a cylinder, so the momentum spectrum is discrete.

Since the detector does not couple to the zero mode, we have

$$\mathbf{k} \in \frac{2\pi}{L} \cdot \mathbb{Z}^n \setminus \{0\}. \quad (32)$$

Note that we have not yet chosen a particular form for the switching function or spatial profile.

From Eq. (27), the only nonvanishing amplitudes are $\mathcal{A}_{1_{\mathbf{k}}, e}^{(1)}$. Therefore the time evolved states will be superpositions of the ground state $|0, g\rangle$ and states of the form $|1_{\mathbf{k}}, e\rangle$, which feature a single quantum in the field. Summing up the squared moduli of the amplitudes and taking the time limits leads to the VEP:

$$P_{0, g \rightarrow e} = \frac{\lambda^2}{2} \sum_{\mathbf{k}} \frac{1}{\omega_{\mathbf{k}}} \left| \int_{\mathbb{R}^n} p(\mathbf{x}_0, \mathbf{y}) \varphi_{\mathbf{k}}(\mathbf{y}) d\mathbf{y} \right|^2 \times \left| \int_{-\infty}^{\infty} \chi(t) e^{i(\Omega + \omega_{\mathbf{k}})t} dt \right|^2. \quad (33)$$

Solving the Klein-Gordon equation in a cavity with periodic boundary conditions yields (see Appendix A) for the spatial part of the mode function

$$\varphi_{\mathbf{k}}(\mathbf{x}) = \frac{1}{\sqrt{L^n}} e^{i\mathbf{k} \cdot \mathbf{x}}, \quad (34)$$

so the final expression for the VEP reads

$$P_{0, g \rightarrow e} = \frac{\lambda^2}{2L^n} \sum_{\mathbf{k}} \frac{1}{\omega_{\mathbf{k}}} \left| \int_{\mathbb{R}^n} p(\mathbf{x}_0, \mathbf{y}) e^{-i\mathbf{k} \cdot \mathbf{y}} d\mathbf{y} \right|^2 \times \left| \int_{-\infty}^{\infty} \chi(t) e^{i(\Omega + \omega_{\mathbf{k}})t} dt \right|^2. \quad (35)$$

2. Dependence on the dimension of spacetime

The momentum sum in Eq. (35) depends on the spatial dimension n , since $\mathbf{k} = (k^1, k^2, \dots, k^n)$. Therefore the convergence behavior of $P_{0, g \rightarrow e}$ also strongly depends on the dimension. To demonstrate this, we assume the detector to be pointlike,

$$p(\mathbf{x}, \mathbf{y}) = \delta(\mathbf{x} - \mathbf{y}), \quad (36)$$

and switch it on and off abruptly (sudden switching) by means of a window function:

$$\chi(t) = \begin{cases} 1 & \text{if } t \in [t_0, t_0 + T] \\ 0 & \text{else} \end{cases}. \quad (37)$$

This is the original UDW detector introduced by DeWitt [3]. Plugging χ and $p(\mathbf{y}, \cdot)$ in Eq. (35) and performing the time integrals, the VEP simplifies to

$$P_{0, g \rightarrow e} = \frac{2\lambda^2}{L^n} \sum_{\mathbf{k}} \frac{1}{\omega_{\mathbf{k}}(\Omega + \omega_{\mathbf{k}})^2} \sin^2 \left(\frac{\Omega + \omega_{\mathbf{k}} T}{2} \right). \quad (38)$$

In the massless case, the momentum sums are made explicit by writing out the dispersion relation

$$\omega_{\mathbf{k}} = |\mathbf{k}| = \frac{2\pi}{L} \sqrt{l_1^2 + l_2^2 + \dots + l_n^2}, \quad (39)$$

where $l_i \in \mathbb{Z} \setminus \{0\}$.

In one spatial dimension, we have

$$P_{0, g \rightarrow e} = \frac{\lambda^2 L^2}{2\pi^3} \sum_{l_1=1}^{\infty} \frac{1}{l_1 \left(\frac{\Omega L}{2\pi} + l_1 \right)^2} \sin^2 \left[\frac{\pi}{L} \left(\frac{\Omega L}{2\pi} + l_1 \right) T \right]. \quad (40)$$

This sum is bounded by

$$P_{0, g \rightarrow e} \leq \frac{\lambda^2 L^2}{2\pi^3} \sum_{l_1=1}^{\infty} \frac{1}{l_1^3},$$

which is convergent.

For dimension $n = 2$, the probability is

$$P_{0,g \rightarrow e} = \frac{\lambda^2 L}{\pi^3} \sum_{l_1=1}^{\infty} \sum_{l_2=1}^{\infty} \left[\sqrt{l_1^2 + l_2^2} \left(\frac{\Omega L}{2\pi} + \sqrt{l_1^2 + l_2^2} \right)^2 \right]^{-1} \times \sin^2 \left[\frac{\pi}{L} \left(\frac{\Omega L}{2\pi} + \sqrt{l_1^2 + l_2^2} \right) T \right], \quad (41)$$

which is similarly bounded by the convergent double sum

$$P_{0,g \rightarrow e} \leq \frac{\lambda^2 L}{\pi^3} \sum_{l_1=1}^{\infty} \sum_{l_2=1}^{\infty} \frac{1}{\sqrt{l_1^2 + l_2^2}^3}.$$

In $n = 3$ dimensions, however, the VEP diverges. Its formal expression is

$$P_{0,g \rightarrow e} = \frac{2\lambda^2}{\pi^3} \sum_{l_1=1}^{\infty} \sum_{l_2=1}^{\infty} \sum_{l_3=1}^{\infty} \left[\sqrt{\sum_{i=1}^3 l_i^2} \left(\frac{\Omega L}{2\pi} + \sqrt{\sum_{i=1}^3 l_i^2} \right)^2 \right]^{-1} \times \sin^2 \left[\frac{\pi}{L} \left(\frac{\Omega L}{2\pi} + \sqrt{\sum_{i=1}^3 l_i^2} \right) T \right]. \quad (42)$$

As $\Omega L(2\pi)^{-1} \geq 0$, we can estimate

$$\frac{\pi^3}{2\lambda^2} P_{0,g \rightarrow e} \geq \sum_{l_1=1}^{\infty} \sum_{l_2=1}^{\infty} \sum_{l_3=1}^{\infty} \left[\frac{\Omega L}{2\pi} + \sqrt{\sum_{i=1}^3 l_i^2} \right]^{-3} \times \sin^2 \left[\frac{\pi}{L} \left(\frac{\Omega L}{2\pi} + \sqrt{\sum_{i=1}^3 l_i^2} \right) T \right]. \quad (43)$$

By exploiting $\cos(x) = \sin(x + \pi/2)$ and the Pythagorean trigonometric identity, it is straightforward to prove that the right-hand side converges for all choices of parameters if and only if

$$\sum_{l_1=1}^{\infty} \sum_{l_2=1}^{\infty} \sum_{l_3=1}^{\infty} \left[A + \sqrt{\sum_{i=1}^3 l_i^2} \right]^{-3}$$

does, where $A = \Omega L(2\pi)^{-1}$. This sum is in turn bounded by

$$\sum_{l_1=1}^{\infty} \sum_{l_2=1}^{\infty} \sum_{l_3=1}^{\infty} [A + l_1 + l_2 + l_3]^{-3}, \quad (44)$$

which diverges logarithmically.

In higher dimensions convergence can only get worse, because even more sums will appear. For any dimension $(1, n)$ with $n \geq 3$, the VEP is divergent [35].

The above results show that the VEP strongly depends on the dimension of the underlying spacetime. In the above example, the vacuum response of a pointlike detector with sudden switching, coupled to a quantized real field is convergent in $(1, 1)$ and $(1, 2)$ dimensions, but divergent in all higher dimensions, necessitating regularization.

3. Regularization through detector profile

Those divergences of the VEP can be understood as a result of the pointlike structure of the detector as well as the sudden switching [35]. In the linear coupling case, the divergences can be regularized by adiabatically switching the detector, or by ‘‘smearing’’ the interaction between detector and field over the spatial profile of the detector. Let us study both possibilities in two separate examples.

Gaussian switching and pointlike detector.— Consider the probability Eq. (35), still with a pointlike detector Eq. (36), but this time employing a Gaussian switching function,

$$\chi(t) = \exp\left(-\frac{t^2}{2T^2}\right), \quad (45)$$

which is known to regularize the response of a resting detector in $(1, 3)$ -dimensional Minkowski spacetime [34]. We generalize this result to $(1, n)$ dimensions: the time integral is readily solved, giving

$$\int_{-\infty}^{\infty} e^{-t^2/(2T^2)} e^{i(\Omega + \omega_{\mathbf{k}})t} dt = \sqrt{2\pi T^2} e^{-(\Omega + \omega_{\mathbf{k}})^2 T^2/2}. \quad (46)$$

Substituting this in Eq. (35) yields

$$P_{0,g \rightarrow e} = \frac{\pi \lambda^2 T^2}{L^n} \sum_{\mathbf{k}} \frac{1}{\omega_{\mathbf{k}}} e^{-(\Omega + \omega_{\mathbf{k}})^2 T^2} \quad (47)$$

which is bounded by the convergent sum

$$P_{0,g \rightarrow e} \leq \frac{2^{n-1} \lambda^2 T^2}{L^{n-1}} \prod_{i=1}^n \sum_{l_i=1}^{\infty} e^{-(2\pi T/L)^2 l_i^2}. \quad (48)$$

This shows that a suitably smooth switching function is able to regularize the leading order excitation probability in arbitrary dimensions.

The excitation probability in this example is finite, but nonzero, even though the detector was in the ground state and the field in the vacuum. This should not be surprising considering that we have a time-dependent Hamiltonian: When the interaction is switched on, the Hamiltonian of the composite system is changed, and the state $|0, g\rangle$ is no longer an energy eigenstate. In consequence, the state begins to evolve nontrivially, and there is a finite probability for the detector to be measured in its excited state

$|e\rangle$. The more adiabatically the interaction is switched on, the lower is the probability to excite the detector [34]. This is reflected in Eq. (47): the larger T , that is, the slower the detector is switched, the smaller $P_{0,g\rightarrow e}$. In the limit $T \rightarrow \infty$, corresponding to adiabatic switching, $P_{0,g\rightarrow e} \rightarrow 0$ as expected.

Sudden switching and Gaussian detector profile.— Now consider a Gaussian detector profile,

$$p(\mathbf{x}_0, \mathbf{y}) = (2\pi\sigma^2)^{-n/2} \exp\left(-\frac{(\mathbf{y} - \mathbf{x}_0)^2}{2\sigma^2}\right), \quad (49)$$

together with a sudden switching. In this case:

$$P_{0,g\rightarrow e} = \frac{2\lambda^2}{L^n} \sum_{\mathbf{k}} \frac{e^{-\mathbf{k}^2\sigma^2}}{\omega_{\mathbf{k}}(\Omega + \omega_{\mathbf{k}})^2} \sin^2\left(\frac{\Omega + \omega_{\mathbf{k}}}{2}T\right), \quad (50)$$

which is bounded by

$$P_{0,g\rightarrow e} \leq \frac{2^{n-2}\lambda^2}{\pi^3 L^{n-3}} \prod_{i=1}^n \sum_{l_i=1}^{\infty} e^{-(2\pi\sigma/L)^2 l_i^2} \quad (51)$$

and therefore again convergent in arbitrary dimensions—the spatial smearing of the interaction between detector and field is also able to regularize the vacuum response of the detector. Moreover, $P_{0,g\rightarrow e} \rightarrow 0$, if the detector is completely delocalized, that is for $\sigma \rightarrow \infty$.

General effect of spacetime profile.— The two preceding examples show that it is possible to regularize the VEP to leading order in perturbation theory. But which combinations of switching function χ and spatial smearing p are able to regularize the VEP? To address this question, it is helpful to use the detector's spacetime profile f : the VEP of the quantized real field in Eq. (35) can be reformulated as

$$P_{0,g\rightarrow e} = \frac{\lambda^2}{2L^n} \sum_{\mathbf{k}} \frac{1}{\omega_{\mathbf{k}}} \left| \tilde{f}(\omega_{\mathbf{k}} + \Omega, \mathbf{k}) \right|^2, \quad (52)$$

where \tilde{f} is the $(1, n)$ -dimensional Fourier transform of the spacetime profile f :

$$\tilde{f}(\omega_{\xi}, \xi) = \int_{\mathbb{R}^n} d\mathbf{x} \int_{-\infty}^{\infty} dt f(\mathbf{x}, t) e^{-i\omega_{\xi}t} e^{i\xi\mathbf{x}}. \quad (53)$$

Therefore, a given spacetime profile does regularize the VEP to leading order in $(1, n)$ dimensions if and only if the modulus squared of its $(1, n)$ -dimensional Fourier transform \tilde{f} decays fast enough in the UV such that the n -fold sum in the above expression is finite.

B. Quadratic coupling to quantized spinor fields

We now turn to the pivotal question: How can we construct a similar particle detector model for quantized spinor fields? To this end, let us begin by investigating and extending a model that has been commonly employed

in the literature, namely, model 4 in Table I pioneered by Takagi in 1985 [33] and extensively used, e.g., in [20, 36–39]. We will assess the physicality of this class of models by considering the vacuum response of spatially smeared detectors.

Let Ψ be a spinor field, that is, a field taking values in some representation space \mathbb{C}^m of the complexified Clifford algebra $\text{Cliff}(1, n)^{\mathbb{C}}$. In order to be able to do explicit calculations, we choose the irreducible Dirac representation of $\text{Cliff}(1, 3)$ on \mathbb{C}^4 in 4 spacetime dimensions. In 2 spacetime dimensions, a related but reducible representation of $\text{Cliff}(1, 1)$ on \mathbb{C}^4 is used, which yields similar spinor mode functions. Details on these conventions and standard results in classical and quantum field theory can be found in Appendix A.

We will work again in the interaction picture, where the operator of the quantized field is

$$\Psi(t, \mathbf{x}) = \sum_{\mathbf{k}, s} a_{\mathbf{k}, s} e^{-i\omega_{\mathbf{k}}t} \psi_{\mathbf{k}, s, +}(\mathbf{x}) + b_{\mathbf{k}, s}^{\dagger} e^{i\omega_{\mathbf{k}}t} \psi_{\mathbf{k}, s, -}(\mathbf{x}). \quad (54)$$

The ladder operators $a_{\mathbf{k}, s}$, $b_{\mathbf{k}, s}$ satisfy the canonical *anti-commutation* relations Eq. (A60). The spinor-valued mode functions $\psi_{\mathbf{k}, s, \epsilon}$ span a solution space of the Dirac equation. Depending on dimension and mass, the mode functions take slightly different forms, namely, (a) Eqs. (A28) and (A37) for massive and massless fields in $(1, 3)$ dimensions; and (b) Eqs. (A28) and (A37) in $(1, 1)$ dimensions.

This quantized spinor field is coupled *quadratically* to a resting UDW-type detector via the interaction Hamiltonian Eq. (15), which is model 4 in Table I. Using Eq. (26) we then obtain the leading order contribution to the time evolution operator:

$$U^{(1)}(t, t_0) = \int_{t_0}^t dt' \chi(t') \mu(t') \times \int_{\mathbb{R}^n} d\mathbf{y} p(\mathbf{x}_0, \mathbf{y}) \bar{\Psi}(t', \mathbf{y}) \Psi(t', \mathbf{y}). \quad (55)$$

The vacuum response Eq. (27) yields

$$P_{0,g\rightarrow e} = \lambda^2 \left| \sum_{\mathbf{k}, s} \int_{\mathbb{R}^n} p(\mathbf{x}_0, \mathbf{y}) \bar{\psi}_{\mathbf{k}, s, -}(\mathbf{y}) \psi_{\mathbf{k}, s, -}(\mathbf{y}) d\mathbf{y} \right|^2 \times \left| \int_{-\infty}^{+\infty} \chi(t) e^{i\Omega t} dt \right|^2 + \lambda^2 \sum_{\mathbf{k}, s} \sum_{\mathbf{p}, r} \left| \int_{\mathbb{R}^n} p(\mathbf{x}_0, \mathbf{y}) \bar{\psi}_{\mathbf{k}, s, +}(\mathbf{y}) \psi_{\mathbf{p}, r, -}(\mathbf{y}) d\mathbf{y} \right|^2 \times \left| \int_{-\infty}^{+\infty} \chi(t) e^{i(\Omega + \omega_{\mathbf{k}} + \omega_{\mathbf{p}})t} dt \right|^2. \quad (56)$$

There are obvious differences to the vacuum response of the usual UDW model (model 1 in Table I, i.e., a

monopole detector linearly coupled to a quantized scalar field). Comparing Eq. (33) with Eq. (55), at leading order in λ , there are two kinds of terms instead of one.

The first term corresponds to excitation of the detector by creation and subsequent annihilation of a field quantum, with amplitude $\mathcal{A}_{0,e}^{(1)}$. More precisely, the detector is excited by creating and annihilating an antiparticle from the vacuum. However, the equivalent process featuring a particle does not occur.

The second term represents processes where the detector is excited by emission of a particle and an antiparticle, with amplitude $\mathcal{A}_{1_{(k,s)},\bar{1}_{(p,r)},e}^{(1)}$. These should be expected in the light of our discussion regarding fermion number conservation in Sec. II B. Note that the momenta of the particle and antiparticle are not related since the detector is “heavy” and can absorb any amount of momentum.

We can make the mode functions $\psi_{\mathbf{k},s,\epsilon}$ explicit using Eqs. (A28), (A37), (A45) and (A53). In all four cases considered here, massive and massless fields in (1, 3) and (1, 1) dimensions, the VEP when coupling quadratically to quantized spinor fields can be brought into the form

$$P_{0,g \rightarrow e} = \frac{\lambda^2}{2L^{2n}} \left[8m^2 \left(\sum_{\mathbf{k}} \frac{1}{\omega_{\mathbf{k}}} \right)^2 \left| \int_{-\infty}^{+\infty} \chi(t) e^{i\Omega t} dt \right|^2 + \sum_{\mathbf{k},\mathbf{p}} \frac{(\omega_{\mathbf{k}} + m)(\omega_{\mathbf{p}} + m)}{\omega_{\mathbf{k}}\omega_{\mathbf{p}}} \left(\frac{\mathbf{k}}{\omega_{\mathbf{k}} + m} - \frac{\mathbf{p}}{\omega_{\mathbf{p}} + m} \right)^2 \times \left| \int_{\mathbb{R}^n} p(\mathbf{x}_0, \mathbf{y}) e^{-i(\mathbf{k}+\mathbf{p})\mathbf{y}} d\mathbf{y} \right|^2 \times \left| \int_{-\infty}^{+\infty} \chi(t) e^{i(\Omega + \omega_{\mathbf{k}} + \omega_{\mathbf{p}})t} dt \right|^2 \right], \quad (57)$$

where $n = 1$ or $n = 3$. The case of a massless field is correctly recovered by setting $m = 0$, such that the first term vanishes. Notice that there is an additional problem with the first term in Eq. (57) for $m \neq 0$. Namely, the term is proportional to $\sum_{\mathbf{k}} \omega_{\mathbf{k}}^{-1}$. Even in the least divergent scenario, i.e. $n = 1$, this sum diverges like $\sum_a a^{-1}$.

This divergency is fundamentally worse behaved than those encountered in the standard bosonic Unruh-DeWitt model, which arise from the pointlike structure of the detector [13, 20], or its overly abrupt switching [34, 35]. The first term in Eq. (57) *cannot be regularized* by way of a smooth spacetime profile, and therefore the divergency in model 4 cannot be cured via this common method. This is because the spatial integral containing the (normalized) detector profile factors out and yields a factor of 1. The time integral here is not momentum dependent and merely contributes an overall factor which cannot regularize the divergent sum.

Comparing with the Unruh-DeWitt model, there are three conceivable origins of this new divergency: (a) it could be algebraic on the level of ladder operators, because we are now dealing with a field obeying Fermi statistics instead of Bose statistics, (b) it could be analytic due to

the field’s spinorial structure and different inner product compared to the scalar fields, (c) or the origin could be the coupling that is now quadratic in the field instead of linear. The question is easily settled by computing the VEP of a *quantized complex* field coupled quadratically to an UDW-type detector, keeping properties (a) and (b) the same as in the usual Unruh-DeWitt model.

C. Quadratic coupling to quantized scalar fields

Let Φ be a quantized real or complex field (models 2 and 3 in Table I, respectively), coupled quadratically to a resting UDW-type detector via the interaction Hamiltonian Eq. (16). Inserting the interaction Hamiltonian in Eq. (26) yields

$$U^{(1)}(t, t_0) = \int_{t_0}^t dt' \chi(t') \mu(t') \int_{\mathbb{R}^n} d\mathbf{y} p(\mathbf{x}_0, \mathbf{y}) \Phi^\dagger(t', \mathbf{y}) \Phi(t', \mathbf{y}), \quad (58)$$

where the field operator (in the interaction picture) is given by Eq. (31) in case of a quantized real field. If the field is complex

$$\Phi(t, \mathbf{x}) = \sum_{\mathbf{k}} \frac{1}{\sqrt{2\omega_{\mathbf{k}}}} \left[a_{\mathbf{k}} e^{-i\omega_{\mathbf{k}}t} \varphi_{\mathbf{k}}(\mathbf{x}) + b_{\mathbf{k}}^\dagger e^{i\omega_{\mathbf{k}}t} \varphi_{\mathbf{k}}^*(\mathbf{x}) \right]. \quad (59)$$

Calculation of the VEP Eq. (27) yields

$$P_{0,g \rightarrow e} = \frac{\lambda^2}{4} \left[\left| \sum_{\mathbf{k}} \frac{1}{\omega_{\mathbf{k}}} \int_{\mathbb{R}^n} p(\mathbf{x}_0, \mathbf{y}) |\varphi_{\mathbf{k}}(\mathbf{y})|^2 d\mathbf{y} \right|^2 \times \left| \int_{-\infty}^{+\infty} \chi(t) e^{i\Omega t} dt \right|^2 + \sum_{\mathbf{k},\mathbf{p}} \frac{1}{\omega_{\mathbf{k}}\omega_{\mathbf{p}}} \left| \int_{\mathbb{R}^n} p(\mathbf{x}_0, \mathbf{y}) \varphi_{\mathbf{k}}^*(\mathbf{y}) \varphi_{\mathbf{p}}^*(\mathbf{y}) d\mathbf{y} \right|^2 \times \left| \int_{-\infty}^{+\infty} \chi(t) e^{i(\Omega + \omega_{\mathbf{k}} + \omega_{\mathbf{p}})t} dt \right|^2 \right] \quad (60)$$

in both cases at leading order. Notice that this is no longer true at higher orders. This expression has two terms like Eq. (56), representing analogue processes: The first term again corresponds to excitation of the detector by emission and reabsorption of an antiparticle with amplitude $\mathcal{A}_{0,e}^{(1)}$, and the second term corresponds to processes where the detector is excited by emission of a particle-antiparticle pair with amplitude $\mathcal{A}_{1_{\mathbf{k}},\bar{1}_{\mathbf{p}},e}^{(1)}$. Explicitly inserting the mode functions Eq. (34) for periodic boundary conditions

gives

$$P_{0,g \rightarrow e} = \frac{\lambda^2}{4L^{2n}} \left[\left(\sum_{\mathbf{k}} \frac{1}{\omega_{\mathbf{k}}} \right)^2 \left| \int_{-\infty}^{+\infty} \chi(t) e^{i\Omega t} dt \right|^2 + \sum_{\mathbf{k}, \mathbf{p}} \frac{1}{\omega_{\mathbf{k}} \omega_{\mathbf{p}}} \left| \int_{\mathbb{R}^n} p(\mathbf{x}_0, \mathbf{y}) e^{-i(\mathbf{k}+\mathbf{p})\mathbf{y}} d\mathbf{y} \right|^2 \times \left| \int_{-\infty}^{+\infty} \chi(t) e^{i(\Omega+\omega_{\mathbf{k}}+\omega_{\mathbf{p}})t} dt \right|^2 \right]. \quad (61)$$

The first term is proportional to $\sum_{\mathbf{k}} \omega_{\mathbf{k}}^{-1}$ and thus divergent in the same way as for spinor fields in Eq. (57). Since this divergence appears in exactly the same form for both scalar and spinor fields, its origin is clearly the quadratic coupling. Also note that for quantized scalar fields the divergence arises even if $m = 0$.

It is not surprising that these divergencies arise: Interactions containing second or higher powers of fields tend to lead to divergencies in observables, which require renormalization. In particular, the spinor field detector model by Iyler and Kumar [32] faces the same problem.

IV. RENORMALIZATION OF QUADRATIC MODELS

Before investigating the renormalization of the quadratically coupled detector models Eqs. (15) and (16), let us briefly review the literature.

A. Literature review

In Ref. [17], Hinton introduces an UDW-type particle detector model coupled to a quantized real field Φ through the interaction Hamiltonian

$$H_{\text{int}} = \lambda \mu \Phi^2[\mathbf{x}(\tau)], \quad (62)$$

which was the template for Eq. (16). Hinton calculates the VEP in [17, eq. (14)], remarks that the expression is formally divergent and requires renormalization but no explicit renormalization scheme is given.

Takagi, who suggested coupling a quantized spinor field quadratically to DeWitt's two-level detector through Eq. (2), followed a different approach. In the original publications, see Refs. [20, 33], Takagi points out an infinite term in the VEP at leading order but argues that this term can be dropped. Later publications employing Takagi's detector model or drawing on his results implicitly follow the same reasoning [36–39]. A key point is that instead of the total excitation probability, excitation *rates* are considered. As is well known, the calculations of rates involves fewer integrations and are therefore generally more regular. In addition, Takagi regularizes the detector response by using a smooth, namely exponential

switching function. As a consequence, in the excitation rate

$$R = \lim_{\substack{t_0 \rightarrow -\infty \\ t \rightarrow +\infty}} \frac{P_{0,g \rightarrow e}(t, t_0)}{t - t_0} \quad (63)$$

the divergence in $P_{0,g \rightarrow e}$ is offset by a divergence in the denominator.

Takagi's expression for the rate [20, eqs. (8.5.2) to (8.5.4)] can easily be obtained in the notation developed earlier by using Eqs. (15), (26) and (27) in Eq. (63) and by using a pointlike detector with exponential switching function:

$$p(\mathbf{x}, \mathbf{y}) = \delta(\mathbf{x} - \mathbf{y}), \quad \chi(t) = e^{-s|t|} \quad (64)$$

The limit $s \rightarrow 0$ is taken at the end of the calculation in Ref. [20] so that ultimately the detector is switched on and off infinitely slowly. One obtains the rate

$$R = \lambda^2 |\langle e|\mu|g \rangle|^2 F(\Omega). \quad (65)$$

Here,

$$F(\Omega) = \lim_{s \rightarrow 0} \lim_{\substack{t_0 \rightarrow -\infty \\ t \rightarrow +\infty}} \int_{t_0}^t dt_1 \int_{t_0}^t dt_2 \frac{1}{t - t_0} \times e^{-s(|t_1|+|t_2|)} e^{-i\Omega(t_1-t_2)} S(t_1 - t_2), \quad (66)$$

which is usually called the *detector response function* [14], and

$$S(t_1 - t_2) = \langle 0|\bar{\Psi}(t_1, \mathbf{x})\Psi(t_1, \mathbf{x})\bar{\Psi}(t_2, \mathbf{x})\Psi(t_2, \mathbf{x})|0 \rangle \quad (67)$$

is a 4-point correlation function. This step is not made explicit in Ref. [20]; rather, Takagi directly argues that the exact form of the switching function is not relevant, since it has only been introduced as a way to regularize the detector response. Therefore, he argues, one is allowed to temporarily replace the exponential switching function with a Gaussian one, and to exploit that only the limits $t \rightarrow \infty$, $t_0 \rightarrow -\infty$ and $s \rightarrow 0$ are of interest—see end of section 3.3 in Ref. [20]. Finally, the Gaussian is replaced *ad hoc* with an exponential function again. If we accept Takagi's reasoning, the above response function can be rewritten as

$$F(\Omega) = \lim_{s \rightarrow 0} \int_{-\infty}^{\infty} dt e^{-i\Omega t} e^{-s|t|} S(t), \quad (68)$$

which indeed corresponds to [20, eqs. (8.5.2) to (8.5.4)] (with two differences: in the original paper, the factor $e^{-s|t|}$ due to the switching function is suppressed, and $\lambda = 1$). In this notation, the divergence we encountered earlier is now hidden in the correlator S : by Wick's theorem it can be expanded as

$$S(t_1 - t_2) = [\text{tr } S^-(0)]^2 + \text{tr}[S^-(t_1 - t_2)S^+(t_1 - t_2)] \quad (69)$$

where S^- , S^+ are the Wightman functions

$$\begin{aligned} S^-(t_1, t_2)_B^A &= \langle 0|\bar{\Psi}_B(t_2, \mathbf{x})\Psi^A(t_1, \mathbf{x})|0 \rangle \\ S^+(t_1, t_2)_B^A &= \langle 0|\Psi^A(t_1, \mathbf{x})\bar{\Psi}_B(t_2, \mathbf{x})|0 \rangle \end{aligned} \quad (70)$$

and the first term is infinite, as expected:

$$\text{tr } S^-(0) \rightarrow \infty . \quad (71)$$

Takagi treats this infinite term as formally constant in Eq. (69), which allows one to obtain a delta distribution from the time integral:

$$F(\Omega) = \delta(\Omega) [\text{tr } S^-(0)]^2 + \lim_{s \rightarrow 0} \int_{-\infty}^{\infty} dt' e^{-i\Omega(t')} e^{-s|t'|} \\ \times \text{tr } S^-(t_2, t_1) S^+(t_1, t_2) . \quad (72)$$

He concludes, therefore, that the term $\text{tr } S^-(0)$ can be dropped, as long as the detector gap is finite, $\Omega > 0$, thereby obtaining a finite excitation rate R .

This argumentation is not entirely satisfactory. In particular, it merely yields a finite excitation rate. This is not enough to fully characterize the response of a particle detector. For that, one would need to be able to compute its full density matrix, which requires computing probability amplitudes, not rates. Takagi's techniques, however, do not avoid divergences in probabilities. The challenge remains to fully renormalize particle detector models with an interaction Hamiltonian that is quadratic in the field.

B. Renormalization at leading order

As we discussed above, the first term in Eqs. (57) and (61) contains a divergence that cannot be regularized by means of a spacetime profile, unlike in the usual linearly coupled UDW model. As we will show now, the occurrence of such divergencies is not surprising from the point of view of a quantum field theoretical renormalization theory, and can be handled straightforwardly. To this end, let us compare the two problematic detector models to quantum electrodynamics (QED). The interaction Hamiltonian of QED, $H_{\text{QED}} \propto A_\mu \bar{\Psi} \gamma^\mu \Psi$, is also quadratic in the spinor field (electron field), the only difference being that the coupling is not to a scalar detector but to the vectorial photon field. Indeed, QED has a similar divergence, namely the well-known divergent tadpole subdiagram. In QED, it is renormalized straightforwardly by normal-ordering the interaction Hamiltonian (see, e.g. [45]). In the following two sections we demonstrate that and how the divergencies in the detector models are related to tadpole diagrams, and we show that normal-ordering of the interaction Hamiltonian renormalizes the detector models as well.

1. Structure of the divergence

As mentioned before, there are two types of perturbative processes that excite the detector at leading order, thereby contributing to the VEP for quantized spinor fields in Eq. (56), or quantized scalar fields in Eq. (60).

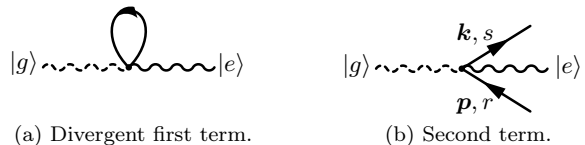


Figure 1. Schematic representation of the processes leading to the state Eq. (73). The wiggly line stands for the detector (dashed when in ground state, solid if excited), the solid straight line for the quantized scalar or spinor field. The time direction is from left to right.

To see this, recall that at leading order, time evolution amounts to applying the interaction Hamiltonian to the initial state $|0, g\rangle$ and integrating over the entire duration of the interaction. In case of a spinor field, the final state is $|e, \psi\rangle$. Given the quadratic coupling in the interaction Hamiltonian $\sim \bar{\Psi} \Psi$ for the fermionic case and $\sim \Phi^\dagger \Phi$ for the bosonic case, the algebraic structure of the leading order time evolved field state is of the form:

$$|\psi\rangle, |\phi\rangle = \sum_{\mathbf{k}} E_{\mathbf{k}} |0\rangle + \sum_{\mathbf{k}, \mathbf{p}} F_{\mathbf{k}, \mathbf{p}} |1_{\mathbf{k}}, \bar{1}_{\mathbf{p}}\rangle . \quad (73)$$

The spinorial degrees of freedom are suppressed and $E_{\mathbf{k}}, F_{\mathbf{k}, \mathbf{p}}$ are coefficients depending on the momenta (and for spinor fields additionally on spins). In other words: When interacting with the field in the vacuum state, the detector can be excited (to leading order in perturbation theory) either by emission and subsequent annihilation of an antiparticle [divergent first term in Eqs. (56), (60) and (73)], or by emitting a particle-antiparticle pair (second term in the same equations). Since we are only interested in the state of the detector after the interaction, both types of processes contribute to the vacuum excitation probability. They are visualized as diagrams in Fig. 1. Note that these simplified diagrams (used for illustration) are not strictly Feynman diagrams since the detector is not yet second quantized, as we will see in more detail in Sec. VIII when we build the detector-field interaction Feynman rules.

The following discussion is limited to the case of a quantized spinor field, but runs analogously for quantized scalar fields. In comparing the spinor field detector with QED, the spinor field corresponds to the electron field in QED, and the detector to the photon field. Thus, the detector ground state translates to the absence of photons, while the excited state corresponds to the presence of one photon. In this sense, the processes in Fig. 1 are analogous to the QED diagrams drawn in Fig. 2. In particular, the problematic first term in Fig. 1 corresponds to the tadpole diagram in Fig. 2. The divergence of its amplitude $\mathcal{A}_{0,e}^{(1)}$ is mirrored by QED: the amplitude of the tadpole diagram is divergent as well; see [45].

While the ‘‘heavy’’ detector guarantees energy and momentum conservation in Fig. 1, both QED processes in Fig. 2 are dynamically forbidden. They may, however, appear as subdiagrams in larger processes, and it is possi-



Figure 2. QED Feynman diagrams corresponding to the processes in Fig. 1.

ble to calculate their contribution to the total amplitudes. Indeed, the analogy between the left-hand diagrams in Figs. 1 and 2 extends to their respective amplitudes: according to Eqs. (27) and (55), the amplitude of the left diagram in Fig. 1 is

$$\begin{aligned} \mathcal{A}_{0,e}^{(1)} &= -i\lambda e^{-i\Omega t} \\ &\times \langle 0, e | \int_{t_0}^t \chi(t') \mu(t') \bar{\Psi}(t', \mathbf{x}) \Psi(t', \mathbf{x}) dt' | 0, g \rangle \\ &\sim \langle 0 | \bar{\Psi}(t', \mathbf{x}) \Psi(t', \mathbf{x}) | 0 \rangle \end{aligned} \quad (74)$$

when suppressing the time integration. The detector was assumed to be pointlike for simplicity, since we know already from Eq. (56) that the spatial profile has no regularizing effect. Using the fermionic time-ordering operator, this can be rewritten as

$$\begin{aligned} \langle 0 | \bar{\Psi}_A(t, \mathbf{x}) \Psi^A(t, \mathbf{x}) | 0 \rangle \\ = - \langle 0 | T \Psi^A(t, \mathbf{x}) \bar{\Psi}_A(t, \mathbf{x}) | 0 \rangle, \end{aligned} \quad (75)$$

which is essentially the Feynman propagator:

$$S_F(x-y)_B^A = \langle 0 | T \Psi^A(x) \bar{\Psi}_B(y) | 0 \rangle. \quad (76)$$

We find

$$\mathcal{A}_{0,e}^{(1)} \sim \text{tr} S_F(0) \rightarrow \infty, \quad (77)$$

where the trace runs over the spinor indices.

By applying position space Feynman rules to the tadpole diagram in Fig. 2, on the other hand, one obtains the amplitude

$$\text{tr}[\gamma^\mu S_F(0)] \rightarrow \infty, \quad (78)$$

(see e.g. [45]). The divergence of the two amplitudes Eqs. (77) and (78) has a common structure: they diverge because the Feynman propagator of the quantized spinor field is ill defined when closed in itself. The gamma matrices in the second amplitude merely appear because electrodynamics has a vector coupling Eq. (3), as opposed to the scalar coupling Eq. (15) for the detector model.

In conclusion, it is justified to interpret the divergence found in the quadratically coupling detector models as the analogue of tadpole diagrams known from quantum field theories such as QED.

2. Renormalization by normal-ordering

Tadpoles are renormalized by normal-ordering of the interaction Hamiltonian. This amounts to setting the amplitude of the tadpole to zero, or—equivalently—ignoring any diagram containing tadpoles as subdiagrams (see, for instance, [45]). The same procedure works for both the detector models as well: normal-ordering the interaction Hamiltonians Eq. (15) leads to

$$\begin{aligned} \mathcal{A}_{0,e}^{(1)} &= -i\lambda e^{-i\Omega t} \\ &\times \langle 0, e | \int_{t_0}^t \chi(t') \mu(t') : \bar{\Psi}(t', \mathbf{x}) \Psi(t', \mathbf{x}) : dt' | 0, g \rangle \\ &= 0 \end{aligned} \quad (79)$$

instead of Eqs. (74) and (77), such that the divergence is renormalized to zero. Equivalently, for detector models coupled quadratically to quantized real or complex fields via the Hamiltonian Eq. (16),

$$\mathcal{A}_{0,e}^{(1)} \sim \langle 0 | : \Phi^\dagger \Phi : | 0 \rangle = 0. \quad (80)$$

The above renormalization can be interpreted as shifting the expectation value of the interaction energy from infinity to zero: If detector and field do not interact, $|0, g\rangle$ is the ground state, with energy eigenvalue zero:

$$\langle 0, g | H | 0, g \rangle = 0. \quad (81)$$

Here, $H = H_d + H_\Phi$ for quantized scalar fields, and $H = H_d + H_\Psi$ for quantized spinor fields as given in Eqs. (5), (A15), (A19) and (A61). However, as soon as the coupling is switched on, $\lambda > 0$, we would naively have

$$\langle 0, g | H + H_{\text{int}} | 0, g \rangle \rightarrow \infty \quad (82)$$

for the interactions quadratic in the field Eqs. (15) and (16). This would be unphysical and normal-ordering the interaction Hamiltonian is therefore appropriate to ensure that

$$\langle 0, g | H + : H_{\text{int}} : | 0, g \rangle = 0. \quad (83)$$

In comparison, for linear coupling Eq. (14) the energy expectation value vanishes automatically.

C. The renormalized models and their VEP

In summary, renormalization of the spinor field detector, model 4 in Table I, is achieved by coupling through the Hamiltonian

$$H_{\text{int}}(t) = \lambda \chi(t) \mu \int_{\mathbb{R}^n} p(\mathbf{x}(t), \mathbf{y}) : \bar{\Psi}(\mathbf{y}) \Psi(\mathbf{y}) : d\mathbf{y}. \quad (84)$$

Detector models 2 and 3 for real or complex fields are similarly renormalized by coupling through

$$H_{\text{int}}(t) = \lambda \chi(t) \mu \int_{\mathbb{R}^n} p(\mathbf{x}(t), \mathbf{y}) : \Phi^\dagger(\mathbf{y}) \Phi(\mathbf{y}) : d\mathbf{y}. \quad (85)$$

The vacuum response of the renormalized spinor field detector is obtained by dropping the first term in Eq. (56):

$$P_{0,g \rightarrow e} = \lambda^2 \sum_{\mathbf{k}, \mathbf{s}} \sum_{\mathbf{p}, \mathbf{r}} \left| \int_{\mathbb{R}^n} p(\mathbf{x}_0, \mathbf{y}) \bar{\psi}_{\mathbf{k}, \mathbf{s}, +}(\mathbf{y}) \psi_{\mathbf{p}, \mathbf{r}, -}(\mathbf{y}) d\mathbf{y} \right|^2 \times \left| \int_{-\infty}^{+\infty} \chi(t) e^{i(\Omega + \omega_{\mathbf{k}} + \omega_{\mathbf{p}})t} dt \right|^2. \quad (86)$$

Explicitly, for periodic boundary conditions:

$$P_{0,g \rightarrow e} = \frac{\lambda^2}{2L^{2n}} \sum_{\mathbf{k}, \mathbf{p}} \frac{(\omega_{\mathbf{k}} + m)(\omega_{\mathbf{p}} + m)}{\omega_{\mathbf{k}} \omega_{\mathbf{p}}} \left(\frac{\mathbf{k}}{\omega_{\mathbf{k}} + m} - \frac{\mathbf{p}}{\omega_{\mathbf{p}} + m} \right)^2 \times \left| \int_{\mathbb{R}^n} p(\mathbf{x}_0, \mathbf{y}) e^{-i(\mathbf{k} + \mathbf{p})\mathbf{y}} d\mathbf{y} \right|^2 \times \left| \int_{-\infty}^{+\infty} \chi(t) e^{i(\Omega + \omega_{\mathbf{k}} + \omega_{\mathbf{p}})t} dt \right|^2. \quad (87)$$

Similarly, the leading-order vacuum response of the renormalized real and complex field detector becomes

$$P_{0,g \rightarrow e} = \frac{\lambda^2}{4} \sum_{\mathbf{k}, \mathbf{p}} \frac{1}{\omega_{\mathbf{k}} \omega_{\mathbf{p}}} \left| \int_{\mathbb{R}^n} p(\mathbf{x}_0, \mathbf{y}) \varphi_{\mathbf{k}}^*(\mathbf{y}) \varphi_{\mathbf{p}}^*(\mathbf{y}) d\mathbf{y} \right|^2 \times \left| \int_{-\infty}^{+\infty} \chi(t) e^{i(\Omega + \omega_{\mathbf{k}} + \omega_{\mathbf{p}})t} dt \right|^2, \quad (88)$$

or explicitly

$$P_{0,g \rightarrow e} = \frac{\lambda^2}{4L^{2n}} \sum_{\mathbf{k}, \mathbf{p}} \frac{1}{\omega_{\mathbf{k}} \omega_{\mathbf{p}}} \left| \int_{\mathbb{R}^n} p(\mathbf{x}_0, \mathbf{y}) e^{-i(\mathbf{k} + \mathbf{p})\mathbf{y}} d\mathbf{y} \right|^2 \times \left| \int_{-\infty}^{+\infty} \chi(t) e^{i(\Omega + \omega_{\mathbf{k}} + \omega_{\mathbf{p}})t} dt \right|^2 \quad (89)$$

by dropping the first term from Eqs. (60) and (61).

As will be demonstrated in the next section, the VEPs Eqs. (87) and (89) may still be divergent even after this renormalization and further regularization of the VEP is necessary. Recall that the VEP of detector model 1 coupling to a quantized scalar field could be rewritten in terms of the Fourier transform of its spacetime profile f in Eq. (52). The same is possible for the quadratically coupling detectors: using the Fourier transformation Eq. (53), the VEP Eq. (89) for quantized scalar fields can be rewritten as

$$P_{0,g \rightarrow e} = \frac{\lambda^2}{4L^{2n}} \sum_{\mathbf{k}, \mathbf{p}} \frac{1}{\omega_{\mathbf{k}} \omega_{\mathbf{p}}} \left| \tilde{f}(-d - \mathbf{k} - \mathbf{p}) \right|^2. \quad (90)$$

The probability in the case of Eq. (87) is

$$P_{0,g \rightarrow e} = \frac{\lambda^2}{2L^{2n}} \sum_{\mathbf{k}, \mathbf{p}} \frac{(\omega_{\mathbf{k}} + m)(\omega_{\mathbf{p}} + m)}{\omega_{\mathbf{k}} \omega_{\mathbf{p}}} \times \left(\frac{\mathbf{k}}{\omega_{\mathbf{k}} + m} - \frac{\mathbf{p}}{\omega_{\mathbf{p}} + m} \right)^2 \left| \tilde{f}(-d - \mathbf{k} - \mathbf{p}) \right|^2. \quad (91)$$

Thus, the UV behavior of its Fourier transform again decides which spacetime profile f is suitable for regularization. Note that the prefactor in front of the \tilde{f} decays faster in the UV for quantized scalar fields than for quantized spinor fields. This means that spinor field detectors require a “stronger” regularization.

V. COMPARISON OF PARTICLE DETECTOR MODELS

So far, we have discussed how to obtain a finite vacuum response through renormalization and regularization for four different detector models. We will now investigate whether any of the three scalar field detector models (1, 2 and 3 in Table I) is comparable to the spinor field detector, in the sense that a comparison of their respective responses offers insight into the properties of the field they probe.

For the different models considered, the relevant features that can have a significant impact on the response of UDW-type detectors for quantized scalar and spinor fields are

1. The nature of the coupling: linear versus quadratic.
2. Internal degrees of freedom of the field: for example, the $U(1)$ charge.
3. The field statistics: bosonic or fermionic.
4. The analytic structure of the field: scalar or spinorial.

From the results obtained in the previous sections, we discuss below each of these points individually.

A. Linear vs quadratic coupling

The coupling has a profound influence on the response of an UDW-type detector: The vacuum response of model 1—i.e. coupling linearly to a quantized real field—given in Eq. (33), is fundamentally different from the response [Eq. (88)] of model 2 to the same field when using the (renormalized) quadratic coupling of Eq. (85). In order to assess the differences between the response of detectors to fermionic (spinor) fields and bosonic (scalar) fields, we will now compare models 2 to 4 that couple to the same power of the fields.

B. Charged vs uncharged field

Quadratic coupling to quantized scalar fields gives the same VEP Eq. (88) for uncharged (i.e. real) and charged

(i.e. complex) quantized scalar fields to leading order in perturbation theory. However, as we shall see in Sec. VIII, the detector response is not identical in general; the field charge does have an influence. Since spinor fields are generally charged, one should always use a charged scalar field when comparing quantized scalar fields with quantized spinor fields in order to single out effects coming exclusively from the field statistics or analytic structure. In other words, only model 3 and model 4 can be rightfully compared.

C. Boson vs fermion statistics

The statistics of the probed field influence the reaction of an UDW-type detector in two ways. First of all, the Pauli exclusion principle will prevent the creation of more than one quantum of a given charge, momentum and spin in a fermionic field. This restricts the set of possible processes that, for example, excite the detector. This would not be the case for bosonic fields. Secondly, the anticommutation of fermionic operators implies that two distinct processes leading to the same final state may have a relative minus sign in their amplitudes. Fermionic fields, unlike bosonic fields, can therefore have cancellations between amplitudes.

Nevertheless, the field statistics do not influence the VEP of the four detector models discussed here at leading order: merely a single quantum (linear coupling), or at most a particle-antiparticle pair (quadratic coupling) is created from the vacuum of the field, so the Pauli exclusion principle has no effect. And since there is only one possible process contributing to the VEP, no cancellation between different processes occurs. This implies that the leading order VEP remains unaffected by the field statistics.

As soon as the field is initially not in its vacuum state, however, the Pauli exclusion principle does affect the response of a particle detector to a fermionic field. And even for the VEP, the exclusion principle and different sign amplitude interference will be relevant at higher orders in perturbation theory. Interestingly, in dimensions larger than two, the spin-statistics theorem ties together field statistics and the spin of a field (which is reflected in its analytic structure). This makes it generally hard to distinguish the effect of the analytic structure and the effect of field statistics. In the leading order vacuum response, however, due to the uniqueness of the leading order VEP described above, it is possible to independently study the effect of the spinor structure versus a scalar structure.

D. Scalar vs spinor field

Comparing Eqs. (86) and (88), one finds that the VEP of model 3 has summands proportional to

$$\begin{aligned} &\propto \frac{1}{4\omega_{\mathbf{k}}\omega_{\mathbf{p}}} \left| \int_{\mathbb{R}^n} p(\mathbf{x}_0, \mathbf{y}) \varphi_{\mathbf{k}}^*(\mathbf{y}) \varphi_{\mathbf{p}}^*(\mathbf{y}) d\mathbf{y} \right|^2 \\ &= \left| \int_{\mathbb{R}^n} p(\mathbf{x}_0, \mathbf{y}) \tilde{\varphi}_{\mathbf{k}}^*(t, \mathbf{y}) \tilde{\varphi}_{\mathbf{p}}^*(t, \mathbf{y}) d\mathbf{y} \right|^2, \end{aligned} \quad (92)$$

while the VEP of the spinor field detector, model 4, has summands proportional to

$$\begin{aligned} &\propto \sum_{s,r} \left| \int_{\mathbb{R}^n} p(\mathbf{x}_0, \mathbf{y}) \bar{\psi}_{\mathbf{k},s,+}(\mathbf{y}) \psi_{\mathbf{p},r,-}(\mathbf{y}) d\mathbf{y} \right|^2 \\ &= \sum_{s,r} \left| \int_{\mathbb{R}^n} p(\mathbf{x}_0, \mathbf{y}) \tilde{\psi}_{\mathbf{k},s,+}(t, \mathbf{y}) \gamma^0 \tilde{\psi}_{\mathbf{p},r,-}(t, \mathbf{y}) d\mathbf{y} \right|^2. \end{aligned} \quad (93)$$

The sum over all spins in the second expression is, of course, not present in the first one for quantized scalar fields. The factor $(4\omega_{\mathbf{k}}\omega_{\mathbf{p}})^{-1}$ in the first expression is simply part of the normalization factor of the scalar mode functions Eq. (A5). This can be made explicit by rewriting both of the above expressions in terms of the full, time-dependent mode functions Eqs. (A5) and (A25) (at arbitrary time t). In this form, it is obvious that the *only* difference between the VEP for scalar and spinor fields is due to the different mode functions.

So does it make any difference at all whether the detector is coupled to a quantized scalar or a spinor field? The answer is yes: Comparing the VEPs Eq. (90) and Eq. (91) at the end of the previous chapter, we found that quantized scalar fields are better behaved for large frequencies since the UV behavior of the mode functions is different; the scalar mode functions generally have a factor $\sim (\omega_{\mathbf{k}})^{-1/2}$ which the spinor mode functions do not: As a simple example, compare the mode functions of massless fields in $(1, 1)$ dimensions: For the quantized (real or complex) scalar field, the particle and antiparticle mode functions are

$$\tilde{\varphi}_{\mathbf{k},\epsilon}^*(t, x) = \frac{1}{\sqrt{2|k|L}} e^{+i|k|t} e^{-ikx} \quad (94)$$

[see Appendix A, Eqs. (A10), (A12) and (A17)], while the corresponding spinor mode functions for particles and antiparticles (in this order) are

$$\begin{aligned} \tilde{\psi}_{\mathbf{k},s,+}^\dagger(t, x) &= \frac{1}{\sqrt{2L}} \left[\begin{array}{c} \xi_s \\ \text{sgn}(k) \sigma^3 \xi_s \end{array} \right]^\dagger e^{+i|k|t} e^{-ikx} \\ \tilde{\psi}_{\mathbf{k},s,-}(t, x) &= \frac{1}{\sqrt{2L}} \left[\begin{array}{c} \text{sgn}(k) \sigma^3 \xi_s \\ \xi_s \end{array} \right] e^{+i|k|t} e^{-ikx} \end{aligned} \quad (95)$$

[see Appendix A, Eqs. (A25), (A45), (A53) and (A58)]. The spinorial parts do not scale with k , while the scalar field has an additional factor $|k|^{-1} = \omega_{\mathbf{k}}^{-1}$.

This difference has notable implications: it causes the quantized scalar fields to exhibit better convergence properties when summing over all momenta—the VEP for detectors coupling quadratically to quantized scalar fields—Eq. (90)—will in general converge better than the VEP for detectors coupling quadratically to quantized spinor fields—Eq. (91). This is a dramatic difference. For instance, there are switching functions and spatial profiles that give a finite VEP for a detector quadratically coupled to a quantized scalar field but yield a divergent VEP for quantized spinor fields. In Sec. V E, examples where this situation actually occurs are discussed.

Superficially, the different normalization conditions, stemming from a mathematically different inner product, are the reason for this difference: The scalar mode functions are orthonormal with respect to

$$\begin{aligned} (\tilde{\varphi}_{\mathbf{k}}, \tilde{\varphi}_{\mathbf{p}}) &\equiv \\ -i \int_B \tilde{\varphi}_{\mathbf{k}}(x) [\partial_0 \tilde{\varphi}_{\mathbf{p}}^*(x)] - [\partial_0 \tilde{\varphi}_{\mathbf{k}}(x)] \tilde{\varphi}_{\mathbf{p}}^*(x) dx & \\ &= \delta_{\mathbf{k}, \mathbf{p}}, \end{aligned} \quad (96)$$

while the spinor mode functions are normalized according to

$$\begin{aligned} \langle \tilde{\psi}_{\mathbf{k}, s, \epsilon}, \tilde{\psi}_{\mathbf{p}, r, \delta} \rangle &\equiv \\ \int_B \tilde{\psi}_{\mathbf{k}, s, \epsilon}^\dagger(x) \tilde{\psi}_{\mathbf{p}, r, \delta}(x) dx &= \delta_{\mathbf{k}, \mathbf{p}} \delta_{s, r} \delta_{\epsilon, \delta}. \end{aligned} \quad (97)$$

The additional time derivative in the product for scalar functions generates a factor $\omega_{\mathbf{k}}$. Thus, the normalization factor of the scalar fields contains an additional factor $(\omega_{\mathbf{k}})^{-1/2}$ compared to the normalization of the spinor fields.

Ultimately, the reason is that the equation of motion of scalar fields, the Klein-Gordon equation, is of second order and features a double time derivative, while the equation of motion of the spinor field, the Dirac equation, is of first order, containing only a single time derivative (see Appendix B).

In order to demonstrate the influence this has on the response of the different detector models, we compare their VEPs in three simple examples on (1, 1) dimensional Minkowski spacetime for massless fields: (1) sudden switching with a pointlike detector, (2) Gaussian switching with a pointlike detector, and (3) sudden switching with a Gaussian detector profile.

E. Examples in (1,1) dimensions

Let us start by recalling the general expressions for the massless (1,1) dimension scenario. For model 3 in Table I (quadratic coupling quantized scalar field detector), the VEP Eq. (89) simplifies in (1, 1) dimensions and for

massless fields to

$$\begin{aligned} P_{0, g \rightarrow e} &= \frac{\lambda^2}{4L^2} \sum_{k, p \neq 0} \frac{1}{|kp|} \left| \int_{-\infty}^{\infty} p(x_0, y) e^{-i(k+p)y} dy \right|^2 \\ &\times \left| \int_{-\infty}^{+\infty} \chi(t) e^{i(\Omega+|k|+|p|)t} dt \right|^2. \end{aligned} \quad (98)$$

On the other hand, for the spinor field detector (model 4 in Table I), one similarly obtains

$$\begin{aligned} P_{0, g \rightarrow e} &= \frac{2\lambda^2}{L^2} \sum_{k, p > 0} \left[\left| \int_{-\infty}^{\infty} p(x_0, y) e^{-i(k-p)y} dy \right|^2 \right. \\ &+ \left. \left| \int_{-\infty}^{\infty} p(x_0, y) e^{-i(p-k)y} dy \right|^2 \right] \left| \int_{-\infty}^{+\infty} \chi(t) e^{i(\Omega+k+p)t} dt \right|^2, \end{aligned} \quad (99)$$

directly from Eq. (86) by plugging in the mode functions and spinors Eqs. (A45) and (A53).

1. Sudden switching and pointlike detector

In the most basic scenario, the detector is pointlike [delta spatial profile as given in Eq. (36)], and it is suddenly coupled to the field as given in Eq. (37). This is the same situation that was considered in Sec. III A 2 for the case of a quantized real field with linear coupling (model 1).

Quantized scalar field.— Plugging Eqs. (36) and (37) in Eq. (98), the resulting VEP for the quantized scalar field is

$$\begin{aligned} P_{0, g \rightarrow e} &= \frac{\lambda^2 L^2}{4\pi^4} \sum_{l_1=1}^{\infty} \sum_{l_2=1}^{\infty} \frac{1}{l_1 l_2 \left(\frac{\Omega L}{2\pi} + l_1 + l_2\right)^2} \\ &\times \sin^2 \left[\frac{\pi}{L} \left(\frac{\Omega L}{2\pi} + l_1 + l_2\right) T \right] \end{aligned} \quad (100)$$

This double sum is convergent: we can estimate

$$\frac{4\pi^4}{\lambda^2 L^2} P_{0, g \rightarrow e} \leq \sum_{l_1=1}^{\infty} \sum_{l_2=1}^{\infty} \frac{1}{l_1 l_2 (l_1 + l_2)^2}.$$

The sums on the right-hand side converge if and only if

$$S = \sum_{l_1=2}^{\infty} \sum_{l_2=2}^{\infty} \frac{1}{l_1 l_2 (l_1 + l_2)^2}$$

does, where the summation starts at 2 instead of 1. We can now exploit that $l_1 l_2 \geq l_1 + l_2$ for all $l_i \geq 2$ to find the upper bound

$$S \leq \sum_{l_1=2}^{\infty} \sum_{l_2=2}^{\infty} \frac{1}{(l_1 + l_2)^3},$$

where the sum on the right-hand side is convergent.

Quantized spinor field.— The formal expression for the VEP in case of a quantized spinor field is obtained by plugging Eqs. (36) and (37) in Eq. (99):

$$P_{0,g \rightarrow e} = \frac{4\lambda^2}{\pi^2} \sum_{l_1=1}^{\infty} \sum_{l_2=1}^{\infty} \frac{1}{\left(\frac{\Omega L}{2\pi} + l_1 + l_2\right)^2} \times \sin^2 \left[\frac{\pi}{L} \left(\frac{\Omega L}{2\pi} + l_1 + l_2 \right) T \right]. \quad (101)$$

Similar to Eq. (43), it is easy to prove that this sum converges if and only if

$$\sum_{l_1=1}^{\infty} \sum_{l_2=1}^{\infty} \frac{1}{\left(\frac{\Omega L}{2\pi} + l_1 + l_2\right)^2}$$

does. However, this sum diverges, since the corresponding integral is ill defined:

$$\int_1^{\infty} dl_1 \int_1^{\infty} dl_2 \frac{1}{(A + l_1 + l_2)^2} = \lim_{a \rightarrow \infty} \ln(a) - \ln(2 + A) \rightarrow \infty.$$

Thus, the VEP Eq. (101) is divergent.

This result nicely illustrates that the detector response to quantized scalar fields is better behaved in the UV: On one hand, all the scalar fields detectors (models 1-3) have a finite VEP in (1, 1) dimensions, even if the detector is simply pointlike and uses sudden switching [see Eqs. (40) and (100)]. On the other hand, in the case of a quantized spinor field the VEP is already divergent in (1, 1) dimensions for this spacetime profile.

2. Gaussian switching and pointlike detector

It was demonstrated in Sec. III A 3 that the original UDW detector (model 1), which has a divergent VEP in dimensions (1, n) for $n \geq 3$, can be regularized by introducing a Gaussian switching function Eq. (45) of width T . We can prove that Gaussian switching also regularizes the spinor field detector, model 4, in (1, 1) dimensions.

Quantized spinor field.— Inserting Eq. (45) in Eq. (99), the VEP for a spinor field reads

$$P_{0,g \rightarrow e} = \frac{8\pi T^2 \lambda^2}{L^2} \sum_{l_1=1}^{\infty} \sum_{l_2=1}^{\infty} e^{-\frac{4\pi^2 T^2}{L^2} \left(\frac{\Omega L}{2\pi} + l_1 + l_2\right)^2}. \quad (102)$$

This excitation probability is now clearly finite: the sum converges if and only if

$$\int_1^{\infty} dl_1 \int_1^{\infty} dl_2 e^{-A(B+l_1+l_2)^2}$$

does, where $A = 4\pi^2 T^2 L^{-2}$ and $B = \Omega L (2\pi)^{-1}$, and the latter expression is bounded from above by

$$\int_1^{\infty} dl_1 e^{-Al_1^2} \int_1^{\infty} dl_2 e^{-Al_2^2} = \frac{\pi}{A}.$$

Quantized scalar field.— For model 3, the same switching function yields

$$P_{0,g \rightarrow e} = \frac{T^2 \lambda^2}{2\pi} \sum_{l_1=1}^{\infty} \sum_{l_2=1}^{\infty} \frac{1}{l_1 l_2} e^{-\frac{4\pi^2 T^2}{L^2} \left(\frac{\Omega L}{2\pi} + l_1 + l_2\right)^2} \quad (103)$$

which is of course also finite since the summand decays faster than in Eq. (102) [and the VEP had been convergent in Eq. (100) even without regularization].

Note that for both field types, $P_{0,g \rightarrow e} \rightarrow 0$ in the adiabatic limit $T \rightarrow \infty$, just like for the linear coupling in Eq. (47).

3. Sudden switching and Gaussian detector profile

The third example discussed in Sec. III A 3 for model 1 demonstrated regularization through a Gaussian detector profile Eq. (49) with variance $\sigma > 0$ and sudden switching. We repeat the example in the present case.

Quantized spinor field.— In case of the quantized spinor field, the probability is

$$P_{0,g \rightarrow e} = \frac{4\lambda^2}{\pi^2} \sum_{l_1=1}^{\infty} \sum_{l_2=1}^{\infty} \frac{e^{-\frac{4\pi^2 \sigma^2}{L^2} (l_1 - l_2)^2}}{\left(\frac{\Omega L}{2\pi} + l_1 + l_2\right)^2} \times \sin^2 \left[\frac{\pi}{L} \left(\frac{\Omega L}{2\pi} + l_1 + l_2 \right) T \right] \quad (104)$$

and convergence is harder to assess than for the Gaussian switching function in Eq. (102): the sine squared is positive, bounded from above by 1 and can thus be ignored. For $l_1 = l_2$, the exponential factor is always 1, but then the denominator decays as l_1^{-2} ; as it happens, this is just fast enough. As a first step, we can estimate

$$\frac{\pi^2}{4\lambda^2} P_{0,g \rightarrow e} \leq \sum_{l_1=1}^{\infty} \sum_{l_2=1}^{\infty} \frac{e^{-A(l_1 - l_2)^2}}{(l_1 + l_2)^2}$$

where $A = 4\pi^2 \sigma^2 L^{-2} > 0$. This sum converges if the corresponding integral

$$I = \int_{l_1=1}^{\infty} dl_1 \int_{l_2=1}^{\infty} dl_2 \frac{e^{-A(l_1 - l_2)^2}}{(l_1 + l_2)^2}$$

does. By substituting $l = l_2 - l_1$,

$$I = \int_{l_1=1}^{\infty} dl_1 \int_{l=1-l_1}^{\infty} dl \frac{e^{-Al^2}}{(l + 2l_1)^2}$$

and since for $l \geq 1 - l_1$ we have $(l + 2l_1)^{-2} < l_1^{-2}$:

$$\begin{aligned} I &< \int_{l_1=1}^{\infty} dl_1 \frac{1}{l_1^2} \int_{l=1-l_1}^{\infty} dl e^{-Al^2} \\ &\leq \int_{l_1=1}^{\infty} dl_1 \frac{1}{l_1^2} \int_{l=-\infty}^{\infty} dl e^{-Al^2} = \sqrt{\frac{\pi}{A}} < \infty. \end{aligned}$$

The VEP Eq. (104) is finite.

Quantized scalar field.— For the quantized scalar field, the probability

$$P_{0,g \rightarrow e} = \frac{\lambda^2 L^2}{8\pi^4} \times \sum_{l_1=1}^{\infty} \sum_{l_2=1}^{\infty} \frac{e^{-\frac{4\pi^2\sigma^2}{L^2}(l_1+l_2)^2} + e^{-\frac{4\pi^2\sigma^2}{L^2}(l_1-l_2)^2}}{l_1 l_2 \left(\frac{\Omega L}{2\pi} + l_1 + l_2\right)^2} \times \sin^2 \left[\frac{\pi}{L} \left(\frac{\Omega L}{2\pi} + l_1 + l_2 \right) T \right] \quad (105)$$

is once again convergent because Eq. (100) already was even without regularization.

Again, $P_{0,g \rightarrow e} \rightarrow 0$ for both fields if the detector is maximally delocalized by $\sigma \rightarrow \infty$.

F. Comparability of the models

From the analysis above we conclude that the differences in the response of models 3 and 4 are only due to the analytic structure of the fields and the field statistics.

The field statistics do not enter the leading order VEP, but will have a profound influence on the detector response at higher orders, or also at leading order if the field is initially not in the vacuum state. On the level of the analytic structure, model 4 is sensitive to the additional spin degree of freedom, and, more importantly, requires stronger regularization since it displays a worse-behaved UV response. Interestingly, it is not enough to regularize with a smooth switching function as opposed to the scalar case. Rather, the spinor model requires a spatial smearing in order to yield finite VEP.

Note that only a qualitative comparison is feasible. A naïve quantitative comparison fails because the coupling strength λ has different dimensions in model 3 and 4: Scalar fields on $(1, n)$ -dimensional spacetime have mass dimension $(n-1)/2$, while spinor fields have mass dimension $n/2$. To obtain a Hamiltonian of mass dimension 1, the respective coupling constants therefore need to be of different dimensions. A direct comparison is therefore only possible with regards to the functional dependence on model parameters like the detector trajectory $x(\tau)$, the detector gap Ω , and more concretely the interaction time T and the detector size σ . In this sense, the leading-order vacuum response of models 3 and 4 is equivalent in all (convergent) examples discussed in Sec. V E.

In conclusion, for finite size detectors after renormalization, the pair of models, model 3 (for quantized complex fields) and model 4 (for quantized spinor fields) can be used to reliably study the differences between fermionic and bosonic fields via particle detectors, at least at leading order in perturbation theory.

VI. COMPUTATION METHODS AT ARBITRARY ORDER

Up to now, the discussion was limited to the leading order in the coupling strength λ . However, potential applications of particle detectors will undoubtedly require calculations to higher orders in perturbation theory: some phenomena that have been investigated for quantized real fields using the original UDW detector, for example, rely on higher-order effects order (see Refs. [23, 46] among others). In preparation of investigations at higher orders, it will be convenient to derive a set of Feynman rules for each detector model. We will adhere to the following roadmap: In this section we develop the computation methods necessary to obtain Feynman rules. In Sec. VII, we will apply these methods to calculations up to second order in the transition amplitudes by way of example, and in Sec. VIII we will generalize the emerging pattern to Feynman rules.

It is to be expected that new divergencies appear at each order in perturbation theory. As in any quantum field theory, there are three sources of divergencies in transition probabilities of UDW-type detector models:

1. The amplitude of a single process can be infinite, as it was the case for the tadpolelike diagram in Fig. 1.
2. Finite amplitudes can still amount to a divergent transition probability of the detector when the field is traced out: the sum over all the ingoing and outgoing field configurations can diverge.
3. The perturbative series itself can diverge when taking into account all orders.

Notice, therefore, it is important to ascertain that those divergences can be regularized and renormalized away in order to be able to fully trust insights gained from using a particle detector model to describe the physics of a quantum field.

Example: vacuum no-response probability.— In order to show which quantities we are going to need to evaluate, let us first consider a transition probability which involves the second order term in the Dyson expansion Eq. (25). Every application of the monopole operator μ Eq. (12) to one of the two energy eigenstates of the detector switches it back and forth between ground state $|g\rangle$ and the excited state $|e\rangle$. In consequence, if the detector starts out in the ground state, only even orders in perturbation theory contribute to the probability for it to remain in the ground state, and only odd orders contribute to the probability for the detector to be excited. There are thus no corrections to the VEP coming from $U^{(2)}$ in Eqs. (25) and (26). Instead, we calculate the probability for the detector to *remain* in the ground state when interacting with a quantum field in the vacuum state, and call this probability the *vacuum no-response probability* (VNRP) $P_{0,g \rightarrow g}$.

Notice, however, that it would not be strictly necessary to go through the $U^{(2)}$ calculation in order to compute the VNRP: Since the same order perturbative corrections to the density matrix are traceless [5], it follows that

$P_{0,g \rightarrow g} = 1 - P_{0,g \rightarrow e}$. We will nevertheless compute it using $U^{(2)}$ to illustrate higher order techniques.

Let F be the probed quantum field, and $\rho(t_0) = |0, g\rangle\langle 0, g|$ the density matrix of the coupled system at starting time t_0 . The VNRP is the (g, g) component after tracing out the field:

$$P_{0,g \rightarrow g}(t, t_0) \equiv \langle g | \text{tr}_F \rho(t) | g \rangle = \sum_a |\langle a, g; t | U(t, t_0) | 0, g; t_0 \rangle|^2 \quad (106)$$

at time $t > t_0$. In the limit $t_0 \rightarrow -\infty$, $t \rightarrow \infty$, the actual duration of the interaction between detector and field is determined by the switching function χ . Using the perturbative expansion Eqs. (25) and (26), the VNRP can be written as

$$P_{0,g \rightarrow g}(t, t_0) = 1 + 2 \sum_a \left[\text{Re} \left(\mathcal{A}_{a,g}^{(0)} \mathcal{A}_{a,g}^{(2)} \right) \right] + \mathcal{O}(\lambda^4), \quad (107)$$

where the transition amplitudes at order n are

$$\mathcal{A}_{a,g}^{(n)} \equiv (-i\lambda)^n \langle a, g; t | U^{(n)}(t, t_0) | 0, g; t_0 \rangle, \quad (108)$$

The contribution at order zero is only nonzero for the final state $|0, g\rangle$ since $U^0 = \mathbf{1}$:

$$\mathcal{A}_{a,g}^{(0)} = \begin{cases} 1 & \text{for } a = 0 \\ 0 & \text{else} \end{cases}. \quad (109)$$

As we have argued earlier, order $n = 1$ does not contribute at all, $\mathcal{A}_{a,g}^{(1)} = 0$. Thus, only the amplitude at order $n = 2$,

$$\mathcal{A}_{a,g}^{(2)} = (-i)^2 \int_{t_0}^t dt_1 \int_{t_0}^t dt_2 \langle a, g; t | T H_{\text{int}}(t_1) H_{\text{int}}(t_2) | 0, g; t_0 \rangle, \quad (110)$$

remains to be evaluated to obtain the VNRP.

As an example, consider the renormalized detector model 3 for quantized complex fields with interaction Hamiltonian Eq. (85). The second order correction is

$$\begin{aligned} \mathcal{A}_{\phi,g}^{(2)} &= (-i\lambda)^2 e^{-i\omega_\phi t} \\ &\times \int_{t_0}^t dt_1 \int_{t_0}^t dt_2 \chi(t_1) \chi(t_2) \langle g | T \mu(t_1) \mu(t_2) | g \rangle \\ &\times \int_{\mathbb{R}^n} d\mathbf{y}_1 \int_{\mathbb{R}^n} d\mathbf{y}_2 p(\mathbf{x}_0, \mathbf{y}_1) p(\mathbf{x}_0, \mathbf{y}_2) \\ &\times \langle \phi | T : \Phi^\dagger(y_1) \Phi(y_1) :: \Phi^\dagger(y_2) \Phi(y_2) : | 0 \rangle. \end{aligned} \quad (111)$$

The main difficulty now rests in evaluating the time-ordered expectation values

$$\langle g | T \mu(t_1) \mu(t_2) | g \rangle \quad (112)$$

and

$$\langle \phi | T : \Phi^\dagger(y_1) \Phi(y_1) :: \Phi^\dagger(y_2) \Phi(y_2) : | 0 \rangle. \quad (113)$$

Higher orders.— Generalizing the above example to order n and arbitrary initial and final states, we need to evaluate expressions of the form

$$\langle g | [\sigma^-]^a [T \mu(t_1) \cdots \mu(t_n)] [\sigma^+]^b | g \rangle \quad (114)$$

for the detector, where $a, b \in \{0, 1\}$ to allow for initial and final states $|g\rangle$ and $|e\rangle$. Similarly, for model 1 and quantized real fields we need to calculate

$$\langle 0 | (a_{\mathbf{p}})_{\mathbf{p}} [T \Phi(y_1) \cdots \Phi(y_n)] (a_{\mathbf{k}}^\dagger)_{\mathbf{k}} | 0 \rangle, \quad (115)$$

where $(a_{\mathbf{k}}^\dagger)_{\mathbf{k}} \equiv a_{\mathbf{k}_1}^\dagger \cdots a_{\mathbf{k}_N}^\dagger$ is an arbitrary product of creation operators [such as, e.g., $(a_{\mathbf{k}}^\dagger)_{\mathbf{k}} = a_{\mathbf{k}_1}^\dagger a_{\mathbf{k}_2}^\dagger a_{\mathbf{k}_3}^\dagger a_{\mathbf{k}_1}^\dagger$ or $(a_{\mathbf{k}}^\dagger)_{\mathbf{k}} = \mathbf{1}$] allowing for arbitrary number eigenstates content in the initial state, and $(a_{\mathbf{p}})_{\mathbf{p}}$ are annihilation operators for arbitrary final states. In case of model 3 (for quantized complex fields), we need

$$\begin{aligned} \langle 0 | (a_{\mathbf{p}})_{\mathbf{p}} (b_{\bar{\mathbf{p}}})_{\bar{\mathbf{p}}} [T : \Phi^\dagger(y_1) \Phi(y_1) : \cdots \\ \cdots : \Phi^\dagger(y_n) \Phi(y_n) :] (a_{\mathbf{k}}^\dagger)_{\mathbf{k}} (b_{\bar{\mathbf{k}}}^\dagger)_{\bar{\mathbf{k}}} | 0 \rangle \end{aligned} \quad (116)$$

and in the case of model 2 (for quantized real fields), the previous expression simplifies because the field is self-adjoint, $\Phi^\dagger = \Phi$, and there is only one type of ladder operators. Finally, for model 4 coupling to quantized spinor fields expressions of the form

$$\begin{aligned} \langle 0 | (a_{\mathbf{p},r})_{\mathbf{p},r} (b_{\bar{\mathbf{p}},\bar{r}})_{\bar{\mathbf{p}},\bar{r}} [T : \bar{\Psi}(y_1) \Psi(y_1) : \cdots \\ \cdots : \bar{\Psi}(y_n) \Psi(y_n) :] (a_{\mathbf{k},s}^\dagger)_{\mathbf{k},s} (b_{\bar{\mathbf{k}},\bar{s}}^\dagger)_{\bar{\mathbf{k}},\bar{s}} | 0 \rangle \end{aligned} \quad (117)$$

appear.

In short, we need to evaluate the vacuum expectation value of time-ordered products of field operators, which may contain normal-ordered subproducts, with a prepended product of annihilation operators and an appended product of creation operators. Since the field operators and the monopole operator are essentially sums of ladder operators as well, a good strategy is to normal-order the entire product by successively commuting (or anticommuting) ladder operators. This procedure will furnish us with variants of *Wick's theorem*. Moreover, the presence of the time-ordering symbol leads to the appearance of *Feynman propagators* instead of ordinary commutators. This approach is closely related to standard techniques in elementary particle physics, where elements of the scattering matrix S are computed to obtain probabilistic predictions about the outcome of scattering experiments. There, the Lehmann-Symanzik-Zimmermann reduction formula similarly allows one to express elements of S in terms of vacuum expectation values of products of time-ordered fields [43, 47].

Time- and normal-ordering.— Let us briefly revise the definition of time-ordering and normal-ordering for bosonic and fermionic fields. In the bosonic case, the time-ordering symbol is defined as

$$\begin{aligned} T \Phi(x) \Phi(y) \\ = \Theta(x^0 - y^0) \Phi(x) \Phi(y) + \Theta(y^0 - x^0) \Phi(y) \Phi(x). \end{aligned} \quad (118)$$

In particular, exchanging two operators inside a time-ordered expression does not engender any change:

$$T\Phi(x)\Phi(y) = T\Phi(y)\Phi(x) . \quad (119)$$

Normal-ordering is achieved by moving all annihilation operators to the right:

$$:a_{\mathbf{k}}a_{\mathbf{p}}^\dagger: = a_{\mathbf{p}}^\dagger a_{\mathbf{k}} , \quad :a_{\mathbf{p}}^\dagger a_{\mathbf{k}}: = a_{\mathbf{p}}^\dagger a_{\mathbf{k}} . \quad (120)$$

For fermionic fields, however,

$$\begin{aligned} T\Psi(x)\Psi(y) \\ = \Theta(x^0 - y^0)\Psi(x)\Psi(y) - \Theta(y^0 - x^0)\Psi(y)\Psi(x) \end{aligned} \quad (121)$$

so exchanging two fields introduces an additional sign

$$T\Psi(x)\Psi(y) = -T\Psi(y)\Psi(x) . \quad (122)$$

Similarly, a sign is introduced when exchanging ladder operators in normal-ordering:

$$:a_{\mathbf{k},s}a_{\mathbf{p},r}^\dagger: = -a_{\mathbf{p},r}^\dagger a_{\mathbf{k},s} , \quad :a_{\mathbf{p},r}^\dagger a_{\mathbf{k},s}: = a_{\mathbf{p},r}^\dagger a_{\mathbf{k},s} . \quad (123)$$

A. The monopole moment as a field

A two-level particle detector is, in a way, a fermionic system: the ladder operators Eq. (6) of the monopole operator satisfy the anticommutation relations

$$\{\sigma^+, \sigma^+\} = 0 , \quad \{\sigma^+, \sigma^-\} = \mathbf{1} , \quad \{\sigma^-, \sigma^-\} = 0 . \quad (124)$$

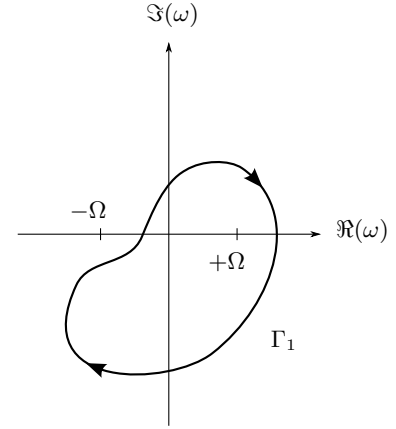
By comparison with the ladder operators of the quantized spinor field it is easy to see that, formally, σ^- , σ^+ correspond to the ladder operators of a fermionic field which (1) has only one mode, (2) does not have spin degrees of freedom, and (3) has particle modes which are their own antiparticles. The analogy extends to the monopole operator: in the Heisenberg picture,

$$\mu(t) = \sigma^+ e^{+i\Omega t} + \sigma^- e^{-i\Omega t} , \quad (125)$$

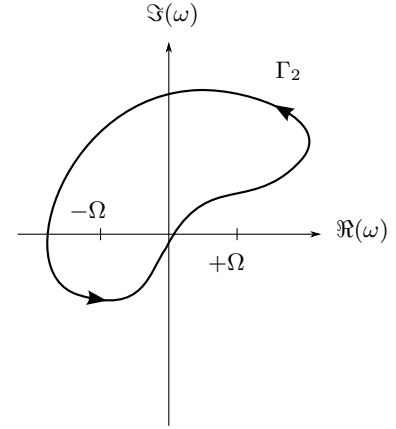
which can be seen as a simplification of the mode expansion of the quantized spinor field Eq. (A58). In the following, we will therefore regard the monopole operator as a fermionic quantum field $\mu(x) = \mu(t, \mathbf{x}) \equiv \mu(t)$ on $(1, n)$ -dimensional Minkowski spacetime which is constant in space, rather than as an observable of a system in first quantization. The time-evolution of this field is described by a Klein-Gordon equation: from Eq. (125) immediately follows $(\partial_t^2 + \Omega^2)\mu(t) = 0$, which can be rewritten as

$$(\square + \Omega^2)\mu(x) = 0 \quad (126)$$

since $\Delta\mu(x) = 0$. While this field is defined on the entire spacetime, it interacts with the quantum field only for a limited time and in a certain place, according to the detector's spacetime profile f .



(a) Contour in eq. (130).



(b) Contour in eq. (131).

Figure 3. Curves for the complex contour integrations in Eqs. (130) and (131).

In terms of particle number eigenstates, this field is very simple: since there is only one mode, no spin quantum numbers and no distinct antiparticles, there can at most be one quantum; excitation of more quanta is forbidden by the Pauli exclusion principle. The two particle number eigenstates are simply the two energy eigenstates of the detector: the ground state $|g\rangle$ for no quantum, the excited state $|e\rangle$ for one quantum. The detector behaves as a sort of completely delocalized Grassman scalar [31, 48, 49].

B. Feynman propagators

Deriving the Feynman propagator D_F of the UDW-type detector (or, more precisely, its monopole moment) runs analogously to the derivation of the Feynman propagator S_F of the quantized spinor field. We will treat the detector first, and generalize to the well-known Feynman propagators of the other fields for the sake of completeness.

1. UDW-type detector

The Feynman propagator of the UDW-type detector is defined as the time-ordered vacuum expectation value

$$D_F(t, s) \equiv \langle g|T\mu(t)\mu(s)|g\rangle, \quad (127)$$

the resulting two 2-point correlators are

$$D_F(t, s) \equiv D_F(t-s) = \begin{cases} e^{-i\Omega(t-s)} & \text{for } t > s \\ -e^{+i\Omega(t-s)} & \text{for } t < s \end{cases}. \quad (128)$$

Note that $D_F(0)$ is ill defined, since $D_F \rightarrow \pm 1$, depending on whether $t < s$ or $t > s$. For $t \neq s$, we may simply express the Feynman propagator using the step function Θ as

$$D_F(t, s) = \Theta(t-s)e^{-i\Omega(t-s)} - \Theta(s-t)e^{+i\Omega(t-s)}. \quad (129)$$

This form of the Feynman propagator has the disadvantage that the exponential factor switches signs depending on which time is larger—in calculations of transition probabilities, one would therefore not end up with the Fourier transform of the spacetime profile f when integrating over all times in the Feynman rules later on. It is therefore useful to rewrite the expression using a complex contour integral (as it is usually for the Feynman propagator of a quantum field [47]). The two cases of time-ordering are then implemented as two different contours.

By the residue theorem, we can rewrite

$$e^{-i\Omega(t-s)} = 2\Omega \oint_{\Gamma_1} \frac{d\omega}{2\pi} \frac{i}{(\omega - \Omega)(\omega + \Omega)} e^{-i\omega(t-s)}, \quad (130)$$

where the curve Γ_1 is given in the first part of Fig. 3 and encloses the pole at $\omega = +\Omega$. Similarly,

$$e^{+i\Omega(t-s)} = 2\Omega \oint_{\Gamma_2} \frac{d\omega}{2\pi} \frac{i}{(\omega - \Omega)(\omega + \Omega)} e^{-i\omega(t-s)} \quad (131)$$

for Γ_2 as shown in the second part of Fig. 3, enclosing the pole at $\omega = -\Omega$. In order to be able to integrate along the real axis, we shift the poles off the axis by $\pm i\epsilon$ and straighten out the curves as shown in Fig. 4. After the evaluation of the integrals, we will take the limit $\epsilon \rightarrow 0$. Since $\Gamma'_1 = \Gamma(r) \cup \Gamma_1(r)$ and $\Gamma'_2 = \Gamma(r) \cup \Gamma_2(r)$ as drawn in Fig. 4, the integral over each of the entire closed curves can be split into two integrals. In the limit $r \rightarrow \infty$, the first integral simply turns into an integral over the entire real line. The second one, on the other hand, evaluates to zero in both cases:

$$\begin{aligned} \Theta(t-s)e^{-i\Omega(t-s)} &= \Theta(t-s) \lim_{\epsilon \rightarrow 0} 2\Omega \\ &\int_{-\infty}^{\infty} \frac{d\omega}{2\pi} \frac{i}{(\omega - \Omega + i\epsilon)(\omega + \Omega - i\epsilon)} e^{-i\omega(t-s)} \end{aligned} \quad (132)$$

and

$$\begin{aligned} \Theta(s-t)e^{+i\Omega(t-s)} &= \Theta(s-t) \lim_{\epsilon \rightarrow 0} 2\Omega \\ &\int_{-\infty}^{\infty} \frac{d\omega}{2\pi} \frac{i}{(\omega - \Omega + i\epsilon)(\omega + \Omega - i\epsilon)} e^{-i\omega(t-s)}. \end{aligned} \quad (133)$$

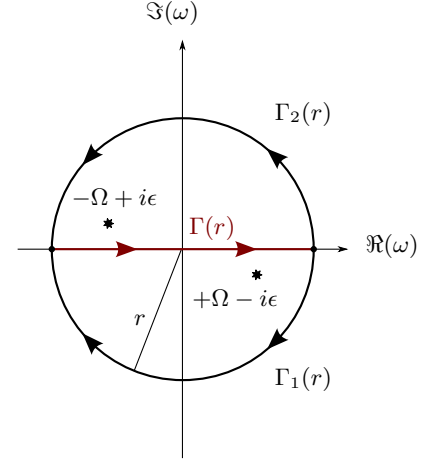


Figure 4. Curves for the complex contour integration in Eqs. (132) and (133).

By introducing time derivatives

$$e^{-i\Omega(t-s)} = \frac{i\partial_t}{\Omega} e^{-i\Omega(t-s)}, \quad e^{+i\Omega(t-s)} = -\frac{i\partial_t}{\Omega} e^{+i\Omega(t-s)} \quad (134)$$

and evaluating them inside the integral, we obtain

$$\begin{aligned} D_F(t-s) &= \\ \lim_{\epsilon \rightarrow 0} 2 \int_{-\infty}^{\infty} \frac{d\omega}{2\pi} \frac{i\omega}{(\omega - \Omega + i\epsilon)(\omega + \Omega - i\epsilon)} e^{-i\omega(t-s)}. \end{aligned} \quad (135)$$

Since in the limit

$$\lim_{\epsilon \rightarrow 0} (\omega - \Omega + i\epsilon)(\omega + \Omega - i\epsilon) = \lim_{\delta \rightarrow 0} \omega^2 - \Omega^2 + i\delta, \quad (136)$$

the above expression is abridged in the usual way to

$$D_F(t-s) = \lim_{\epsilon \rightarrow 0} 2 \int_{-\infty}^{\infty} \frac{d\omega}{2\pi} \frac{i\omega}{\omega^2 - \Omega^2 + i\epsilon} e^{-i\omega(t-s)}. \quad (137)$$

If the arguments of the propagator are exchanged, a sign is picked up,

$$D_F(s-t) = -D_F(t-s), \quad (138)$$

since $T\mu(t)\mu(s) = -T\mu(s)\mu(t)$.

2. Quantized scalar field

Although well known in the literature, we repeat the definition of the Feynman propagator for quantized scalar fields:

$$G_F(x-y) \equiv \langle 0|T\Phi(x)\Phi^\dagger(y)|0\rangle. \quad (139)$$

It can be expressed as

$$G_F(x-y) = \lim_{\epsilon \rightarrow 0} \frac{1}{L^n} \sum_{\mathbf{k}} \int_{-\infty}^{\infty} \frac{dk^0}{2\pi} \frac{i}{k^2 - m^2 + i\epsilon} e^{-ik(x-y)}, \quad (140)$$

see, for example, Ref. [47]. Note that for $x = y$,

$$G_F(0) = \frac{1}{2L^n} \sum_{\mathbf{k}} \frac{1}{\omega_{\mathbf{k}}} \rightarrow \infty. \quad (141)$$

Unlike for the detector, no sign is picked up under exchange of the arguments:

$$G_F(x-y) = G_F(y-x). \quad (142)$$

3. Quantized spinor field

The Feynman propagator of the quantized spinor field is, by definition,

$$S_F(x-y)_B^A \equiv \langle 0 | T \Psi^A(x) \bar{\Psi}_B(y) | 0 \rangle, \quad (143)$$

and can be expressed as [47]

$$S_F(x-y)_B^A = \lim_{\epsilon \rightarrow 0} \frac{1}{L^n} \sum_{\mathbf{k}} \int_{-\infty}^{\infty} \frac{dk^0}{2\pi} \frac{i [k \cdot \gamma + m]_B^A}{k^2 - m^2 + i\epsilon} e^{-ik(x-y)}. \quad (144)$$

The above expression is valid in $(1, n)$ dimensions, for both $n = 1$ and $n = 3$; the massless case is correctly recovered by setting $m = 0$.

It is straightforward to check that the Feynman propagator diverges in the coincidence limit

$$S_F(0) \rightarrow \infty. \quad (145)$$

Unlike for the detector, where the exchange of the propagator's argument only produced a sign, there is no simple relation between $S_F(x-y)$ and $S_F(y-x)$:

$$\begin{aligned} S_F(y-x)_B^A &= \\ &= - \lim_{\epsilon \rightarrow 0} \frac{1}{L^n} \sum_{\mathbf{k}} \int_{-\infty}^{\infty} \frac{dk^0}{2\pi} \frac{i [k \cdot \gamma - m]_B^A}{k^2 - m^2 + i\epsilon} e^{-ik(x-y)}. \end{aligned} \quad (146)$$

C. Wick's theorem

In this section we will first address Wick's theorem for quantized scalar fields. Then, we will formulate the fermionic version of the theorem for spinor fields, and subsequently simplify it in order to arrive to the case of the detector (monopole field). Notice that full proofs of the theorems are given in Appendix C.

1. Quantized complex field

Ultimately, we want to calculate expectation values like Eq. (116), or more generally:

$$\langle 0 | (a_{\mathbf{p}})_{\mathbf{p}} (b_{\bar{\mathbf{p}}})_{\bar{\mathbf{p}}} [T \Phi^{\epsilon_1}(x_1) \cdots \cdots \Phi^{\epsilon_n}(x_n)] (a_{\mathbf{k}}^\dagger)_{\mathbf{k}} (b_{\bar{\mathbf{k}}}^\dagger)_{\bar{\mathbf{k}}} | 0 \rangle, \quad (147)$$

where the index ϵ_i indicates that the fields may be conjugated or not. Since the vacuum expectation value of normal-ordered products of operators vanishes, it is useful to rewrite the original sequence of operators as a sum of normal-ordered expressions. To achieve normal-ordering, the fields need to be expanded in terms of ladder operators, and the ladder operators commuted with each other until normal-ordering is reached. The well-known Wick theorem allows to do so systematically. We will proceed in two steps in evaluating the above expression. In the first step, we present Wick theorem for time-ordered products of field operators. In the second step, we then extend this theorem and allow for more ladder operators to be prepended and appended.

It is useful to decompose the field operator into a part containing the creation operators and a second one containing the annihilation operators:

$$\Phi(x) = \Phi_a(x) + \Phi_b^\dagger(x), \quad (148)$$

where

$$\Phi_a(x) \equiv \sum_{\mathbf{k}} a_{\mathbf{k}} \varphi_{\mathbf{k}}(x), \quad \Phi_b(x) \equiv \sum_{\mathbf{k}} b_{\mathbf{k}} \varphi_{\mathbf{k}}(x) \quad (149)$$

and $\varphi_{\mathbf{k}}$ are the mode functions of the quantised scalar field.

Time-ordered product of quantized complex fields.— The above separation facilitates normal-ordering series of fields. If there are only a few field operators, this can still rapidly be done by hand. For example,

$$\Phi(x)\Phi^\dagger(y) = : \Phi(x)\Phi^\dagger(y) : + [\Phi_a(x), \Phi_a^\dagger(y)]. \quad (150)$$

It is straightforward to check that the commutator is identical to a nontrivial two-point function of the quantized complex field:

$$[\Phi_a(x), \Phi_a^\dagger(y)] = \mathbf{1} \langle 0 | \Phi(x)\Phi^\dagger(y) | 0 \rangle. \quad (151)$$

Thus, time-ordering of the fields introduces the Feynman propagator, such that for example:

$$T \Phi(x)\Phi^\dagger(y) = : \Phi(x)\Phi^\dagger(y) : + \mathbf{1} G_F(x-y). \quad (152)$$

These results are readily generalized if more fields are included. To keep the notation light, Feynman propagators are customarily written as *contractions*

$$\begin{aligned} \overbrace{\Phi(x)\Phi^\dagger(y)} &\equiv \mathbf{1} G_F(x-y), & \overbrace{\Phi(x)\Phi(y)} &\equiv 0, \\ \overbrace{\Phi^\dagger(x)\Phi(y)} &\equiv \mathbf{1} G_F(x-y), & \overbrace{\Phi^\dagger(x)\Phi^\dagger(y)} &\equiv 0. \end{aligned} \quad (153)$$

Theorem VI.1 (Wick's theorem for time-ordered quantized complex fields). *A product of n time-ordered field operators of the quantized complex field Φ , which may contain subproducts that are normal-ordered, can be rewritten as follows:*

$$\begin{aligned}
& T\Phi^{\epsilon_1}(x_1)\Phi^{\epsilon_2}(x_2)\cdots\Phi^{\epsilon_n}(x_n) \\
& = : \Phi^{\epsilon_1}(x_1)\Phi^{\epsilon_2}(x_2)\cdots\Phi^{\epsilon_n}(x_n) : \\
& + \sum_{\text{single}} : \overbrace{\Phi^{\epsilon_1}(x_1)\cdots\Phi^{\epsilon_i}(x_i)\cdots\Phi^{\epsilon_j}(x_j)\cdots\Phi^{\epsilon_n}(x_n)} : \\
& + \sum_{\text{double}} : \overbrace{\Phi^{\epsilon_1}(x_1)\cdots\Phi^{\epsilon_i}(x_i)\cdots\Phi^{\epsilon_j}(x_j)\cdots} \\
& \quad \cdots \overbrace{\Phi^{\epsilon_k}(x_k)\cdots\Phi^{\epsilon_l}(x_l)} : + \cdots . \tag{154}
\end{aligned}$$

Two contracted fields belonging to different normal-ordered subproducts are to be replaced as follows:

$$\begin{aligned}
& \overbrace{\Phi^\dagger(x_i)\cdots\Phi(x_j)} = \mathbf{1} G_F(x_i - x_j) \\
& \overbrace{\Phi(x_i)\cdots\Phi^\dagger(x_j)} = \mathbf{1} G_F(x_i - x_j) \\
& \overbrace{\Phi(x_i)\cdots\Phi(x_j)} = 0 \\
& \overbrace{\Phi^\dagger(x_i)\cdots\Phi^\dagger(x_j)} = 0 . \tag{155}
\end{aligned}$$

Contraction of any pair of fields belonging to the same normal-ordered subproduct vanish.

For three fields, for example,

$$\begin{aligned}
& T\Phi(x) : \Phi^\dagger(y)\Phi(z) : \\
& = : \Phi(x)\Phi^\dagger(y)\Phi(z) : + : \overbrace{\Phi(x)\Phi^\dagger(y)} \Phi(z) : \\
& = : \Phi(x)\Phi^\dagger(y)\Phi(z) : + \mathbf{1} G_F(x - y)\Phi(z) . \tag{156}
\end{aligned}$$

This theorem is a canonical result in quantum field theory [43, 47].

Theorem VI.2 (Wick's theorem for full expectation values of the quantized complex field). *Consider a time-ordered product of quantized complex fields $T\Phi^{\epsilon_1}(x_1)\cdots\Phi^{\epsilon_n}(x_n)$ that may contain normal-ordered subproducts. The indices $\epsilon_i \in \{\circ, \dagger\}$ indicate whether the field operator is conjugated ($\epsilon_i = \dagger$, such that $\Phi^{\epsilon_i} = \Phi^\dagger$) or not ($\epsilon_i = \circ$, such that $\Phi^{\epsilon_i} = \Phi$). Then prepend products of annihilation operators*

$$(a_{\mathbf{p}})_{\mathbf{p}} \equiv a_{\mathbf{p}_1} \cdots a_{\mathbf{p}_M} , \quad (b_{\mathbf{p}})_{\mathbf{p}} \equiv b_{\mathbf{p}_1} \cdots b_{\mathbf{p}_M} \tag{157}$$

and append products of creation operators

$$(a_{\mathbf{k}}^\dagger)_{\mathbf{k}} \equiv a_{\mathbf{k}_1}^\dagger \cdots a_{\mathbf{k}_N}^\dagger , \quad (b_{\mathbf{k}}^\dagger)_{\mathbf{k}} \equiv b_{\mathbf{k}_1}^\dagger \cdots b_{\mathbf{k}_N}^\dagger . \tag{158}$$

The vacuum expectation value of the resulting product of operators vanishes if the total number of operators is odd.

If it is even, it can be expressed as the sum over all full contractions:

$$\begin{aligned}
& \langle 0 | (a_{\mathbf{p}})_{\mathbf{p}} (b_{\mathbf{p}})_{\mathbf{p}} [T\Phi^{\epsilon_1}(x_1)\cdots\Phi^{\epsilon_n}(x_n)] (a_{\mathbf{k}}^\dagger)_{\mathbf{k}} (b_{\mathbf{k}}^\dagger)_{\mathbf{k}} | 0 \rangle \\
& = \sum_{\text{all full}} \overbrace{a_{\mathbf{p}_1} \cdots \Phi^{\epsilon_i}(x_i) \cdots \Phi^{\epsilon_j}(x_j) \cdots \Phi^{\epsilon_k}(x_k) \cdots} \\
& \quad \cdots \overbrace{\Phi^{\epsilon_l}(x_l) \cdots b_{\mathbf{k}_N}^\dagger} . \tag{159}
\end{aligned}$$

The contractions between fields that do not belong to the same normal-ordered subproducts are

$$\overbrace{\Phi^\dagger(x_i)\cdots\Phi(x_j)} = \mathbf{1} G_F(x_i - x_j) = \overbrace{\Phi(x_i)\cdots\Phi^\dagger(x_j)} , \tag{160}$$

the contractions between ladder operators

$$\overbrace{a_{\mathbf{p}} \cdots a_{\mathbf{p}}^\dagger} = \mathbf{1} \delta_{\mathbf{k}, \mathbf{p}} = \overbrace{b_{\mathbf{k}} \cdots b_{\mathbf{p}}^\dagger} , \tag{161}$$

and, finally, the mixed contractions

$$\begin{aligned}
& \overbrace{a_{\mathbf{k}} \cdots \Phi^\dagger(x)} = \mathbf{1} \varphi_{\mathbf{k}}^*(x) , & \overbrace{\Phi(x) \cdots a_{\mathbf{k}}^\dagger} = \mathbf{1} \varphi_{\mathbf{k}}(x) \\
& \overbrace{b_{\mathbf{k}} \cdots \Phi(x)} = \mathbf{1} \varphi_{\mathbf{k}}^*(x) , & \overbrace{\Phi^\dagger(x) \cdots b_{\mathbf{k}}^\dagger} = \mathbf{1} \varphi_{\mathbf{k}}(x) . \tag{162}
\end{aligned}$$

All other contractions vanish, in particular contractions between fields belonging to the same normal-ordered subproducts.

A proof of this theorem is given in Appendix C 1.

2. Quantized real field

Note that the field operator can be separated as

$$\Phi(x) = \Phi_a(x) + \Phi_a^\dagger(x) . \tag{163}$$

Unlike for the quantized complex field, the commutator

$$[\Phi_a(x), \Phi(y)] = \langle 0 | \Phi(x)\Phi(y) | 0 \rangle \tag{164}$$

does not vanish. This changes the contractions in the equivalent of theorem VI.1 for the quantized real field: contractions between $\Phi(x)$ and $\Phi(y)$ do not vanish for the quantized real field. Similarly, the contraction between $a_{\mathbf{k}}$ and $\Phi(x)$ does not vanish in the equivalent of theorem VI.2, since

$$\begin{aligned}
& [a_{\mathbf{k}}, \Phi(x)] = \mathbf{1} \varphi_{\mathbf{k}}^*(x) \\
& [\Phi(x), a_{\mathbf{k}}^\dagger] = \mathbf{1} \varphi_{\mathbf{k}}(x) \tag{165}
\end{aligned}$$

are now nonzero. Keeping this in mind, we can immediately state:

Theorem VI.3 (Wick's theorem for full expectation values of the quantized real field). *Consider a time-ordered product of quantized real fields $T\Phi(x_1)\cdots\Phi(x_n)$ that may*

contain normal-ordered subproducts. Then prepend products of annihilation operators

$$(a_{\mathbf{p}})_{\mathbf{p}} \equiv a_{\mathbf{p}_1} \cdots a_{\mathbf{p}_M} \quad (166)$$

and append products of creation operators

$$(a_{\mathbf{k}}^\dagger)_{\mathbf{k}} \equiv a_{\mathbf{k}_1}^\dagger \cdots a_{\mathbf{k}_N}^\dagger . \quad (167)$$

The vacuum expectation value of the resulting product of operators vanishes if the total number of operators is odd. If it is even, it can be expressed as the sum over all full contractions:

$$\begin{aligned} & \langle 0 | (a_{\mathbf{p}})_{\mathbf{p}} [T\Phi(x_1) \cdots \Phi(x_n)] (a_{\mathbf{k}}^\dagger)_{\mathbf{k}} | 0 \rangle \\ &= \sum_{\text{all full contractions}} \overbrace{a_{\mathbf{p}_1} \cdots \Phi(x_i) \cdots \Phi(x_j) \cdots \Phi(x_k) \cdots \Phi(x_l) \cdots a_{\mathbf{k}_N}^\dagger} \end{aligned} \quad (168)$$

The contractions between fields that do not belong to the same normal-ordered subproduct are

$$\overbrace{\Phi(x_i) \cdots \Phi(x_j)} = \mathbf{1} G_F(x_i - x_j) , \quad (169)$$

the contractions between ladder operators

$$\overbrace{a_{\mathbf{k}} \cdots a_{\mathbf{p}}^\dagger} = \mathbf{1} \delta_{\mathbf{k}, \mathbf{p}} , \quad (170)$$

and the mixed contractions

$$\overbrace{a_{\mathbf{k}} \cdots \Phi(x)} = \mathbf{1} \varphi_{\mathbf{k}}^*(x) \quad \overbrace{\Phi(x) \cdots a_{\mathbf{k}}^\dagger} = \mathbf{1} \varphi_{\mathbf{k}}(x) . \quad (171)$$

All other contractions vanish, in particular contractions between fields belonging to the same normal-ordered subproducts.

3. Quantized spinor field

For spinor fields, we need to work out how to evaluate vacuum expectation values of the form

$$\langle 0 | (a_{\mathbf{p}, r})_{\mathbf{p}, r} (b_{\bar{\mathbf{p}}, \bar{r}})_{\bar{\mathbf{p}}, \bar{r}} [T\Psi^{\epsilon_1}(x_1) \cdots \Psi^{\epsilon_n}(x_n)] (a_{\mathbf{k}, s}^\dagger)_{\mathbf{k}, s} (b_{\bar{\mathbf{k}}, \bar{s}}^\dagger)_{\bar{\mathbf{k}}, \bar{s}} | 0 \rangle \quad (172)$$

where once more the index ϵ_i indicates whether the field is conjugated ($\bar{\Psi}$), or not (Ψ). Let us again split the field in two parts, according to the ladder operators, by defining

$$\begin{aligned} \Psi_a(x) &\equiv \sum_{\mathbf{k}, s} a_{\mathbf{k}, s} \psi_{\mathbf{k}, s, +}(x) \\ \Psi_b(x) &\equiv \sum_{\mathbf{k}, s} b_{\mathbf{k}, s}^\dagger \psi_{\mathbf{k}, s, -}(x) , \end{aligned} \quad (173)$$

such that

$$\begin{aligned} \Psi(x) &= \Psi_a(x) + \Psi_b(x) \\ \bar{\Psi}(x) &= \bar{\Psi}_a(x) + \bar{\Psi}_b(x) . \end{aligned} \quad (174)$$

Note that this convention varies slightly from Eqs. (148) and (149) used for quantized scalar fields.

Time-ordered products of quantized spinor fields.— Two spinor fields are easily normal-ordered by hand, for example:

$$\Psi(x)\bar{\Psi}(y) = : \Psi(x)\bar{\Psi}(y) : + \{\Psi_a(x), \bar{\Psi}_a(y)\} . \quad (175)$$

The anticommutators can be evaluated using Eq. (A36) for massive fields in (1, 3) dimensions [and the analogous equations for massless fields, and in (1, 1) dimensions respectively]. It is straightforward to see that

$$\{\Psi_a^A(x), \bar{\Psi}_{a, B}(y)\} = \mathbf{1} \langle 0 | \Psi^A(x) \bar{\Psi}_B(y) | 0 \rangle . \quad (176)$$

The Feynman propagator appears again if the fields are time-ordered. For example,

$$T\Psi(x)\bar{\Psi}(y) = : \Psi(x)\bar{\Psi}(y) : + \mathbf{1} S_F(x - y) , \quad (177)$$

where we have used that $: \bar{\Psi}(y)\Psi(x) : = - : \Psi(x)\bar{\Psi}(y) :$.

The generalization of the above is given by the fermionic version of Wick's theorem for spinor fields:

Theorem VI.4 (Wick's theorem for time-ordered quantized spinor fields). *Consider a time-ordered product of spinor fields $T\Psi^{\epsilon_1}(x_1) \cdots \Psi^{\epsilon_n}(x_n)$ which may contain normal-ordered subproducts. The indices $\epsilon_i \in \{\circ, \bar{\cdot}\}$ indicate whether the field operator is Dirac conjugated ($\epsilon_i = \bar{\cdot}$, such that $\Psi^{\epsilon_i} = \bar{\Psi}$) or not ($\epsilon_i = \circ$, such that $\Psi^{\epsilon_i} = \Psi$). It can be normal-ordered as follows:*

$$\begin{aligned} & T\Psi^{\epsilon_1}(x_1) \Psi^{\epsilon_2}(x_2) \cdots \Psi^{\epsilon_n}(x_n) \\ &= : \Psi^{\epsilon_1}(x_1) \Psi^{\epsilon_2}(x_2) \cdots \Psi^{\epsilon_n}(x_n) : \\ &+ \sum_{\text{single contractions}} : \Psi^{\epsilon_1}(x_1) \cdots \overbrace{\Psi^{\epsilon_i}(x_i) \cdots \Psi^{\epsilon_j}(x_j)} \cdots \Psi^{\epsilon_n}(x_n) : \\ &+ \sum_{\text{double contractions}} : \Psi^{\epsilon_1}(x_1) \cdots \overbrace{\Psi^{\epsilon_i}(x_i) \cdots \Psi^{\epsilon_j}(x_j)} \cdots \\ &\quad \cdots \overbrace{\Psi^{\epsilon_k}(x_k) \cdots \Psi^{\epsilon_l}(x_l)} : + \cdots . \end{aligned} \quad (178)$$

Contractions of any pair of fields belonging to the same normal-ordered subproduct vanish. Two contracted fields belonging to different normal-ordered subproducts are to be replaced as follows:

$$\begin{aligned} \overbrace{\bar{\Psi}_{A_i}(x_i) \Psi^{A_j}(x_j)} &= -\mathbf{1} S_F(x_j - x_i)_{A_i}^{A_j} \\ \overbrace{\Psi^{A_i}(x_i) \bar{\Psi}_{A_j}(x_j)} &= +\mathbf{1} S_F(x_i - x_j)_{A_i}^{A_j} \\ \overbrace{\Psi(x_i) \Psi(x_j)} &= 0 \\ \overbrace{\bar{\Psi}(x_i) \bar{\Psi}(x_j)} &= 0 . \end{aligned} \quad (179)$$

If contracted operators are not adjacent, the term has to be reordered until they are, with every exchange of two operators introducing an overall factor of (-1) to the term.

The last requirement that contracted operators need to be adjacent means for example that

$$\begin{aligned} & \overbrace{\Psi(x_1)\Psi(x_2)\Psi(x_3)\Psi(x_4)} \\ & = (-1)^3 : \overbrace{\Psi(x_4)\Psi(x_1)\Psi(x_2)\Psi(x_3)} : \end{aligned} \quad (180)$$

Since this is again a canonical result [43, 47], we abstain from giving the proof here.

Theorem VI.5 (Wick's theorem for full expectation values of the quantized spinor field). *Consider a time-ordered product of spinor fields $T\Psi^{\epsilon_1}(x_1)\cdots\Psi^{\epsilon_n}(x_n)$ like in theorem VI.4. Then prepend products of annihilation operators*

$$\begin{aligned} (a_{\mathbf{p},r})_{\mathbf{p},r} &\equiv a_{(\mathbf{p},r)_1}\cdots a_{(\mathbf{p},r)_M} \\ (b_{\bar{\mathbf{p}},\bar{r}})_{\bar{\mathbf{p}},\bar{r}} &\equiv b_{(\bar{\mathbf{p}},\bar{r})_1}\cdots b_{(\bar{\mathbf{p}},\bar{r})_{\bar{M}}}, \end{aligned} \quad (181)$$

and append products of creation operators

$$\begin{aligned} (a_{\mathbf{k},s}^\dagger)_{\mathbf{k},s} &\equiv a_{(\mathbf{k},s)_1}^\dagger\cdots a_{(\mathbf{k},s)_N}^\dagger \\ (b_{\bar{\mathbf{k}},\bar{s}}^\dagger)_{\bar{\mathbf{k}},\bar{s}} &\equiv b_{(\bar{\mathbf{k}},\bar{s})_1}^\dagger\cdots b_{(\bar{\mathbf{k}},\bar{s})_{\bar{N}}}^\dagger. \end{aligned} \quad (182)$$

The vacuum expectation value of the resulting product of operators vanishes if the total number of operators is odd. If it is even, it can be expressed as the sum over all full contractions:

$$\begin{aligned} & \langle 0 | (a_{\mathbf{p},r})_{\mathbf{p},r} (b_{\bar{\mathbf{p}},\bar{r}})_{\bar{\mathbf{p}},\bar{r}} [T\Psi^{\epsilon_1}(x_1)\cdots \\ & \quad \cdots \Psi^{\epsilon_n}(x_n)] (a_{\mathbf{k},s}^\dagger)_{\mathbf{k},s} (b_{\bar{\mathbf{k}},\bar{s}}^\dagger)_{\bar{\mathbf{k}},\bar{s}} | 0 \rangle \\ & = \sum_{\text{all full contract.}} \overbrace{a_{(\mathbf{p},r)_1}\cdots\Psi^{\epsilon_i}(x_i)\cdots\Psi^{\epsilon_j}(x_j)\cdots\Psi^{\epsilon_k}(x_k)\cdots} \\ & \quad \cdots \overbrace{\Psi^{\epsilon_l}(x_l)\cdots b_{(\bar{\mathbf{k}},\bar{s})_{\bar{N}}}^\dagger} \cdot \end{aligned} \quad (183)$$

The contractions between fields that do not belong to the same normal-ordered subproduct are

$$\begin{aligned} \overbrace{\Psi_{A_i}(x_i)\Psi^{A_j}(x_j)} &= -\mathbf{1} S_F(x_j - x_i)_{A_i}^{A_j} \\ \overbrace{\Psi^{A_i}(x_i)\Psi_{A_j}(x_j)} &= +\mathbf{1} S_F(x_i - x_j)_{A_j}^{A_i}, \end{aligned} \quad (184)$$

the contractions between ladder operators

$$\overbrace{a_{\mathbf{k},s} a_{\mathbf{p},r}^\dagger} = \mathbf{1} \delta_{\mathbf{k},\mathbf{p}} \delta_{s,r} = \overbrace{b_{\mathbf{k},s} b_{\mathbf{p},r}^\dagger}, \quad (185)$$

and the mixed contractions

$$\begin{aligned} \overbrace{a_{\mathbf{k},s} \Psi_A(x)} &= \mathbf{1} \bar{\psi}_{\mathbf{k},s,+A}(x) \\ \overbrace{\Psi^A(x) a_{\mathbf{k},s}^\dagger} &= \mathbf{1} \psi_{\mathbf{k},s,+}^A(x) \\ \overbrace{b_{\mathbf{k},s} \Psi^A(x)} &= \mathbf{1} \psi_{\mathbf{k},s,-}^A(x) \\ \overbrace{\Psi_A(x) b_{\mathbf{k},s}^\dagger} &= \mathbf{1} \bar{\psi}_{\mathbf{k},s,-A}(x). \end{aligned} \quad (186)$$

If contracted operators are not adjacent, the term has to be reordered until they are, with every exchange of two operators introducing an overall factor of (-1) to the term. All other contractions vanish, in particular contractions between fields belonging to the same normal-ordered subproduct.

A proof is given in Appendix C 2.

4. UDW-type detector

Last but not least, we would like to compute vacuum expectation values of the from given in Eq. (114),

$$\langle g | [\sigma^-]^a [T\mu(t_1)\cdots\mu(t_n)] [\sigma^+]^b | g \rangle \quad (187)$$

As before, we decompose the monopole operator into a creation and an annihilation part,

$$\mu_-(t) \equiv e^{-i\Omega t} \sigma^-, \quad \mu_+(t) \equiv e^{+i\Omega t} \sigma^+, \quad (188)$$

such that

$$\mu(t) = \mu_-(t) + \mu_+(t). \quad (189)$$

Time-ordered products of monopole operators.— For two monopole operators, normal-ordering is swiftly accomplished and yields

$$\mu(t_1)\mu(t_2) = : \mu(t_1)\mu(t_2) : + \{\mu_-(t_1), \mu_+(t_2)\}, \quad (190)$$

where

$$\{\mu_-(t_1), \mu_+(t_2)\} = \mathbf{1} e^{-i\Omega(t_1-t_2)}. \quad (191)$$

Now consider what happens if the product of monopole operators is time-ordered. For example,

$$T\mu(t_1)\mu(t_2) = : \mu(t_1)\mu(t_2) : + \mathbf{1} D_F(t_1 - t_2), \quad (192)$$

using the definition of the Feynman propagator Eq. (129). Since the monopole operator $\mu(x)$ (as a field) has basically the same structure as the quantized spinor field, we can directly conclude that the generalization to n operators is given by

Theorem VI.6 (Wick's theorem for time-ordered monopole operators). *A product of n time-ordered monopole operators μ can be rewritten as a sum of normal-ordered products as follows:*

$$\begin{aligned} & T\mu(t_1)\cdots\mu(t_n) \\ & = : \mu(t_1)\cdots\mu(t_n) : \\ & \quad + \sum_{\text{single contractions}} : \mu(t_1)\cdots\overbrace{\mu(t_i)\cdots\mu(t_j)}\cdots\mu(t_n) : \\ & \quad + \sum_{\text{double contractions}} : \mu(t_1)\cdots\overbrace{\mu(t_i)\cdots\mu(t_k)\cdots\mu(t_j)}\cdots\mu(t_1)\cdots \\ & \quad \cdots\mu(t_n) : + \cdots \end{aligned} \quad (193)$$

The contraction of adjacent operators is defined as

$$\overline{\mu(t_i)\mu(t_j)} \equiv \mathbf{1} D_F(t_i - t_j) . \quad (194)$$

If contracted operators are not adjacent, the term has to be reordered until they are, with every exchange of two operators introducing an overall factor of (-1) to the term.

Similar to the spinor field, this last remark implies, for example,

$$\begin{aligned} : \overline{\mu(t_1)\mu(t_2)\mu(t_3)\mu(t_4)} : &= - : \overline{\mu(t_1)\mu(t_3)\mu(t_2)\mu(t_4)} : \\ &= -\mathbf{1} e^{-i\Omega(t_1+t_2-t_3-t_4)} . \end{aligned} \quad (195)$$

5. Full expectation value

When prepending zero or one annihilation operator σ^- and appending zero or one creation operator σ^+ and taking the vacuum expectation value, more contractions appear:

Theorem VI.7 (Wick's theorem for the full expectation value of the detector). *Consider a product of n time-ordered monopole operators μ with $a \in \{0, 1\}$ annihilation operators and $b \in \{0, 1\}$ creation operators. Its vacuum expectation value is*

$$\begin{aligned} &\langle g | [\sigma^-]^a [T\mu(t_1) \cdots \mu(t_n)] [\sigma^+]^b | g \rangle \\ &= \sum_{\substack{\text{all full} \\ \text{contractions}}} \overline{\sigma^- \cdots \mu(t_i) \cdots \mu(t_k) \cdots \mu(t_j) \cdots \mu(t_l) \cdots \sigma^+} . \end{aligned} \quad (196)$$

The contraction between two adjacent monopole fields is defined as

$$\overline{\mu(t_i)\mu(t_j)} \equiv \mathbf{1} D_F(t_i - t_j) , \quad (197)$$

the contraction between ladder operator and monopole field

$$\overline{\sigma^- \mu(t)} = \mathbf{1} e^{+i\Omega t} , \quad \overline{\mu(t) \sigma^+} = \mathbf{1} e^{-i\Omega t} , \quad (198)$$

and finally the contraction between ladder operators

$$\overline{\sigma^- \sigma^+} = \mathbf{1} . \quad (199)$$

If contracted operators are not adjacent, the term has to be reordered until they are, with every exchange of two operators introducing an overall factor of (-1) to the term.

The proof is presented in Appendix C 3.

D. Diagrammatic computation

A usual way to visualize the contractions between field operators in the above theorems, as well as the next step towards Feynman diagrams, is the use of line diagrams. Operators in a given product are represented by points (vertices), and contractions are visualized as lines between the vertices. The vacuum expectation value of a given product of operators can be obtained in a structured manner by drawing such a diagram for every nontrivial full contraction (meaning that there are no wholly unconnected vertices), assigning the corresponding contraction as a factor to each line, and then summing up the terms obtained from each diagram.

To distinguish them from the fully fledged Feynman diagrams that we will develop in Sec. VIII, we will in the following sometimes refer to these diagrams as *auxiliary diagrams*.

1. UDW-type detector

The following set of rules can be applied as a help in evaluating expectation values of the form Eq. (187) using theorem VI.7:

Auxiliary diagrams for the detector.

1. If a creation operator is present, draw a vertex on the left end of the diagram. If an annihilation operator is present, draw a vertex on the right end of the diagram. These vertices will be referred to as external vertices (ingoing on the left and outgoing on the right).
2. In the middle, draw a horizontal series of vertices, one for each t_i , starting with t_n on the left, and label them accordingly. These vertices will be referred to as internal vertices.
3. To account for the nontrivial contractions Eqs. (197) to (199), connect all vertices by lines such that each external and internal vertex has one line attached to it.
4. Draw one diagram for every way to connect all vertices using the rules in 3, such that no vertex is left completely unconnected. If this is impossible, the expectation value is zero.
5. Associate the following factors to each line in a diagram:
 - $\mathbf{1}$ to a line connecting two external vertices
 - $e^{-i\Omega t_i}$ to a line connecting an ingoing vertex with an internal vertex t_i
 - $e^{+i\Omega t_i}$ to a line connecting an outgoing vertex with an internal vertex t_i
 - $D_F(t_i - t_j)$ to a line connecting two internal vertices t_i, t_j ; since $D_F(t_i - t_j) = -D_F(t_j - t_i)$, and the overall sign is determined in other ways, the order is irrelevant.
6. To obtain the correct overall sign of a diagram, fall back to the interaction picture and reorder the op-

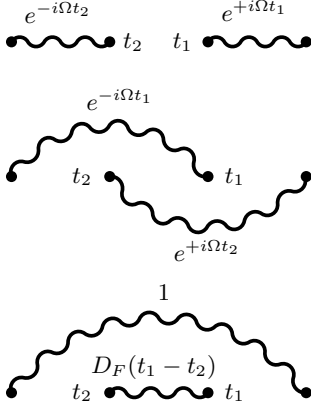


Figure 5. The three diagrams belonging to the example for the monopole operator.

erators such that contracted pairs are adjacent, as described in theorem VI.7.

7. The vacuum expectation value is obtained by summing up the values associated with each diagram.

Example.— Assume the detector is excited both at the beginning and at the end. Including second order corrections to the amplitude, one encounters the expectation value

$$E = \langle 0 | \sigma^- [T\mu(t_1)\mu(t_2)] \sigma^+ | 0 \rangle . \quad (200)$$

There are three full contractions which can be written as follows:

$$\begin{aligned} E &= \langle 0 | \overline{\sigma^- [T\mu(t_1)\mu(t_2)]} \sigma^+ | 0 \rangle \\ &\quad + \langle 0 | \overline{\sigma^- [T\mu(t_1)\mu(t_2)]} \sigma^+ | 0 \rangle \\ &\quad + \langle 0 | \overline{\sigma^- [T\mu(t_1)\mu(t_2)]} \sigma^+ | 0 \rangle \\ &\quad + \overline{\sigma^- \mu(t_1)\mu(t_2)} \sigma^+ - \overline{\sigma^- \mu(t_2)\mu(t_1)} \sigma^+ \\ &\quad + \overline{\sigma^- \sigma^+ \mu(t_1)\mu(t_2)} \\ &= e^{+i\Omega(t_1-t_2)} - e^{-i\Omega(t_1-t_2)} + D_F(t_1 - t_2) , \quad (201) \end{aligned}$$

according to theorem VI.7. Up to the signs, the same is obtained from the three corresponding diagrams shown in Fig. 5.

2. Linear coupling to quantized real fields

To simplify the use of theorem VI.3 to evaluate the vacuum expectation values of the form

$$\langle 0 | (a_{\mathbf{p}})_{\mathbf{p}} [T\Phi(y_1) \cdots \Phi(y_n)] (a_{\mathbf{k}}^\dagger)_{\mathbf{k}} | 0 \rangle , \quad (202)$$

the following equivalent diagrammatic method can be used:

Auxiliary diagrams for quantized real fields, linear coupling.

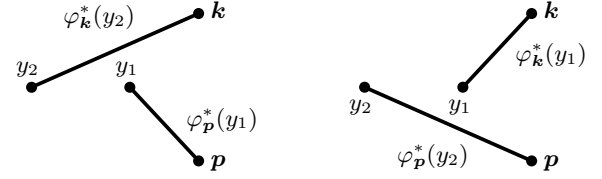


Figure 6. The two diagrams belonging to the example for linear coupling to quantized real fields.

1. On the left end of the diagram, draw vertices for every creation operator, and label them by their momenta. Similarly, draw vertices for every annihilation operator on the right-hand side and label them by their momenta. As before, these vertices will be referred to as external vertices (ingoing on the left and outgoing on the right).
2. In the middle, draw a horizontal series of vertices, one for each y_i , starting with y_n on the left, and label them accordingly. Once again, these are the internal vertices.
3. To account for the nontrivial contractions Eqs. (169) to (171), connect all vertices by lines in the following way:
 - both external and internal vertices have one line attached
 - direct connections between ingoing vertices are forbidden; direct connections between outgoing vertices are forbidden
4. Draw one diagram for every way to connect all vertices using the rules in 3. If this is not possible, the expectation value is zero.
5. Associate the following factors to each line in a diagram:
 - $\delta_{\mathbf{k},\mathbf{p}}$ to a line connecting two external vertices \mathbf{k} and \mathbf{p}
 - $\varphi_{\mathbf{k}}(y_i)$ to a line connecting an ingoing vertex \mathbf{k} with an internal vertex y_i
 - $\varphi_{\mathbf{k}}^*(y_i)$ to a line connecting an outgoing vertex \mathbf{k} with an internal vertex y_i
 - $G_F(y_i - y_j)$ to a line connecting two internal vertices y_i, y_j ; since $G_F(x_i - x_j) = G_F(x_j - x_i)$, the order is irrelevant.
6. The vacuum expectation value is obtained by summing up the values associated with each diagram.

Example.— Add two annihilation operators in front of the two time-ordered fields. The calculations can still be performed by hand in a reasonable time, yielding:

$$\begin{aligned} \langle 0 | a_{\mathbf{k}} a_{\mathbf{p}} [T\Phi(y_1)\Phi(y_2)] | 0 \rangle \\ = \varphi_{\mathbf{k}}^*(y_2) \varphi_{\mathbf{p}}^*(y_1) + \varphi_{\mathbf{k}}^*(y_1) \varphi_{\mathbf{p}}^*(y_2) . \quad (203) \end{aligned}$$

Indeed, applying the above diagrammatic rules results in the two diagrams depicted in Fig. 6 and gives the same result.

3. Quadratic coupling to quantized real fields

If the detector model 2 coupling quadratically to a quantized real field is used instead, expectation values of the following type are encountered:

$$\langle 0 | (a_{\mathbf{p}})_{\mathbf{p}} [T : \Phi(y_1)\Phi(y_1) : \dots \dots : \Phi(y_n)\Phi(y_n) :] (a_{\mathbf{k}}^\dagger)_{\mathbf{k}} | 0 \rangle . \quad (204)$$

Since there are now normal-ordered subproducts of fields with the same argument, the above rules have to be adapted.

Auxiliary diagrams for quantized real fields, quadratic coupling.

The rules for quantized real fields and linear coupling still apply, with one exception in point 3: internal vertices have two lines attached; these are not interchangeable.

Example.— We evaluate an expectation value similar to the example for linear coupling. There are four ways to contract two fields $\Phi(y_1)$, $\Phi(y_2)$, and then two ways to contract the remaining fields with the ladder operators. In consequence there are eight terms in total, yielding:

$$\begin{aligned} & \langle 0 | a_{\mathbf{k}} a_{\mathbf{p}} [T : \Phi(y_1)\Phi(y_1) : : \Phi(y_2)\Phi(y_2) :] | 0 \rangle \\ & = 4 G_F(y_1 - y_2) [\varphi_{\mathbf{k}}^*(y_2) \varphi_{\mathbf{p}}^*(y_1) + \varphi_{\mathbf{k}}^*(y_1) \varphi_{\mathbf{p}}^*(y_2)] . \end{aligned} \quad (205)$$

The corresponding diagrams are drawn in Fig. 7. The same result can be obtained more economically by dropping the distinction between the two lines attached to each internal vertex, leading to merely two distinct diagrams in Fig. 8. To compensate, we assign an additional symmetry factor of four to the line between the two vertices, which counts the different ways the fields $\Phi(y_1)$ and $\Phi(y_2)$ can be contracted while now resulting in the same diagram. In accordance with the convention in particle physics, we will in the following use symmetry factors rather than distinguishing different legs of the same vertex.

4. Quadratic coupling to quantized complex fields

Theorem VI.2 is useful to evaluate the vacuum expectation values of the form

$$\langle 0 | (a_{\mathbf{p}})_{\mathbf{p}} (b_{\overline{\mathbf{p}}})_{\overline{\mathbf{p}}} [T : \Phi^\dagger(y_1)\Phi(y_1) : \dots \dots : \Phi^\dagger(y_n)\Phi(y_n) :] (a_{\mathbf{k}}^\dagger)_{\mathbf{k}} (b_{\overline{\mathbf{k}}}^\dagger)_{\overline{\mathbf{k}}} | 0 \rangle , \quad (206)$$

which arise when calculating the response of the quadratically coupling detector model 3. Here, the existence of two independent types of ladder operators (and accordingly the fact that the field is no longer self-adjoint) has to be taken into account. This is most conveniently achieved by giving the connection lines between vertices a direction, that is, by turning them into arrows. The following rules can be used to apply the theorem:

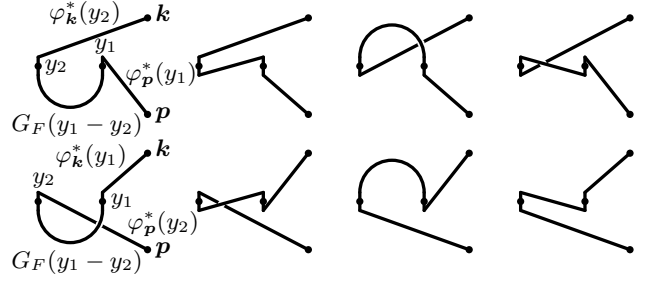


Figure 7. The eight diagrams belonging to the example for quadratic coupling to quantized real fields. In each of the two lines, all four ways to connect the two internal vertices are realized. In the upper line, one field $\Phi(y_2)$ is always contracted with $a_{\mathbf{k}}$, and one field $\Phi(y_1)$ with $a_{\mathbf{p}}$. In the lower line, the inverse case is accounted for.

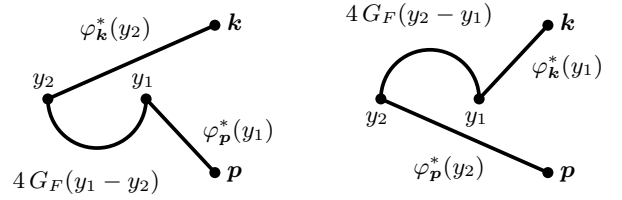


Figure 8. Diagrams belonging to the example for quadratic coupling to quantized real fields, reduced to two distinct diagrams by dropping the distinction between upwards and downwards lines of internal vertices. To compensate, an additional factor four is assigned to their contraction.

Auxiliary diagrams for quantized complex fields, quadratic coupling.

1. On the left end of the diagram, draw vertices for every creation operator $a_{\mathbf{k}_1}^\dagger$ and $b_{\overline{\mathbf{k}_2}}^\dagger$, and label them by their momenta with \mathbf{k}_1 , $\overline{\mathbf{k}_2}$, where the bar is used to mark antiparticle operators. Similarly, draw vertices for every annihilation operator $a_{\mathbf{p}_1}$ and $b_{\overline{\mathbf{p}_2}}$ on the right-hand side and label them by their momenta \mathbf{p}_1 and $\overline{\mathbf{p}_2}$.
2. In the middle, draw a horizontal series of vertices for each y_i , starting with y_n on the left, and label them accordingly.
3. To account for the nontrivial contractions Eqs. (160) to (162), connect all vertices by arrows in the following way:
 - vertices representing a^\dagger and b are origins of one arrow each
 - vertices representing a and b^\dagger are endpoints of one arrow each
 - vertices representing y_i are origin of one arrow, and endpoint of one arrow each
 - direct connections between ingoing vertices are forbidden; direct connections between outgoing vertices are forbidden
 - connecting an internal vertex with itself is for-

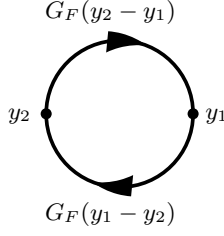


Figure 9. Diagram belonging to Example 1 for quantized complex fields.

bidden

- *arrow directions must not collide*
4. *Draw one diagram for every way to connect all vertices using the rules in 3. If this is not possible, the expectation value is zero.*
 5. *Associate the following factors to each arrow in a diagram:*
 - $\delta_{\mathbf{k}, \mathbf{p}}$ *to an arrow connecting two external vertices \mathbf{k} and \mathbf{p}*
 - $\varphi_{\mathbf{k}}(y_i)$ *to an arrow connecting an ingoing vertex \mathbf{k} with an internal vertex y_i*
 - $\varphi_{\mathbf{k}}^*(y_i)$ *to an arrow connecting an outgoing vertex \mathbf{k} with an internal vertex y_i*
 - $G_F(y_i - y_j)$ *to an arrow connecting two internal vertices y_i, y_j*
 6. *The vacuum expectation value is obtained by summing up the values associated with each diagram.*

Example 1.— Consider the term

$$\langle 0 | T : \Phi^\dagger(y_1) \Phi(y_1) :: \Phi^\dagger(y_2) \Phi(y_2) : | 0 \rangle . \quad (207)$$

There is only one contributing diagram, drawn in Fig. 9, and we can immediately read off that

$$\langle 0 | T : \Phi^\dagger(y_1) \Phi(y_1) :: \Phi^\dagger(y_2) \Phi(y_2) : | 0 \rangle = [G_F(y_1 - y_2)]^2 , \quad (208)$$

where we have used that $G_F(y_2 - y_1) = G_F(y_1 - y_2)$. The same result is obtained when doing the ladder operator algebra directly by hand.

Example 2.— Now consider the analogue of the expectation value from the example for quadratic coupling to quantized real fields. Both annihilation operators have to be contracted, and according to theorem VI.2, they can only (nontrivially) be contracted with conjugated fields $\Phi^\dagger(y_i)$. This only leaves $\Phi(y_1), \Phi(y_2)$, whose contraction vanishes – unlike for the quantized real field, this expectation value vanishes for a quantized complex field:

$$\langle 0 | a_{\mathbf{k}} a_{\mathbf{p}} [T : \Phi^\dagger(y_1) \Phi(y_1) :: \Phi^\dagger(y_2) \Phi(y_2) :] | 0 \rangle = 0 . \quad (209)$$

This is reflected in the diagrammatic rules through the orientation of the lines, and is the manifestation of $U(1)$ charge conservation.

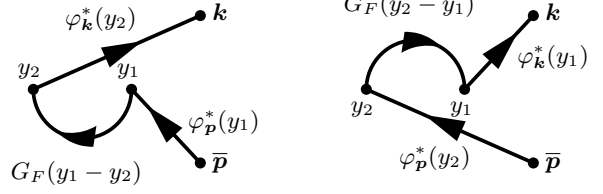


Figure 10. The two diagrams belonging to Example 3 for quantized complex fields.

Example 3.— We replace one outgoing particle state with an antiparticle state. The two corresponding diagrams are shown in Fig. 10, and give

$$\begin{aligned} \langle 0 | a_{\mathbf{k}} b_{\mathbf{p}} [T : \Phi^\dagger(y_1) \Phi(y_1) :: \Phi^\dagger(y_2) \Phi(y_2) :] | 0 \rangle \\ = G_F(y_1 - y_2) [\varphi_{\mathbf{k}}^*(y_2) \varphi_{\mathbf{p}}^*(y_1) + \varphi_{\mathbf{k}}^*(y_1) \varphi_{\mathbf{p}}^*(y_2)] . \end{aligned} \quad (210)$$

Unlike in the example for quadratic coupling to quantized real fields, there is only one possibility to draw a diagram if y_2 is connected to \mathbf{k} instead of four, and a second possibility if y_2 is connected to \mathbf{p} ; in total, there are thus two instead of eight diagrams.

5. Quadratic coupling to quantized spinor fields

For spinor fields, the rules need to be extended once more to account for the fermionic nature of the field. To evaluate expressions of the type

$$\langle 0 | (a_{\mathbf{p}, r})_{\mathbf{p}, r} (b_{\bar{\mathbf{p}}, \bar{r}})_{\bar{\mathbf{p}}, \bar{r}} [T : \bar{\Psi}_{A_1}(y_1) \Psi^{A_1}(y_1) \cdots \cdots \bar{\Psi}_{A_n}(y_n) \Psi^{A_n}(y_n) :] (a_{\mathbf{k}, s}^\dagger)_{\mathbf{k}, s} (b_{\bar{\mathbf{k}}, \bar{s}}^\dagger)_{\bar{\mathbf{k}}, \bar{s}} | 0 \rangle \quad (211)$$

using theorem VI.5, the following set of rules may be employed:

Auxiliary diagrams for quantized spinor fields, quadratic coupling.

1. *On the left end of the diagram, draw vertices for every creation operator $a_{\mathbf{k}_1, s_1}^\dagger$ and $b_{\bar{\mathbf{k}}_2, s_2}^\dagger$, and label them by their momenta and spins (\mathbf{k}_1, s) , $(\bar{\mathbf{k}}_2, s_2)$, where the bar is used to mark antiparticle operators. Similarly, draw vertices for every annihilation operator $a_{\mathbf{p}_1, r_1}$ and $b_{\bar{\mathbf{p}}_2, r_2}$ on the right-hand side and label them by their momenta and spins (\mathbf{p}_1, r_1) and $(\bar{\mathbf{p}}_2, r_2)$. Include a horizontal setoff between all vertices, such that the leftmost annihilation operator ends up at the very right, and the rightmost creation operator on the very left. The ordering of all vertices has to be inverse to the ordering of the corresponding ladder operators.*
2. *In the middle, draw a horizontal series of vertices for each y_i , starting with y_n on the left, and label*

them accordingly. Also, indicate the appropriate spinor index A_i .

3. To account for the nontrivial contractions Eqs. (184) to (186), connect all vertices by arrows in the following way:
 - external vertices representing a^\dagger and b are origins of one arrow each
 - external vertices representing a and b^\dagger are endpoints of one arrow each
 - internal vertices representing y_i are origin of one arrow, and endpoint of one arrow each
 - direct connections between ingoing vertices are forbidden; direct connections between outgoing vertices are forbidden
 - connecting an internal vertex with itself is forbidden
 - arrow directions must not collide
4. Draw one diagram for every way to connect all vertices using the rules in 3. If this is not possible, the expectation value is zero.
5. Associate the following factors to each arrow in a diagram:
 - $\delta_{\mathbf{k},\mathbf{p}} \delta_{s,r}$ to an arrow connecting two external vertices (\mathbf{k}, s) , (\mathbf{p}, r) (or their antiparticle pendants)
 - $\psi_{\mathbf{k},s,+}^A(x)$ to an arrow connecting an ingoing particle vertex (\mathbf{k}, s) with an internal vertex (x, A)
 - $\psi_{\mathbf{k},s,-,A}(x)$ to an arrow connecting an ingoing antiparticle vertex $(\overline{\mathbf{k}}, s)$ with an internal vertex (x, A)
 - $\bar{\psi}_{\mathbf{p},r,+,A}(x)$ to an arrow connecting an outgoing particle vertex (\mathbf{p}, r) with an internal vertex (x, A)
 - $\psi_{\mathbf{p},r,-}^A(x)$ to an arrow connecting an outgoing antiparticle vertex $(\overline{\mathbf{p}}, r)$ with an internal vertex (x, A)
 - $S_F(x-y)_B^A$ to an arrow going from an internal vertex (y, B) to an internal vertex (x, A)
6. To determine the overall sign of a diagram, fall back to the interaction picture calculations and order the operators according to the contractions, as described in theorem VI.5.
7. The vacuum expectation value is obtained by summing up the values associated with each diagram.

Example 1.— Consider the following term, which allows only one nontrivial contraction according to theorem VI.5:

$$\begin{aligned} & \langle 0 | T : \bar{\Psi}(y_1) \Psi(y_1) :: \bar{\Psi}(y_2) \Psi(y_2) | 0 \rangle \\ &= \langle 0 | T : \overbrace{\bar{\Psi}_A(y_1) \Psi^A(y_1)} :: \underbrace{\bar{\Psi}_B(y_2) \Psi^B(y_2)} | 0 \rangle \\ &= -\text{tr } S_F(y_1 - y_2) S_F(y_2 - y_1), \quad (212) \end{aligned}$$

where the trace is over spinor indices. The same factors are obtained diagrammatically from Fig. 11.

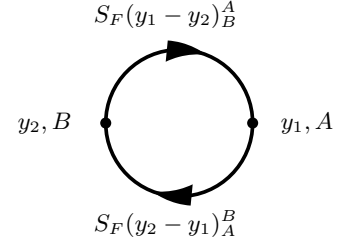


Figure 11. Diagram belonging to Example 1 for quantized spinor fields.

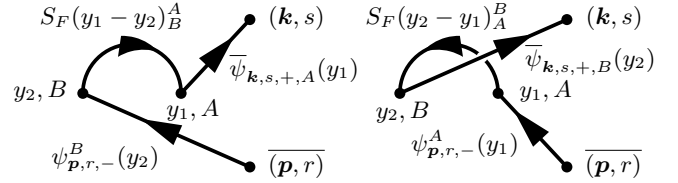


Figure 12. The two diagrams belonging to Example 2 for quantized spinor fields.

Example 2.— Consider the term

$$E = \langle 0 | a_{\mathbf{k},s} b_{\mathbf{p},r} [T : \bar{\Psi}(y_1) \Psi(y_1) :: \bar{\Psi}(y_2) \Psi(y_2) :] | 0 \rangle. \quad (213)$$

According to theorem VI.5, there are two nontrivial ways to contract. By reordering and writing out the contractions it can be cast into the form:

$$\begin{aligned} E &= (-1)^3 \overbrace{a_{\mathbf{k},s} \bar{\Psi}_A(y_1)} \overbrace{\Psi^A(y_1) \bar{\Psi}_B(y_2)} \overbrace{b_{\mathbf{p},r} \Psi^B(y_2)} \\ &+ (-1)^5 \overbrace{a_{\mathbf{k},s} \bar{\Psi}_B(y_2)} \overbrace{\Psi^B(y_2) \bar{\Psi}_A(y_1)} \overbrace{b_{\mathbf{p},r} \Psi^A(y_1)} \\ &= -\text{tr } \bar{\psi}_{\mathbf{k},s,+}(y_1) S_F(y_1 - y_2) \psi_{\mathbf{p},r,-}(y_2) \\ &\quad - \text{tr } \bar{\psi}_{\mathbf{k},s,+}(y_2) S_F(y_2 - y_1) \psi_{\mathbf{p},r,-}(y_1). \quad (214) \end{aligned}$$

The two corresponding diagrams are shown in Fig. 12.

VII. SECOND ORDER: VACUUM NO-RESPONSE PROBABILITY

We now turn to calculating the VNRP Eq. (107) for all four detector models up to second order as an example. The emerging patterns can then easily be generalized to full Feynman rules. We have already determined the transition amplitudes $\mathcal{A}_{a,g}^{(0)}$ in Eq. (109), and $\mathcal{A}_{a,g}^{(1)}$ vanishes. Only the second order amplitude $\mathcal{A}_{a,g}^{(2)}$ given in Eq. (110) remains to be evaluated.

A. Linear coupling to quantized real fields

To calculate the VNRP for the original UDW detector, model 1 in Table I, we insert the interaction Hamiltonian Eq. (14) in the amplitude Eq. (110). Combining the switching function and the spatial profile into the spacetime profile f gives the amplitude

$$\mathcal{A}_{\phi,g}^{(2)} = (-i\lambda)^2 e^{-i\omega\phi} \int dy_1 f(y_1) \int dy_2 f(y_2) \times \langle g|T\mu(y_1)\mu(y_2)|g\rangle \langle\phi|T\Phi(y_1)\Phi(y_2)|0\rangle, \quad (215)$$

where each integration runs over $[t_0, t] \times \mathbb{R}^n$, and $|\phi\rangle$ are energy eigenstates with energy ω_ϕ . Theorem VI.3 and theorem VI.7, and their diagrammatic representations can now be applied to evaluate these amplitudes for any given final state ϕ of the quantized real field. If the final state is the vacuum, $|\phi\rangle = |0\rangle$, there is only one way to contract all fields:

$$\mathcal{A}_{0,g}^{(2)} = (-i\lambda)^2 \int dy_1 f(y_1) \int dy_2 f(y_2) \times \langle g|T\overline{\mu(y_1)}\mu(y_2)|g\rangle \langle 0|T\overline{\Phi(y_1)}\Phi(y_2)|0\rangle. \quad (216)$$

The corresponding auxiliary diagrams for detector and field share the same vertices, and can be combined as shown in Fig. 13. Writing the propagators out introduces factors of the form $e^{\pm id \cdot y_i}$ —where $d = (\omega, \mathbf{0})$ —in case of the detector, and $e^{\pm ik \cdot y_i}$ in case of the field. This allows to perform the integration over the y_i ; for example:

$$\int dy_1 f(y_1) e^{-i(d+k)y_1} \equiv \tilde{f}(d+k), \quad (217)$$

where the domain of integration is $[t_0, t] \times \mathbb{R}^n$. In the limit $t_0 \rightarrow -\infty$, $t \rightarrow \infty$, this is just the Fourier transform of f as defined in Eq. (53). For simplicity, the same symbol \tilde{f} will be used both for finite times and in the limit $\pm\infty$. The amplitude then reads

$$\mathcal{A}_{0,g}^{(2)} = \lim_{\epsilon \rightarrow 0} \lim_{\delta \rightarrow 0} \int_{-\infty}^{\infty} \frac{d\omega}{2\pi} \frac{1}{L^n} \sum_{\mathbf{k}} \int_{-\infty}^{\infty} \frac{dk^0}{2\pi} (-i\lambda) \tilde{f}(d+k) \times \frac{2i\omega}{\omega^2 - \Omega^2 + i\epsilon} \frac{i}{k^2 - m^2 + i\delta} (-i\lambda) \tilde{f}(-d-k). \quad (218)$$

The factors and integrals that now additionally appear in the amplitude can be incorporated directly into the diagrammatic rules to obtain Feynman rules: For example, the last amplitude as a whole can be represented by the Feynman diagram shown in Fig. 14. To regain the amplitude from the diagram, we simply have to integrate (sum) the product of all the factors over the energies and momenta d, k running in the loop (with the appropriate measure).

If the final state contains one particle, $|\phi\rangle = |1_{\mathbf{k}}\rangle$, the amplitude vanishes,

$$\mathcal{A}_{1_{\mathbf{k}},g}^{(2)} \sim \langle 0|a_{\mathbf{k}}T\Phi(y_1)\Phi(y_2)|0\rangle = 0, \quad (219)$$

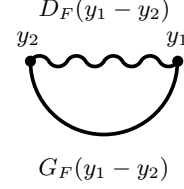


Figure 13. Linear coupling to quantized real field: auxiliary diagram for detector and field if final state $|\phi\rangle = |0\rangle$.

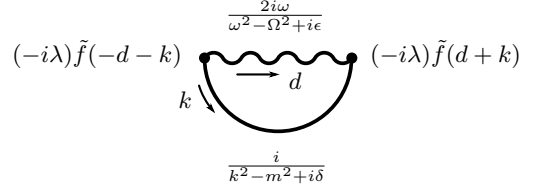


Figure 14. Linear coupling to quantized real field: Feynman diagram at second order for the VNRP amplitude, final state $|\phi\rangle = |0\rangle$.

since the presence of three operators does not allow for a full contraction.

If the final state is $|\phi\rangle = |1_{\mathbf{k}}, 1_{\mathbf{p}}\rangle$, there are two ways to contract the operators in the field part:

$$\mathcal{A}_{1_{\mathbf{k}},1_{\mathbf{p}},g}^{(2)} = (-i\lambda)^2 e^{-i(\omega_{\mathbf{k}} + \omega_{\mathbf{p}})t} \times \int dy_1 f(y_1) \int dy_2 f(y_2) \langle g|T\overline{\mu(y_1)}\mu(y_2)|g\rangle \times \left[\langle 0|a_{\mathbf{k}}a_{\mathbf{p}}T\overline{\Phi(y_1)}\Phi(y_2)|0\rangle + \langle 0|a_{\mathbf{k}}a_{\mathbf{p}}T\overline{\Phi(y_1)}\Phi(y_2)|0\rangle \right]. \quad (220)$$

We have already calculated these contractions in Eq. (203); the corresponding diagrams were drawn in Fig. 6. The resulting amplitude is

$$\mathcal{A}_{1_{\mathbf{k}},1_{\mathbf{p}},g}^{(2)} = \frac{1}{\sqrt{2\omega_{\mathbf{k}}L^n}} e^{-i\omega_{\mathbf{k}}t} \frac{1}{\sqrt{2\omega_{\mathbf{p}}L^n}} e^{-i\omega_{\mathbf{p}}t} \times \int_{-\infty}^{\infty} \frac{d\omega}{2\pi} \frac{2i\omega}{\omega^2 - \Omega^2 + i\epsilon} \times \left[(-i\lambda)\tilde{f}(d-p) (-i\lambda)\tilde{f}(-d-k) + (-i\lambda)\tilde{f}(d-k) (-i\lambda)\tilde{f}(-d-p) \right], \quad (221)$$

where we have suppressed the limit $\epsilon \rightarrow 0$, the two corresponding Feynman diagrams are drawn in Fig. 15. Note that both diagrams essentially have the same amplitude since the two outgoing momenta \mathbf{k}, \mathbf{p} appear symmetrically.

Final states $|\phi\rangle$ with more outgoing field quanta cannot contribute, because there are only two fields available to contract annihilation operators (outgoing states) with. Equivalently, on the level of Feynman diagrams, there are no further diagrams at second order. The vacuum

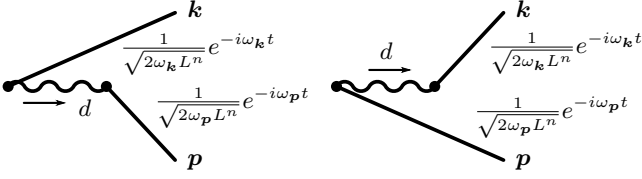


Figure 15. Linear coupling to quantized real field: Feynman diagrams at second order for the VNRP amplitude, final state $|\phi\rangle = |1_{\mathbf{k}}, 1_{\mathbf{p}}\rangle$. The vertex factors and the detector propagator are not shown.

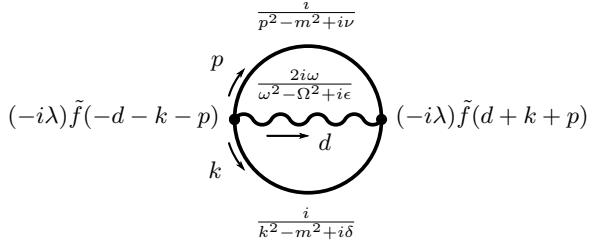


Figure 16. Quadratic coupling to quantized real field: Feynman diagram contributing to $\mathcal{A}_{0,g}^{(2)}$.

no-response probability is now obtained by inserting all amplitudes in Eq. (107); we refrain from writing it out here.

B. Quadratic coupling to quantized scalar fields

1. Quantized real fields

For model 2 with the interaction Hamiltonian Eq. (85), there are three nonzero amplitudes of the form

$$\begin{aligned} \mathcal{A}_{\phi,g}^{(2)} &= (-i\lambda)^2 e^{-i\omega\phi} \int dy_1 f(y_1) \int dy_2 f(y_2) \\ &\quad \times \langle g|T\mu(y_1)\mu(y_2)|g\rangle \\ &\quad \times \langle \phi|T:\Phi(y_1)\Phi(y_1)::\Phi(y_2)\Phi(y_2):|0\rangle. \end{aligned} \quad (222)$$

For final state $|0\rangle$, there are two ways to contract all field operators. There is a single corresponding Feynman diagram, drawn in Fig. 16, its amplitude therefore contains a symmetry factor of two:

$$\begin{aligned} \mathcal{A}_{0,g}^{(2)} &= 2 \int_{-\infty}^{\infty} \frac{d\omega}{2\pi} \frac{1}{L^n} \sum_{\mathbf{k}} \int_{-\infty}^{\infty} \frac{dk^0}{2\pi} \frac{1}{L^n} \sum_{\mathbf{p}} \int_{-\infty}^{\infty} \frac{dp^0}{2\pi} \\ &\quad \times (-i\lambda) \tilde{f}(d+k+p) \frac{2i\omega}{\omega^2 - \Omega^2 + i\epsilon} \frac{i}{k^2 - m^2 + i\delta} \\ &\quad \times \frac{i}{p^2 - m^2 + i\nu} (-i\lambda) \tilde{f}(-d-k-p). \end{aligned} \quad (223)$$

If the final state contains two field quanta, the expectation value in the field part corresponds to Eq. (205).

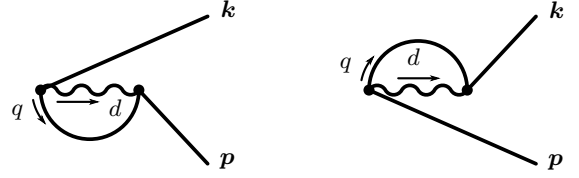


Figure 17. Quadratic coupling to quantized real field: two out of eight Feynman diagrams contributing to $\mathcal{A}_{1_{\mathbf{k}}, 1_{\mathbf{p}}, g}^{(2)}$.

Recall that there are eight ways to fully contract this expression; the two corresponding diagrams are drawn in Fig. 8. The complete Feynman diagrams are drawn in Fig. 17 and have symmetry factor four. The sum of the corresponding amplitudes is

$$\begin{aligned} \mathcal{A}_{1_{\mathbf{k}}, 1_{\mathbf{p}}, g}^{(2)} &= \\ &= 4 \frac{e^{-i\omega_k t}}{\sqrt{2\omega_k L^n}} \frac{e^{-i\omega_p t}}{\sqrt{2\omega_p L^n}} \int_{-\infty}^{\infty} \frac{d\omega}{2\pi} \frac{1}{L^n} \sum_{\mathbf{q}} \int_{-\infty}^{\infty} \frac{dq^0}{2\pi} \\ &\quad \times \left[(-i\lambda) \tilde{f}(d-p+q) \frac{2i\omega}{\omega^2 - \Omega^2 + i\epsilon} \right. \\ &\quad \times \frac{i}{q^2 - m^2 + i\delta} (-i\lambda) \tilde{f}(-d-k-q) \\ &\quad \left. + (-i\lambda) \tilde{f}(d-k+q) \frac{2i\omega}{\omega^2 - \Omega^2 + i\epsilon} \right. \\ &\quad \left. \times \frac{i}{q^2 - m^2 + i\delta} (-i\lambda) \tilde{f}(-d-p-q) \right]. \end{aligned} \quad (224)$$

Finally, if the final state has four particles, there are four ladder operators for the outgoing states that must be contracted with four field operators, which gives $4! = 24$ possible combinations. Figure 18 shows the six corresponding distinct Feynman diagrams. The symmetry factor for each diagram is four, and their amplitude totals to

$$\begin{aligned} \mathcal{A}_{1_{\mathbf{k}}, 1_{\mathbf{p}}, 1_{\mathbf{q}}, 1_{\mathbf{l}}}^{(2)} &= 4 \frac{e^{-i\omega_k t}}{\sqrt{2\omega_k L^n}} \frac{e^{-i\omega_p t}}{\sqrt{2\omega_p L^n}} \frac{e^{-i\omega_q t}}{\sqrt{2\omega_q L^n}} \frac{e^{-i\omega_l t}}{\sqrt{2\omega_l L^n}} \\ &\quad \times \int_{-\infty}^{\infty} \frac{d\omega}{2\pi} (-i\lambda)^2 \frac{2i\omega}{\omega^2 - \Omega^2 + i\epsilon} \\ &\quad \left[\tilde{f}(d-p-q) \tilde{f}(-d-k-l) + \tilde{f}(d-p-l) \tilde{f}(-d-k-q) \right. \\ &\quad \left. + \tilde{f}(d-q-l) \tilde{f}(-d-k-p) + \tilde{f}(d-k-q) \tilde{f}(-d-p-l) \right. \\ &\quad \left. + \tilde{f}(d-k-p) \tilde{f}(-d-q-l) + \tilde{f}(d-k-l) \tilde{f}(-d-p-q) \right]. \end{aligned} \quad (225)$$

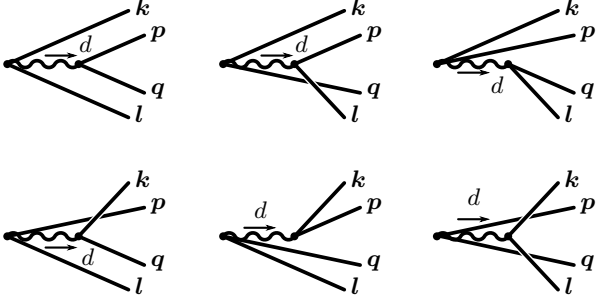


Figure 18. Quadratic coupling to quantized real field: six out of 24 Feynman diagrams contributing to $\mathcal{A}_{1k,1p,1q,1l,g}^{(2)}$.

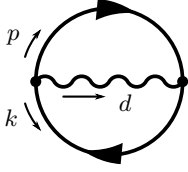


Figure 19. Quadratic coupling to quantized complex field: Feynman diagram corresponding to $\mathcal{A}_{0,g}^{(2)}$.

2. Quantized complex fields

When considering model 3 for the quantized complex field, there are again three nonzero amplitudes of the form

$$\begin{aligned} \mathcal{A}_{\phi,g}^{(2)} &= (-i\lambda)^2 e^{-i\omega\phi} \int dy_1 f(y_1) \int dy_2 f(y_2) \\ &\quad \times \langle g|T\mu(y_1)\mu(y_2)|g\rangle \\ &\quad \times \langle \phi|T:\Phi^\dagger(y_1)\Phi(y_1)::\Phi^\dagger(y_2)\Phi(y_2):|0\rangle. \end{aligned} \quad (226)$$

If the final state is the vacuum, there is only one way to fully contract, unlike for the quantized real field. The expression in the field part was already evaluated in Eq. (207), the corresponding auxiliary diagram is given in Fig. 9. In combination with the diagram of the detector's Feynman propagator, it becomes the Feynman diagram Fig. 19. Its amplitude is simply half of the amplitude in the case of a quantized real field as given in Eq. (223).

If the final state of the quantized complex field contains one particle and one antiparticle, the amplitude admits two different ways to fully contract. The expression in the field has already been calculated in Eq. (210); the two corresponding Feynman diagrams based on Fig. 10 are given in Fig. 20. The resulting amplitude is

$$\mathcal{A}_{1k,\bar{1}p,g}^{(2)} = \frac{1}{4} \mathcal{A}_{1k,1p,g}^{(2)}, \quad (227)$$

differing from $\mathcal{A}_{1k,1p,g}^{(2)}$ in Eq. (224) only by lack of the symmetry factor.

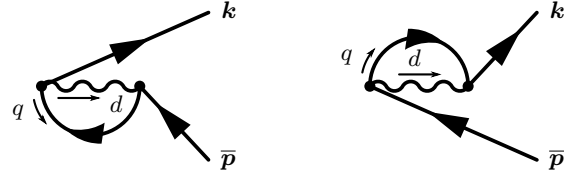


Figure 20. Quadratic coupling to quantized complex field: the two Feynman diagrams contributing to $\mathcal{A}_{1k,\bar{1}p,g}^{(2)}$.

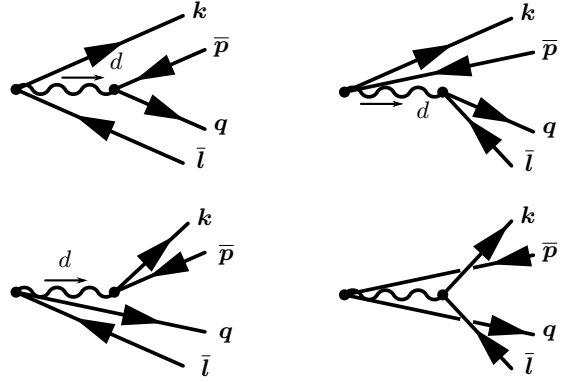


Figure 21. Quadratic coupling to quantized complex field: the four Feynman diagrams contributing to $\mathcal{A}_{1k,\bar{1}p,1q,\bar{1}l,g}^{(2)}$.

If the final state has two particles and two antiparticles, there are only four full contractions possible, as opposed to the quantized real field with 24 contractions. They correspond to the diagrams in Fig. 21, and the resulting amplitude is

$$\begin{aligned} \mathcal{A}_{1k,\bar{1}p,1q,\bar{1}l}^{(2)} &= \frac{e^{-i\omega_k t}}{\sqrt{2\omega_k L^n}} \frac{e^{-i\omega_p t}}{\sqrt{2\omega_p L^n}} \frac{e^{-i\omega_q t}}{\sqrt{2\omega_q L^n}} \frac{e^{-i\omega_l t}}{\sqrt{2\omega_l L^n}} \\ &\times \int_{-\infty}^{\infty} \frac{d\omega}{2\pi} (-i\lambda)^2 \frac{2i\omega}{\omega^2 - \Omega^2 + i\epsilon} \left[\tilde{f}(d-p-q) \tilde{f}(-d-k-l) \right. \\ &+ \tilde{f}(d-q-l) \tilde{f}(-d-k-p) + \tilde{f}(d-k-p) \tilde{f}(-d-q-l) \\ &\left. + \tilde{f}(d-k-l) \tilde{f}(-d-p-q) \right]. \end{aligned} \quad (228)$$

C. Quadratic coupling to quantized spinor fields

For the spinor field detector, model 4, the missing amplitudes are of the form

$$\begin{aligned} \mathcal{A}_{\psi,g}^{(2)} &= (-i\lambda)^2 e^{-i\omega\psi t} \int dy_1 f(y_1) \int dy_2 f(y_2) \\ &\quad \times \langle g|T\mu(y_1)\mu(y_2)|g\rangle \\ &\quad \times \langle \psi|T:\bar{\Psi}(y_1)\Psi(y_1)::\bar{\Psi}(y_2)\Psi(y_2):|0\rangle. \end{aligned} \quad (229)$$

If the final state is $|0\rangle$, there is only one full contraction. The expression involving the field operators has already

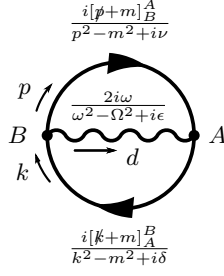


Figure 22. Quadratic coupling to quantized spinor field: Feynman diagram with factors corresponding to $\mathcal{A}_{0,g}^{(2)}$. Note that the sign of the momentum in the spinor field propagator is such that it flows into the direction of the field line (fermion flow).

been evaluated in Eq. (212) and yields twice the Feynman propagator of the spinor field. Writing it out according to Eq. (144), the amplitude can be expressed as

$$\begin{aligned} \mathcal{A}_{0,g}^{(2)} = & - \int_{-\infty}^{\infty} \frac{d\omega}{2\pi} \frac{1}{L^n} \sum_{\mathbf{k}} \int_{-\infty}^{\infty} \frac{dk^0}{2\pi} \frac{1}{L^n} \sum_{\mathbf{p}} \int_{-\infty}^{\infty} \frac{dp^0}{2\pi} \\ & \times (-i\lambda) \tilde{f}(d - k + p) \times \frac{2i\omega}{\omega^2 - \Omega^2 + i\epsilon} \frac{i[\not{k} + m]_A^B}{k^2 - m^2 + i\delta} \\ & \times \frac{i[\not{p} + m]_B^A}{p^2 - m^2 + i\nu} (-i\lambda) \tilde{f}(-d + k - p), \quad (230) \end{aligned}$$

where we have used Feynman slash notation $\not{k} = k \cdot \gamma$. Combining the two auxiliary diagrams corresponding to this contraction yields the Feynman diagram Fig. 22. Note the overall sign -1 of the amplitude that arises from the reordering of the fermionic field operators.

If there are two field quanta in the final state (particle and antiparticle), there are two ways to fully contract, analogous to the quantized complex field. The expression in the field part is similar to the one given in Eq. (214), but the annihilation operators are exchanged. This introduces an overall sign -1 , such that

$$\begin{aligned} \mathcal{A}_{1\mathbf{k},s,\bar{1}\mathbf{p},r,g}^{(2)} = & \sqrt{\frac{m}{\omega_{\mathbf{k}} L^n}} e^{-i\omega_{\mathbf{k}} t} \bar{u}_{\mathbf{k},s,B} \sqrt{\frac{m}{\omega_{\mathbf{p}} L^n}} e^{-i\omega_{\mathbf{p}} t} v_{\mathbf{p},r}^A \int_{-\infty}^{\infty} \frac{d\omega}{2\pi} \\ & \times \frac{1}{L^n} \sum_{\mathbf{q}} \int_{-\infty}^{\infty} \frac{dq^0}{2\pi} (-i\lambda) \tilde{f}(d - p - q) \frac{2i\omega}{\omega^2 - \Omega^2 + i\epsilon} \\ & \times \frac{i[\not{q} + m]_A^B}{q^2 - m^2 + i\delta} (-i\lambda) \tilde{f}(-d - k - q) \\ & + \sqrt{\frac{m}{\omega_{\mathbf{k}} L^n}} e^{-i\omega_{\mathbf{k}} t} \bar{u}_{\mathbf{k},s,A} \sqrt{\frac{m}{\omega_{\mathbf{p}} L^n}} e^{-i\omega_{\mathbf{p}} t} v_{\mathbf{p},r}^B \int_{-\infty}^{\infty} \frac{d\omega}{2\pi} \\ & \times \frac{1}{L^n} \sum_{\mathbf{q}} \int_{-\infty}^{\infty} \frac{dq^0}{2\pi} (-i\lambda) \tilde{f}(d - k + q) \frac{2i\omega}{\omega^2 - \Omega^2 + i\epsilon} \\ & \times \frac{i[\not{q} + m]_A^B}{q^2 - m^2 + i\delta} (-i\lambda) \tilde{f}(-d - p - q). \quad (231) \end{aligned}$$

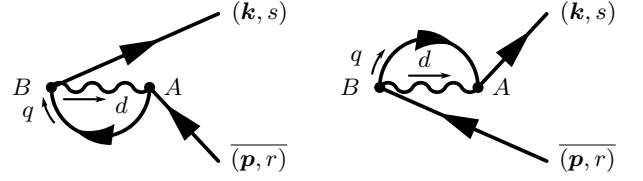


Figure 23. Quadratic coupling to quantized spinor field: the two Feynman diagrams contributing to $\mathcal{A}_{1\mathbf{k},s,\bar{1}\mathbf{p},r,g}^{(2)}$.

The expression for massless fields is recovered by $m\omega_{\mathbf{k}}^{-1}L^{-n} \rightarrow L^{-n}$. The corresponding Feynman diagrams are drawn in Fig. 23.

The only other final state with nonzero probability amplitude contains two particle states and two antiparticle states. Note that the fermionic nature of the field requires $(\mathbf{k}, s) \neq (\mathbf{q}, u)$ and $(\mathbf{p}, r) \neq (\mathbf{l}, v)$ due to the Pauli exclusion principle. As for the quantized complex field in the comparable situation, there are four possible contractions—see Fig. 24 for the corresponding Feynman diagrams. For massive fields, the amplitude is

$$\begin{aligned} \mathcal{A}_{1\mathbf{k},s,\bar{1}\mathbf{p},r,1\mathbf{q},u,\bar{1}\mathbf{l},v,g}^{(2)} = & (-i\lambda)^2 \sqrt{\frac{m}{\omega_{\mathbf{k}} L^n}} e^{-i\omega_{\mathbf{k}} t} \sqrt{\frac{m}{\omega_{\mathbf{p}} L^n}} e^{-i\omega_{\mathbf{p}} t} \\ & \times \sqrt{\frac{m}{\omega_{\mathbf{q}} L^n}} e^{-i\omega_{\mathbf{q}} t} \sqrt{\frac{m}{\omega_{\mathbf{l}} L^n}} e^{-i\omega_{\mathbf{l}} t} \int_{-\infty}^{\infty} \frac{d\omega}{2\pi} \frac{2i\omega}{\omega^2 - \Omega^2 + i\epsilon} \\ & \times \left[\tilde{f}(d - p - q) \tilde{f}(-d - k - l) (\bar{u}_{\mathbf{q},u,A} v_{\mathbf{p},r}^A) (\bar{u}_{\mathbf{k},s,B} v_{\mathbf{l},v}^B) \right. \\ & + \tilde{f}(d - q - l) \tilde{f}(-d - k - p) (\bar{u}_{\mathbf{q},u,A} v_{\mathbf{l},v}^A) (\bar{u}_{\mathbf{k},s,B} v_{\mathbf{p},r}^B) \\ & + \tilde{f}(d - k - p) \tilde{f}(-d - q - l) (\bar{u}_{\mathbf{k},s,A} v_{\mathbf{p},r}^A) (\bar{u}_{\mathbf{q},u,B} v_{\mathbf{l},v}^B) \\ & \left. + \tilde{f}(d - k - l) \tilde{f}(-d - p - q) (\bar{u}_{\mathbf{k},s,A} v_{\mathbf{l},v}^A) (\bar{u}_{\mathbf{q},u,B} v_{\mathbf{p},r}^B) \right], \quad (232) \end{aligned}$$

and the case of a massless field is recovered like for Eq. (231).

VIII. FEYNMAN RULES FOR DETECTOR MODELS

Feynman diagrams and Feynman rules can be understood as an extension of the diagrammatic representation of Wick's theorem. In order to obtain a transition amplitude, there are additional factors and summations (integrations) to be performed. Since their occurrence also follows simple patterns, it is straightforward to include them into the diagrammatic rules: Combining the auxiliary diagrams of the different field types into one diagram containing all field types gives us a Feynman diagram, and incorporating all additional operations into the rules for evaluating auxiliary diagrams gives Feynman rules.

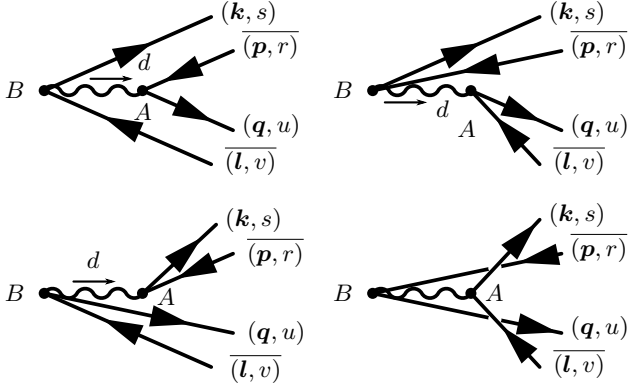


Figure 24. Quadratic coupling to quantized spinor field: the four Feynman diagrams contributing to $\mathcal{A}_{1_{\mathbf{k},s}, \bar{1}_{\mathbf{p},r}, 1_{\mathbf{q},u}, \bar{1}_{\mathbf{l},v}, g}^{(2)}$.

Note that the formalism presented here does not make use of asymptotic free states, in contrast to the usual Feynman rules of particle physics. Rather, ingoing and outgoing states are tensor products of Fock states of the noninteracting systems.

A. Towards Feynman rules

Feynman diagrams.— Consider, for example, the expression

$$\begin{aligned} & \langle g | \sigma^- T \mu(y_1) \mu(y_2) \sigma^+ | g \rangle \\ & \times \langle 0 | b_{\mathbf{p},r} a_{\mathbf{k},s} T : \bar{\Psi}(y_1) \Psi(y_1) : : \bar{\Psi}(y_2) \Psi(y_2) : | 0 \rangle . \end{aligned} \quad (233)$$

The detector part allows for three different contractions, giving rise to three terms and the three corresponding diagrams drawn in Fig. 5. The field part has two possible contractions, with diagrams shown in Fig. 12. Since these two parts are multiplied, one arrives at six summands in total. Both the diagrams for the detector and the field always have the same amount of vertices (equal to the order in perturbation theory), and can be combined into six Feynman diagrams which simultaneously show contractions for the detector and the field.

Feynman rules.— From the VNRP calculations in Sec. VII, we can directly deduce that outgoing quanta contribute the factors

$$\begin{aligned} & e^{-i\Omega t_0} , \quad \frac{1}{\sqrt{2\omega_{\mathbf{k}} L^n}} e^{-i\omega_{\mathbf{k}} t_0} , \\ & \frac{m}{\sqrt{\omega_{\mathbf{k}} L^n}} e^{-i\omega_{\mathbf{k}} t_0} u_{\mathbf{k},s}^A , \quad \frac{m}{\sqrt{\omega_{\mathbf{k}} L^n}} e^{-i\omega_{\mathbf{k}} t_0} \bar{v}_{\mathbf{k},s,A} \end{aligned} \quad (234)$$

to the amplitude [for the detector, quantized scalar fields, quantized spinor field particles and (massive) spinor field antiparticles from left to right and top to bottom]. Internal lines between vertices give (Fourier transformed) Feynman propagators as usual; for the detector, scalar

fields, and (massive) spinor fields from left to right:

$$\frac{2i\omega}{\omega^2 - \Omega^2 + i\epsilon} , \quad \frac{i}{k^2 - m^2 + i\epsilon} , \quad \frac{i[k+m]_B^A}{k^2 - m^2 + i\epsilon} . \quad (235)$$

Each vertex contributes $\tilde{f}(k)$ where k is the energy-momentum flowing into the vertex. Finally, all internal momenta (the ones in the propagators) need to be integrated or summed according to

$$\int_{-\infty}^{\infty} \frac{d\omega}{2\pi} , \quad \frac{1}{L^n} \sum_{\mathbf{k}} \int_{-\infty}^{\infty} \frac{dk^0}{2\pi} \quad (236)$$

for the detector (left) and the fields (right).

Let us now consider the factors associated with incoming quanta on one hand, and cases where two ladder operators are contracted, i.e., diagrammatically, when an incoming line is directly connected to an outgoing line. The contractions related to the first case are $\overline{\sigma^- \mu(t_i)} = \mathbf{1} e^{+i\Omega t_i}$ for the detector, $\overline{a_{\mathbf{k}} \cdots \Phi^\dagger(x)} = \mathbf{1} \varphi_{\mathbf{k}}^*(x)$ for a quantized real field, and so on. The exponential functions simply contribute to the Fourier transform of f , such that the incoming momenta appear in the momentum balance of the vertex they are attached to. The normalization factors and spinors are left over and assigned to the incoming diagram leg. Moreover, since we are working in the interaction picture, there is a time-dependent phase in addition to the ladder operator creating the state, for example,

$$|e; t_0\rangle = e^{+i\Omega t_0} |e\rangle , \quad |1_{\mathbf{k}}; t_0\rangle = e^{+i\omega_{\mathbf{k}} t_0} |1_{\mathbf{k}}\rangle . \quad (237)$$

Altogether, the incoming legs of the diagram contribute factors

$$\begin{aligned} & e^{+i\Omega t} , \quad \frac{1}{\sqrt{2\omega_{\mathbf{k}} L^n}} e^{+i\omega_{\mathbf{k}} t} , \\ & \frac{m}{\sqrt{\omega_{\mathbf{k}} L^n}} e^{+i\omega_{\mathbf{k}} t} \bar{u}_{\mathbf{k},s,A} , \quad \frac{m}{\sqrt{\omega_{\mathbf{k}} L^n}} e^{+i\omega_{\mathbf{k}} t} v_{\mathbf{k},s}^A \end{aligned} \quad (238)$$

in the same order as before.

If two ladder operators are contracted, they merely contribute Kronecker deltas ensuring that both are of the same type (momentum, spin) according to Eqs. (161), (170), (185) and (199). In the full amplitude, they additionally contribute phases from the interaction picture. For example, in case of a quantized real field:

$$\langle 1_{\mathbf{k}}, g; t | U^{(0)}(t, t_0) | 1_{\mathbf{p}}, g; t_0 \rangle = e^{-i\omega_{\mathbf{k}}(t-t_0)} \delta_{\mathbf{k},\mathbf{p}} . \quad (239)$$

Similar results hold for the monopole moment, and the remaining fields. Disconnected lines from the left to the right end of the diagram will thus contribute

$$e^{-i\Omega(t-t_0)} , \quad e^{-i\omega_{\mathbf{k}}(t-t_0)} \delta_{\mathbf{k},\mathbf{p}} , \quad e^{-i\omega_{\mathbf{k}}(t-t_0)} \delta_{\mathbf{k},\mathbf{p}} \delta_{s,r} \quad (240)$$

for the detector, quantized scalar fields, and quantized spinor fields, in that order.

The Feynman diagrams presented in this chapter, as well as the auxiliary diagrams in Sec. VID, do not contain lines for the detector in its ground state—in this they differ from the representations we used in Secs. III and IV and it differs from the diagrams used in [21]. The reason for this is that Feynman diagrams generally describe the energy-momentum flows involved in the interaction processes. The detectors (as macroscopic physical objects) do carry energy and momentum, but in the UDW-type detector models, only the excitations of its internal degree of freedom couple to the field. This is why lines are drawn not for the detector itself but instead for the excitation, i.e., for the quantum of energy, that the detector can carry.

B. Feynman rules for single detectors

We summarize the Feynman rules for all four UDW-type detector models considered in this work. The rules are applicable for detectors on Minkowski spacetime, the trajectory of the detector is determined by its spacetime profile f : if the spatial dependence varies with time in the restframe of the field, the detector is moving. Assume the field is initially in the number eigenstate $|a_i\rangle$ at time t_0 , and the detector in the state $|\beta_i\rangle$ (which may either be the ground state $|g\rangle$ or the excited state $|e\rangle$). The aim is to calculate the probability amplitude

$$\mathcal{A} = \langle a_f, \beta_f; t | U(t, t_0) | a_i, \beta_i; t_0 \rangle \quad (241)$$

for the detector to end up in the state $|\beta_f\rangle$ and the field in $|a_f\rangle$ at time $t > t_0$ to order λ^n in perturbation theory. In general, this is accomplished by combining the perturbative expansion Eqs. (25) and (26) of the time-evolution operator with the appropriate Wick theorem.

The calculations can be organized using a set of Feynman rules; the procedure itself is independent of the detector model and the type of field:

Generic Feynman rules. *In order to calculate a probability amplitude of the type Eq. (241) to order λ^n in perturbation theory, proceed as follows:*

1. *At a given order $k \leq n$, draw all possible Feynman diagrams using the rules appropriate for the detector model and field in question, as described in the following sections.*
2. *Evaluate the amplitude $\mathcal{A}_i^{(k)}$ of each diagram by first multiplying the factors associated with the individual parts of that diagram, and then summing (integrating) over all undetermined energies and momenta.*
3. *Sum up the amplitudes at order k : their contribution to the total amplitude \mathcal{A} is*

$$\mathcal{A}^{(k)} = \sum_i \mathcal{A}_i^{(k)} \quad (242)$$

4. *Repeat the above steps for every order $0 \leq k \leq n$,*

and add the resulting amplitudes to obtain \mathcal{A} :



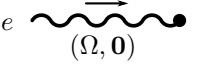
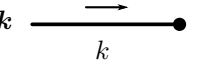
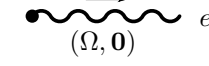
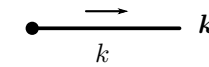
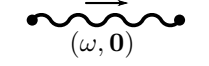
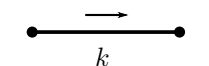
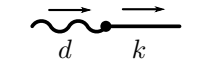
$$\mathcal{A} = \sum_{k=0}^n \frac{1}{k!} \mathcal{A}^{(k)} \quad (243)$$

The four sections below specify how to draw and evaluate the Feynman diagrams at a given order k for the different detector models and fields.

1. Linear coupling to quantized real fields

The Feynman diagrams for the detector model 1 coupling a single UDW-type detector to a quantized real field consist of the seven different types of elements listed below. Each element is associated with a factor in the amplitude $\mathcal{A}_i^{(k)}$ of an individual diagram. The corresponding factor is printed to the right of each element. Straight lines represent excitations of the quantized scalar field, wiggly lines excitations of the UDW-type detector.

Elements in Feynman diagrams.

- | | | |
|----|--|--|
| 1. |  | $e^{-i\Omega(t-t_0)}$ |
| 2. |  | $e^{-i\omega_k(t-t_0)} \delta_{\mathbf{k},\mathbf{p}}$ |
| 3. |  | $e^{+i\Omega t_0}$ |
| 4. |  | $\frac{1}{\sqrt{2\omega_k L^n}} e^{+i\omega_k t_0}$ |
| 5. |  | $e^{-i\Omega t}$ |
| 6. |  | $\frac{1}{\sqrt{2\omega_k L^n}} e^{-i\omega_k t}$ |
| 7. |  | $\frac{2i\omega}{\omega^2 - \Omega^2 + i\epsilon}$ |
| 8. |  | $\frac{i}{k^2 - m^2 + i\epsilon}$ |
| 9. |  | $(-i\lambda) \tilde{f}(d-k)$ |

Here,

$$\tilde{f}(d-k) = \int_{t_0}^t dx^0 \int_{\mathbb{R}^n} d\mathbf{x} f(x) e^{-ix(d-k)} \quad (244)$$

is the temporally cutoff Fourier transform of the detector's spacetime profile f . Momentum flowing into a vertex has sign $+1$ and is indicated by an arrow pointing towards

the vertex, momentum flowing out of a vertex has sign -1 and is indicated by an arrow pointing away from the vertex. Depending on the situation, the direction of any momentum in the vertex (element 9) could of course be reversed.

Constructing a Feynman diagram. *To construct a Feynman diagram at order k and evaluate its amplitude $\mathcal{A}_i^{(k)}$, adhere to the following rules:*

1. Draw a horizontal series of k vertices. These will be referred to as internal vertices.
2. If the detector is initially excited, $|\beta_i\rangle = |e\rangle$, draw a wiggly line entering the diagram from the left (element 3).
3. For every quantum in the initial state of the field $|a_i\rangle$, draw a plain line entering the diagram from the left (element 4).
4. If the detector is excited in the end, $|\beta_f\rangle = |e\rangle$, draw a wiggly line leaving the diagram on the right (element 5).
5. For every quantum in the final state of the field $|a_f\rangle$, draw a plain line leaving the diagram on the right (element 6).
6. Connect the ingoing lines with outgoing lines (elements 1 and 2) or vertices, and the remaining outgoing lines with vertices as well. Connect the vertices with each other (elements 7 and 8). In the end, each vertex has to have one detector line and one field line attached (element 9).
7. If this is impossible, $\mathcal{A}_i^{(k)} = 0$ and $\mathcal{A}^{(k)} = 0$.
8. Else, multiply the factors corresponding to the elements in the diagram, integrate over the momenta running in the propagators (elements 7 and 8) by

$$\int_{-\infty}^{\infty} \frac{d\omega}{2\pi}, \quad \frac{1}{L^n} \sum_{\mathbf{k}} \int_{-\infty}^{\infty} \frac{dk^0}{2\pi} \quad (245)$$

and finally take the limit $\epsilon \rightarrow 0$ for any propagator present to obtain the amplitude $\mathcal{A}_i^{(k)}$ of the diagram.

2. Quadratic coupling to quantized real fields

The Feynman rules for the detector model 2 coupling quadratically to quantized real fields through Eq. (85) (renormalized at leading order) are largely equal to the ones given in the previous section.

Elements in Feynman diagrams.

Having quadratic coupling instead of linear coupling merely changes the vertex, all other elements are identical to the ones listed in the previous section:

9'.  $(-i\lambda) \tilde{f}(d - k - p)$

Constructing a Feynman diagram. *Construction of a Feynman diagram at a given order k proceeds as before, with the exception of*

- 6'. [...] *In the end, each vertex has to have one detector line and two field lines attached (element 9').*


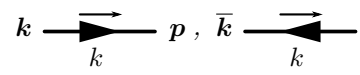
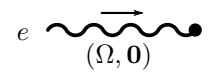
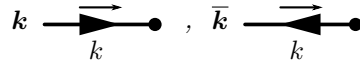
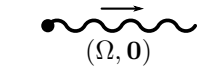
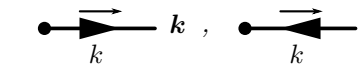
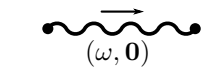
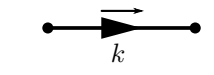
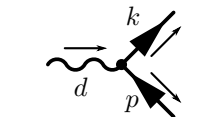
and the appearance of symmetry factors because each vertex corresponds to two identical field operators $\Phi(y_i)\Phi(y_i)$:

9. *Multiply the amplitude with the symmetry factor of the diagram (compare Sec. VID 3).*

3. Quadratic coupling to quantized complex fields

In case of the (leading order renormalized) model 3 and a quantized complex field, one additionally has to distinguish between particle and antiparticle quanta. Diagrammatically, this is achieved by turning field lines into arrows.

Elements in Feynman diagrams.

1.  $e^{-i\Omega(t-t_0)}$
2.  $e^{-i\omega_{\mathbf{k}}(t-t_0)} \delta_{\mathbf{k},\mathbf{p}}$
3.  $e^{+i\Omega t_0}$
4.  $\frac{1}{\sqrt{2\omega_{\mathbf{k}}L^n}} e^{+i\omega_{\mathbf{k}}t_0}$
5.  $e^{-i\Omega t}$
6.  $\frac{1}{\sqrt{2\omega_{\mathbf{k}}L^n}} e^{-i\omega_{\mathbf{k}}t}$
7.  $\frac{2i\omega}{\omega^2 - \Omega^2 + i\epsilon}$
8.  $\frac{i}{k^2 - m^2 + i\epsilon}$
9.  $(-i\lambda) \tilde{f}(d - k - p)$

Constructing a Feynman diagram. *For quantized complex fields, step 6. from Sec. VIII B 1 has to be amended once more:*


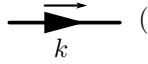
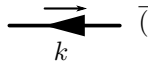
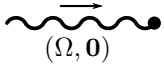


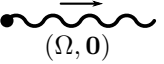
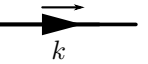
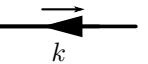
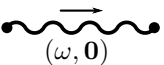
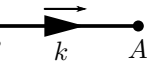
- 6'. [...] *In the end, each vertex has to have one detector line and two field lines attached (element 9'). Arrow directions must not collide.*

Unlike for the quantized real field, there is no need for introducing symmetry factors, since the two field operators underlying a vertex, $\Phi^\dagger(y_i)\Phi(y_i)$, are not identical (see Sec. VID 4).

4. Quadratic coupling to quantized spinor fields

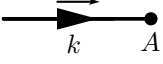

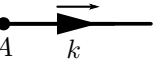
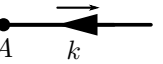
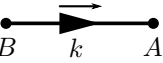
For a quantized spinor field coupled to an UDW-type detector through Eq. (84), the same elements appear, but are assigned different factors:

Elements in Feynman diagrams – massive field.

1. e  e $e^{-i\Omega(t-t_0)}$
2. (\mathbf{k}, s)  (\mathbf{p}, r) $e^{-i\omega_{\mathbf{k}}(t-t_0)} \delta_{\mathbf{k},\mathbf{p}} \delta_{s,r}$
3. $\overline{(\mathbf{k}, s)}$  $\overline{(\mathbf{p}, r)}$ $e^{-i\omega_{\mathbf{k}}(t-t_0)} \delta_{\mathbf{k},\mathbf{p}} \delta_{s,r}$
4. e  $e^{+i\Omega t_0}$
5. (\mathbf{k}, s)  $\frac{m}{\sqrt{\omega_{\mathbf{k}} L^n}} e^{+i\omega_{\mathbf{k}} t_0} u_{\mathbf{k},s}^A$
6. $\overline{(\mathbf{k}, s)}$  $\frac{m}{\sqrt{\omega_{\mathbf{k}} L^n}} e^{+i\omega_{\mathbf{k}} t_0} \bar{v}_{\mathbf{k},s,A}$
7.  e $e^{-i\Omega t}$
8. A  (\mathbf{k}, s) $\frac{m}{\sqrt{\omega_{\mathbf{k}} L^n}} e^{+i\omega_{\mathbf{k}} t_0} \bar{u}_{\mathbf{k},s,A}$
9. A  $\overline{(\mathbf{k}, s)}$ $\frac{m}{\sqrt{\omega_{\mathbf{k}} L^n}} e^{+i\omega_{\mathbf{k}} t_0} v_{\mathbf{k},s}^A$
10.  $\frac{2i\omega}{\omega^2 - \Omega^2 + i\epsilon}$
11. B  A $\frac{i[k+m]_B^A}{k^2 - m^2 + i\epsilon}$

When dealing with massless fields, the redefinition of the normalization factors in the mode functions (see Appendix A 2) requires redefinition of part of the Feynman rules just stated:

Elements in Feynman diagrams – massless field.

- 5'. (\mathbf{k}, s)  $\frac{1}{\sqrt{L^n}} e^{+i\omega_{\mathbf{k}} t_0} u_{\mathbf{k},s}^A$
- 6'. $\overline{(\mathbf{k}, s)}$  $\frac{1}{\sqrt{L^n}} e^{+i\omega_{\mathbf{k}} t_0} \bar{v}_{\mathbf{k},s,A}$
- 8'. A  (\mathbf{k}, s) $\frac{1}{\sqrt{L^n}} e^{+i\omega_{\mathbf{k}} t_0} \bar{u}_{\mathbf{k},s,A}$
- 9'. A  $\overline{(\mathbf{k}, s)}$ $\frac{1}{\sqrt{L^n}} e^{+i\omega_{\mathbf{k}} t_0} v_{\mathbf{k},s}^A$
- 11'. B  A $\frac{i k_B^A}{k^2 + i\epsilon}$

Constructing a Feynman diagram. For spinor fields, the steps from Sec. VIII B 3 are still applicable, but it is convenient keep track of spinor indices in addition:

- 1'. Draw a horizontal series of k vertices, and label each one with a spinor index A_i . These will be referred to as internal vertices.

Note that these rules do *not* provide the overall sign of the amplitude $\mathcal{A}_i^{(k)}$ of an individual diagram at order k . As for the auxiliary diagrams in Sec. VID, the sign is most easily determined by writing out the underlying contractions and reordering the operators explicitly.

C. Feynman rules for multiple detectors

For questions in relativistic quantum information theory, often two or more detectors coupled to the same quantum field F are considered. Each detector i has its own Hilbert space, and a monopole operator $\mu^{(i)}$ acting on it. For N detectors, the Hamiltonian of the entire system is

$$H = H_F + \sum_{i=1}^N H_d^{(i)} + H_{\text{int}}^{(i)} \quad (246)$$

where each $H_d^{(i)}$ is the Hamiltonian of a free detector as given in Eq. (5), and each detector by itself interacts with the field as before. The above Feynman rules readily generalize to such situations: each additional detector is equivalent to an additional monopole field $\mu^{(i)}(x)$. Because each of these has its own Hilbert space, quanta (and the corresponding lines in Feynman diagrams) of different detectors always need to be distinguished. Since there are only two fields (for linear coupling) or three fields (for quadratic coupling) present in each interaction Hamiltonian, there are still only two- or three-legged vertices, respectively. While direct interactions of the detectors

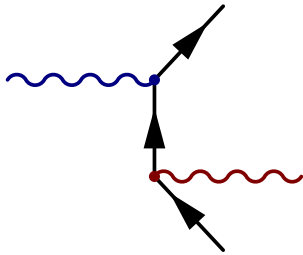


Figure 25. Example of a leading-order process involving two different detectors, blue and red (upper and lower wavy lines), quadratically interacting with a quantized complex or spinor field. Initially, the blue (upper) detector is excited. By exchange of a field quantum, the excitation is swapped to the red (lower) detector under emission of a particle-antiparticle pair.

do not occur in this model, they can of course interact indirectly through the quantum field they probe—Fig. 25 demonstrates such a process.

IX. CONCLUSIONS AND OUTLOOK

A key feature of Unruh-DeWitt detectors, i.e., of first quantized systems that are coupled to quantum fields, is that they can be localized in space and time. UDW detectors therefore provide an excellent tool for extracting spatiotemporal information from quantum fields, at least in gedanken experiments. So far, most studies have used the simplest kind of Unruh-DeWitt detectors, namely detectors that couple linearly to a bosonic real scalar field. The use of those Unruh-DeWitt detector models has yielded important results, for example about the Unruh and Hawking effects [2, 15, 50–52], and, more recently, about the extraction of entanglement from the vacuum and communication via quantum fields [4, 5].

These successes motivate the development of Unruh-DeWitt detector models also for the detection of quanta other than real scalar bosons, such as fermionic and complex quanta. There are pioneering studies in this direction [17, 20, 32, 33], but so far they have not gone further than the calculation of transition rates. Indeed, we found that a direct application of these models beyond the computation of transition rates leads to divergencies that cannot be regularized in the usual fashion, i.e., through spatial smearing and smooth switching functions.

Here, we introduced improved Unruh-DeWitt type detector models that cure these divergencies by means of renormalization. The new UDW detector models therefore possess the full versatility of the usual bosonic Unruh-DeWitt detectors. For example, they now allow for the investigation of the entanglement structure of the fermionic vacuum.

To this end, we started by analyzing the four different particle detector models summarized in Table I. We then

showed that, without further treatment, the vacuum excitation probability is already divergent at leading order in perturbation theory for the models 2-4, which are coupling quadratically in the field. These divergences cannot be regularized by the introduction of a spacetime profile (switching function and spatial smearing), unlike divergencies appearing in the case of the traditional linearly coupled UDW detector [13, 20, 34, 35].

We found the origin of these divergences to be the fact that the quadratic coupling gives rise to loop diagrams (see left side of Fig. 1) which are the exact equivalent of tadpole diagrams in quantum electrodynamics (QED) [45], with the detector playing the role of the electromagnetic field. Motivated by the analogy to QED we renormalized models 2-4 at leading order in perturbation theory by normal-ordering the interaction Hamiltonian. Physically, this corresponds to setting the (otherwise infinite) interaction energy to zero.

Finally, we derived Feynman rules for all four detector models in Sec. VIII. The Feynman rules allow for the systematic, graph-based calculation and renormalization of, for example, transition probabilities to arbitrary order, in the way familiar from particle physics.

With the Feynman rules for the various detector models at hand, one can now straightforwardly study the behaviors not only of bosonic but also of fermionic fields, for example, concerning the communication between two first quantized quantum systems (UDW detectors) via a quantum field, or the harvesting or farming of entanglement from the vacuum. In particular, the latter may now also allow one to develop quantitative tools to measure entanglement in the fermionic vacuum.

There are various further promising possibilities, in particular for applying the new renormalized detector model for spinor fields. Among others, this detector model can now be used to study the fermionic Unruh effect beyond the detector transition rates. This should allow one to study the universality and the thermalization of a detector in the fermionic Unruh effect [46] and to study possible finite time effects (see for instance [53]).

We also addressed the question of which bosonic detector model allows for a fair comparison with a fermionic model. We found that the leading order behavior of the renormalized models 3 and 4 can be compared on equal footing.

Finally, while UDW detectors are of great value for gedanken experiments, let us recall that the UDW detector for bosonic fields can be viewed as an idealization of a realistic system, such as the lowest two energy levels of an atom or molecule [27, 28]. The atom detects photons by internal excitation that can later be measured via standard experimental procedures. It should be interesting to explore to what extent the UDW detector for fermionic fields, model 4 in Table I, can also be viewed as a simple idealization of a realistic system, such as the optical cavity envisioned in the introduction, which would detect fermions through electromagnetic mode excitations. More generally, it should be interesting to further investigate

how the proposed detector models along with their mode selection and switching functions could find experimental realizations.

Appendix A: Notes on quantum fields

In this section, we summarize results of the classical and quantum field theory of scalar fields on Minkowski spacetime, as well as spinor fields on $\mathbb{R}^{1,1}$ and $\mathbb{R}^{1,3}$. All fields are spatially restricted to the cavity

$$B = [-L/2, L/2]^n \subset \mathbb{R}^n \quad (\text{A1})$$

with periodic boundary conditions

$$\Phi(t, \mathbf{x} + \boldsymbol{\delta}) = \Phi(t, \mathbf{x}) \quad \forall \boldsymbol{\delta} \in L \cdot \mathbb{Z}^n \quad (\text{A2})$$

The objective is to establish notation and provide a reference basis for the main body of this paper. These results are obtained in close analogy to the standard treatment of unrestricted fields, see e.g. [43, 47].

1. Scalar fields

a. Results in classical theory

Consider a real or complex field Φ on Minkowski spacetime. The dynamics of this field are determined by the Lagrangian densities

$$\begin{aligned} \mathcal{L}_\Phi &= \frac{1}{2}(\partial_\mu \Phi)(\partial^\mu \Phi) - \frac{1}{2}m^2 \Phi^2 \\ \mathcal{L}_\Phi^c &= (\partial_\mu \Phi^*)(\partial^\mu \Phi) - m^2 \Phi^* \Phi \end{aligned} \quad (\text{A3})$$

(for the real and the complex field, respectively), which both yield Klein-Gordon equation

$$(\partial_\mu \partial^\mu + m^2)\Phi(t, \mathbf{x}) = 0 \quad (\text{A4})$$

as equation of motion. A solution space to the Klein-Gordon equation is spanned by the family of mode functions

$$\tilde{\varphi}_{\mathbf{k}}(t, \mathbf{x}) = \frac{1}{\sqrt{2\omega_{\mathbf{k}}L^n}} e^{-ik \cdot x}, \quad (\text{A5})$$

where the momentum takes the following values:

$$\mathbf{k} \in 2\pi/L \cdot \mathbb{Z}^n. \quad (\text{A6})$$

The energy $\omega_{\mathbf{k}}$ is determined by the dispersion relation

$$\omega_{\mathbf{k}} = \sqrt{|\mathbf{k}|^2 + m^2}. \quad (\text{A7})$$

These mode functions have been normalized according to the condition

$$(\tilde{\varphi}_{\mathbf{k}}, \tilde{\varphi}_{\mathbf{p}}) = \delta_{\mathbf{k}, \mathbf{p}} \quad (\text{A8})$$

with respect to the Klein-Gordon product

$$\begin{aligned} (\Phi_1, \Phi_2) &\equiv -i \int_B \Phi_1(t, \mathbf{x}) [\partial_0 \Phi_2^*(t, \mathbf{x}) \\ &\quad - [\partial_0 \Phi_1(t, \mathbf{x})] \Phi_2^*(t, \mathbf{x})] d\mathbf{x}. \end{aligned} \quad (\text{A9})$$

It is useful to define purely spatial mode functions

$$\varphi_{\mathbf{k}}(\mathbf{x}) = \frac{1}{\sqrt{L^n}} e^{ik \cdot \mathbf{x}}. \quad (\text{A10})$$

These are orthonormal with respect to the L^2 -scalar product

$$\langle \varphi_{\mathbf{k}}, \varphi_{\mathbf{p}} \rangle = \int_B \varphi_{\mathbf{k}}^*(\mathbf{x}) \varphi_{\mathbf{p}}(\mathbf{x}) d\mathbf{x} = \delta_{\mathbf{k}, \mathbf{p}}. \quad (\text{A11})$$

To avoid cluttered notation, we will sometimes drop the tilde distinguishing time-dependent from time-independent mode functions.

b. Elements of canonical quantization

Canonical quantization of the free real field leads to the mode expansion

$$\Phi(t, \mathbf{x}) = \sum_{\mathbf{k}} a_{\mathbf{k}} \tilde{\varphi}_{\mathbf{k}}(t, \mathbf{x}) + a_{\mathbf{k}}^\dagger \tilde{\varphi}_{\mathbf{k}}^*(t, \mathbf{x}) \quad (\text{A12})$$

for the Heisenberg picture field operator in terms of the annihilators $a_{\mathbf{k}}$ and creators $a_{\mathbf{k}}^\dagger$. In the Schrödinger picture,

$$\Phi(\mathbf{x}) = \sum_{\mathbf{k}} \frac{1}{\sqrt{2\omega_{\mathbf{k}}}} [a_{\mathbf{k}} \varphi_{\mathbf{k}}(\mathbf{x}) + a_{\mathbf{k}}^\dagger \varphi_{\mathbf{k}}^*(\mathbf{x})]. \quad (\text{A13})$$

The field operator is self-adjointed, $\Phi^\dagger = \Phi$, and the ladder operators satisfy the canonical commutation relations

$$\begin{aligned} [a_{\mathbf{k}}, a_{\mathbf{p}}^\dagger] &= \mathbb{1} \delta_{\mathbf{k}, \mathbf{p}} \\ [a_{\mathbf{k}}, a_{\mathbf{p}}] &= 0 = [a_{\mathbf{k}}^\dagger, a_{\mathbf{p}}^\dagger]. \end{aligned} \quad (\text{A14})$$

After renormalizing the vacuum energy by normal-ordering, the dynamics of the system are determined by the Hamilton operator

$$H_\Phi = \sum_{\mathbf{k}} \omega_{\mathbf{k}} a_{\mathbf{k}}^\dagger a_{\mathbf{k}}. \quad (\text{A15})$$

Particle number eigenstates are created by acting on the vacuum state with creation operators

$$|(n_{\mathbf{k}})_{\mathbf{k}}\rangle = \prod_{\mathbf{k}} \frac{1}{\sqrt{n_{\mathbf{k}}!}} (a_{\mathbf{k}}^\dagger)^{n_{\mathbf{k}}} |0\rangle. \quad (\text{A16})$$

Creation operators commute, so their ordering is not relevant.

Quantization of the free complex field leads to the mode expansion

$$\Phi(t, \mathbf{x}) = \sum_{\mathbf{k}} \frac{1}{\sqrt{2\omega_{\mathbf{k}}}} \left[a_{\mathbf{k}} e^{-i\omega_{\mathbf{k}}t} \varphi_{\mathbf{k}}(\mathbf{x}) + b_{\mathbf{k}}^{\dagger} e^{+i\omega_{\mathbf{k}}t} \varphi_{\mathbf{k}}^*(\mathbf{x}) \right] \quad (\text{A17})$$

in the Heisenberg picture. The field operator is *not* self-adjoint, the ladder operators satisfy the canonical commutation relations

$$[a_{\mathbf{k}}, a_{\mathbf{p}}^{\dagger}] = \mathbf{1} \delta_{\mathbf{k}, \mathbf{p}}, \quad [b_{\mathbf{k}}, b_{\mathbf{p}}^{\dagger}] = \mathbf{1} \delta_{\mathbf{k}, \mathbf{p}}, \quad (\text{A18})$$

and all other commutators not yet fixed by these relations vanish. The Hamilton operator of the free complex field is

$$H = \sum_{\mathbf{k}} \omega_{\mathbf{k}} \left(a_{\mathbf{k}}^{\dagger} a_{\mathbf{k}} + b_{\mathbf{k}}^{\dagger} b_{\mathbf{k}} \right), \quad (\text{A19})$$

and particle number eigenstates are again generated by applying the creation operators on the vacuum. The complex field has $U(1)$ charge, so we need to distinguish between particle states created by a and antiparticle states created by b :

$$|(n_{\mathbf{k}})_{\mathbf{k}}, (\bar{n}_{\mathbf{p}})_{\mathbf{p}}\rangle = \prod_{\mathbf{k}} \frac{1}{\sqrt{n_{\mathbf{k}}!}} (a_{\mathbf{k}}^{\dagger})^{n_{\mathbf{k}}} \prod_{\mathbf{p}} \frac{1}{\sqrt{\bar{n}_{\mathbf{p}}!}} (b_{\mathbf{p}}^{\dagger})^{\bar{n}_{\mathbf{p}}} |0\rangle. \quad (\text{A20})$$

2. Spinor fields

a. Results in classical theory

Let Ψ be a spinor field on Minkowski spacetime $\mathbb{R}^{1,1}$ or $\mathbb{R}^{1,3}$, taking values in \mathbb{C}^4 as a representation space of the Clifford algebras $\text{Cliff}(1,1)$ or $\text{Cliff}(1,3)$, respectively. In $(1,3)$ dimensions we choose the irreducible Dirac representation, generated by the Dirac matrices

$$\gamma^0 = \begin{bmatrix} \mathbf{1}_2 & 0 \\ 0 & -\mathbf{1}_2 \end{bmatrix}, \quad \gamma^i = \begin{bmatrix} 0 & \sigma_i \\ -\sigma_i & 0 \end{bmatrix}, \quad (\text{A21})$$

where $\mathbf{1}_2$ is the two-dimensional identity matrix, and

$$\sigma_1 = \begin{pmatrix} 0 & 1 \\ 1 & 0 \end{pmatrix}, \quad \sigma_2 = \begin{pmatrix} 0 & -i \\ i & 0 \end{pmatrix}, \quad \sigma_3 = \begin{pmatrix} 1 & 0 \\ 0 & -1 \end{pmatrix} \quad (\text{A22})$$

are the Pauli matrices. The Dirac matrices satisfy the anticommutation relations

$$\{\gamma^{\mu}, \gamma^{\nu}\} = 2\eta^{\mu\nu} \mathbf{1}_2$$

for $\mu, \nu \in \{0, 1, 2, 3\}$, and therefore generate a representation of the Clifford algebra $\text{Cliff}(1,3)^{\mathbb{C}}$ on \mathbb{C}^4 . In $(1,1)$ dimensions, we use γ^0 and γ^3 to generate a (reducible)

representation of $\text{Cliff}(1,1)$ on \mathbb{C}^4 very similar to the Dirac representation.

The dynamics of the field are governed by the Lagrange density

$$\mathcal{L}_{\Psi} = \bar{\Psi} (i\gamma^{\mu} \partial_{\mu} - m) \Psi, \quad (\text{A23})$$

leading to the Dirac equation:

$$(i\gamma^{\mu} \partial_{\mu} - m) \Psi(t, \mathbf{x}) = 0. \quad (\text{A24})$$

Here γ^{μ} are the Dirac matrices. Solutions to the Dirac equation are linear combinations of the mode functions

$$\tilde{\psi}_{\mathbf{k},s,\epsilon}(t, \mathbf{x}) = \psi_{\mathbf{k},s,\epsilon}(\mathbf{x}) e^{-\epsilon i\omega_{\mathbf{k}}t}, \quad (\text{A25})$$

where $s \in \{-1/2, 1/2\}$ describes the spin degree of freedom, and \mathbf{k} and ϵ can take the same values as in Eq. (A6). These mode functions are taken to be normalized according to the condition

$$\langle \tilde{\psi}_{\mathbf{k},s,\epsilon}, \tilde{\psi}_{\mathbf{p},r,\delta} \rangle = \delta_{\mathbf{k},\mathbf{p}} \delta_{s,r} \delta_{\epsilon,\delta} = \langle \psi_{\mathbf{k},s,\epsilon}, \psi_{\mathbf{p},r,\delta} \rangle, \quad (\text{A26})$$

where we use the (generalized) scalar product

$$\langle \Psi_1, \Psi_2 \rangle \equiv \int_B \Psi_1^{\dagger}(t, \mathbf{x}) \Psi_2(t, \mathbf{x}) d\mathbf{x}. \quad (\text{A27})$$

Again, to lighten notation, we will sometimes drop the tilde if safely possible.

The solution of the Dirac equation in the cavity B can be accomplished in close analogy to the case of a free spinor field, a detailed treatment of the latter can e.g. be found in [43]. The actual form and the properties of the mode functions depend on the spatial dimension as well as on the mass parameter m .

(1,3) dimensions.— In case of a finite mass $m \neq 0$, the mode functions in three spatial dimensions can be decomposed as

$$\psi_{\mathbf{k},s,\epsilon}(\mathbf{x}) = \sqrt{\frac{m}{\omega_{\mathbf{k}} L^3}} u_{\mathbf{k},s,\epsilon} e^{+i\mathbf{k}\mathbf{x}}, \quad (\text{A28})$$

where the spatial dependence has been separated from the spinorial part. For the latter, we will use the well-established notation $u_{\mathbf{k},s,\epsilon=+1} = u_{\mathbf{k},s}$ and $u_{\mathbf{k},s,\epsilon=-1} = v_{\mathbf{k},s}$. Explicitly, they are

$$u_{\mathbf{k},s} = \sqrt{\frac{\omega_{\mathbf{k}} + m}{2m}} \begin{bmatrix} \xi_s \\ \frac{1}{\omega_{\mathbf{k}} + m} \left(\sum_{i=1}^3 \sigma^i k^i \right) \xi_s \end{bmatrix} \quad (\text{A29})$$

$$v_{\mathbf{k},s} = \sqrt{\frac{\omega_{\mathbf{k}} + m}{2m}} \begin{bmatrix} \frac{1}{\omega_{\mathbf{k}} + m} \left(\sum_{i=1}^3 \sigma^i k^i \right) \xi_s \\ \xi_s \end{bmatrix},$$

where σ^i are the Pauli matrices, and

$$\xi_{1/2} = \begin{pmatrix} 1 \\ 0 \end{pmatrix}, \quad \xi_{-1/2} = \begin{pmatrix} 0 \\ 1 \end{pmatrix} \quad (\text{A30})$$

are eigenvectors of σ^3 . Multiplying two spinors yields

$$\begin{aligned} \bar{u}_{\mathbf{k},s} u_{\mathbf{p},r} &= \frac{1}{2m} \left[\sqrt{(\omega_{\mathbf{k}} + m)(\omega_{\mathbf{p}} + m)} \right. \\ &\quad \left. - \frac{2si(k^1 p^2 - k^2 p^1) + \mathbf{k} \cdot \mathbf{p}}{\sqrt{(\omega_{\mathbf{k}} + m)(\omega_{\mathbf{p}} + m)}} \right] \delta_{s,r} \\ &\quad + \frac{1}{2m} \frac{2s(k^1 p^3 - k^3 p^1) - i(k^2 p^3 - k^3 p^2)}{\sqrt{(\omega_{\mathbf{k}} + m)(\omega_{\mathbf{p}} + m)}} \delta_{s,-r} \end{aligned} \quad (\text{A31})$$

$$\begin{aligned} \bar{u}_{\mathbf{k},s} v_{\mathbf{p},r} &= \frac{\sqrt{(\omega_{\mathbf{k}} + m)(\omega_{\mathbf{p}} + m)}}{2m} \\ &\quad \times \left[\left(\frac{2sp^3}{\omega_{\mathbf{p}} + m} - \frac{2sk^3}{\omega_{\mathbf{k}} + m} \right) \delta_{s,r} \right. \\ &\quad \left. + \left(\frac{p^1 - 2sip^2}{\omega_{\mathbf{p}} + m} - \frac{k^1 - 2sik^2}{\omega_{\mathbf{k}} + m} \right) \delta_{s,-r} \right] \end{aligned} \quad (\text{A32})$$

and

$$\bar{v}_{\mathbf{k},s} v_{\mathbf{p},r} = -\bar{u}_{\mathbf{k},s} u_{\mathbf{p},r} \quad (\text{A33})$$

$$\bar{v}_{\mathbf{k},s} u_{\mathbf{p},r} = -(\bar{u}_{\mathbf{k},s} v_{\mathbf{p},r})^* \quad (\text{A34})$$

The bar indicates the Dirac conjugate $\bar{u} = u^\dagger \gamma^0$ as usual. In particular, the normalization is chosen such that for $\mathbf{k} = \mathbf{p}$ all products simplify to

$$\bar{u}_{\mathbf{k},s,\epsilon} u_{\mathbf{k},r,\delta} = \epsilon \delta_{s,r} \delta_{\epsilon,\delta} \quad (\text{A35})$$

Moreover, products with the inverse order of spinors (such that they multiply to a 4×4 matrix) can be brought into a compact form as well:

$$\begin{aligned} \sum_s u_{\mathbf{k},s}^A \bar{u}_{\mathbf{k},s,B} &= \frac{1}{2m} [k \cdot \gamma + \mathbf{1}_4 m]_B^A \\ \sum_s v_{\mathbf{k},s}^A \bar{v}_{\mathbf{k},s,B} &= \frac{1}{2m} [k \cdot \gamma - \mathbf{1}_4 m]_B^A \end{aligned} \quad (\text{A36})$$

For vanishing mass $m = 0$, the mode functions

$$\psi_{\mathbf{k},s,\epsilon}(\mathbf{x}) = \frac{1}{\sqrt{L^3}} u_{\mathbf{k},s,\epsilon} e^{+i\mathbf{k} \cdot \mathbf{x}} \quad (\text{A37})$$

are simply the limit $m \rightarrow 0$ of Eq. (A28), but the normalization of the spinor parts is changed:

$$\begin{aligned} u_{\mathbf{k},s} &= \frac{1}{\sqrt{2}} \left[\frac{\xi_s}{|\mathbf{k}|} \left(\sum_{i=1}^3 \sigma^i k^i \right) \xi_s \right] \\ v_{\mathbf{k},s} &= \frac{1}{\sqrt{2}} \left[\frac{1}{|\mathbf{k}|} \left(\sum_{i=1}^3 \sigma^i k^i \right) \xi_s \right] \end{aligned} \quad (\text{A38})$$

This ensures that products of spinors are still finite. Explicitly,

$$\begin{aligned} \bar{u}_{\mathbf{k},s} u_{\mathbf{p},r} &= \\ &\quad \frac{1}{2} \left[1 - \frac{1}{|\mathbf{k}||\mathbf{p}|} (2si(k^1 p^2 - k^2 p^1) + \mathbf{k} \cdot \mathbf{p}) \right] \delta_{s,r} \\ &\quad + \frac{1}{2} \frac{1}{|\mathbf{k}||\mathbf{p}|} [2s(k^1 p^3 - k^3 p^1) - i(k^2 p^3 - k^3 p^2)] \delta_{s,-r} \end{aligned} \quad (\text{A39})$$

$$\begin{aligned} \bar{u}_{\mathbf{k},s} v_{\mathbf{p},r} &= \frac{1}{2} \left(\frac{2sp^3}{|\mathbf{p}|} - \frac{2sk^3}{|\mathbf{k}|} \right) \delta_{s,r} \\ &\quad \frac{1}{2} \left(\frac{p^1 - 2sip^2}{|\mathbf{p}|} - \frac{k^1 - 2sik^2}{|\mathbf{k}|} \right) \delta_{s,-r} \end{aligned} \quad (\text{A40})$$

$$\bar{v}_{\mathbf{k},s} v_{\mathbf{p},r} = -\bar{u}_{\mathbf{k},s} u_{\mathbf{p},r} \quad (\text{A41})$$

$$\bar{v}_{\mathbf{k},s} u_{\mathbf{p},r} = -(\bar{u}_{\mathbf{k},s} v_{\mathbf{p},r})^* \quad (\text{A42})$$

and for $\mathbf{k} = \mathbf{p}$ all products vanish:

$$\bar{u}_{\mathbf{k},s,\epsilon} u_{\mathbf{k},r,\delta} = 0 \quad (\text{A43})$$

Note that these products are *not* simply the limits $m \rightarrow 0$ of Eqs. (A32) and (A35). Finally,

$$\begin{aligned} \sum_s u_{\mathbf{k},s}^A \bar{u}_{\mathbf{k},s,B} &= \frac{1}{2|\mathbf{k}|} [k \cdot \gamma]_B^A \\ \sum_s v_{\mathbf{k},s}^A \bar{v}_{\mathbf{k},s,B} &= \frac{1}{2|\mathbf{k}|} [k \cdot \gamma]_B^A \end{aligned} \quad (\text{A44})$$

(1,1) dimension.— For finite mass $m \neq 0$, the mode functions can be decomposed as

$$\psi_{\mathbf{k},s,\epsilon}(x) = \sqrt{\frac{m}{\omega_{\mathbf{k}} L}} u_{\mathbf{k},s,\epsilon} e^{+i\mathbf{k} \cdot \mathbf{x}} \quad (\text{A45})$$

where the spinorial parts are

$$\begin{aligned} u_{\mathbf{k},s} &= \sqrt{\frac{\omega_{\mathbf{k}} + m}{2m}} \left[\frac{\xi_s}{\omega_{\mathbf{k}} + m} \sigma^3 \xi_s \right] \\ v_{\mathbf{k},s} &= \sqrt{\frac{\omega_{\mathbf{k}} + m}{2m}} \left[\frac{k}{\omega_{\mathbf{k}} + m} \sigma^3 \xi_s \right] \end{aligned} \quad (\text{A46})$$

Here, σ^3 is the third Pauli matrix. The products of spinors are

$$\begin{aligned} \bar{u}_{\mathbf{k},s} u_{\mathbf{p},r} &= \frac{\sqrt{(\omega_{\mathbf{k}} + m)(\omega_{\mathbf{p}} + m)}}{2m} \\ &\quad \times \left[1 - \frac{kp}{(\omega_{\mathbf{k}} + m)(\omega_{\mathbf{p}} + m)} \right] \delta_{s,r} \end{aligned} \quad (\text{A47})$$

$$\begin{aligned} \bar{u}_{\mathbf{k},s} v_{\mathbf{p},r} &= \frac{\sqrt{(\omega_{\mathbf{k}} + m)(\omega_{\mathbf{p}} + m)}}{2m} \\ &\quad \times \left(\frac{2sp}{\omega_{\mathbf{p}} + m} - \frac{2sk}{\omega_{\mathbf{k}} + m} \right) \delta_{s,r} \end{aligned} \quad (\text{A48})$$

$$\bar{v}_{k,s} v_{p,r} = -\bar{u}_{k,s} u_{p,r} \quad (\text{A49})$$

$$\bar{v}_{k,s} u_{p,r} = -\bar{u}_{k,s} v_{p,r} . \quad (\text{A50})$$

For $k = p$, all relations simplify to

$$\bar{u}_{k,s,\epsilon} u_{k,r,\delta} = \epsilon \delta_{s,r} \delta_{\epsilon,\delta} \quad (\text{A51})$$

as before. Finally,

$$\begin{aligned} \sum_s u_{\mathbf{k},s}^A \bar{u}_{\mathbf{k},s,B} &= \frac{1}{2m} [k_\mu \gamma^\mu + \mathbf{1}_4 m]_B^A \\ \sum_s v_{\mathbf{k},s}^A \bar{v}_{\mathbf{k},s,B} &= \frac{1}{2m} [k_\mu \gamma^\mu - \mathbf{1}_4 m]_B^A , \end{aligned} \quad (\text{A52})$$

where here $k_\mu \gamma^\mu = k^0 \gamma^0 - k^3 \gamma^3 \equiv \omega_{\mathbf{k}} \gamma^0 - k \gamma^3$.

In case of vanishing mass $m = 0$, the mode functions can be decomposed as

$$\psi_{k,s,\epsilon}(x) = \frac{1}{\sqrt{L}} u_{k,s,\epsilon} e^{+i k x} \quad (\text{A53})$$

with spinors

$$\begin{aligned} u_{k,s} &= \frac{1}{\sqrt{2}} \begin{bmatrix} \xi_s \\ \text{sgn } k \sigma^3 \xi_s \end{bmatrix} \\ v_{k,s} &= \frac{1}{\sqrt{2}} \begin{bmatrix} \text{sgn } k \sigma^3 \xi_s \\ \xi_s \end{bmatrix} . \end{aligned} \quad (\text{A54})$$

The products then read

$$\begin{aligned} \bar{u}_{k,s} u_{p,r} &= \frac{1}{2} [1 - \text{sgn}(kp)] \delta_{s,r} \\ \bar{u}_{k,s} v_{p,r} &= s [\text{sgn } p - \text{sgn } k] \delta_{s,r} \\ \bar{v}_{k,s} v_{p,r} &= -\bar{u}_{k,s} u_{p,r} \\ \bar{v}_{k,s} u_{p,r} &= -\bar{u}_{k,s} v_{p,r} , \end{aligned} \quad (\text{A55})$$

and for $k = p$ all products vanish like in four dimensions

$$\bar{u}_{k,s,\epsilon} u_{k,r,\delta} = 0 . \quad (\text{A56})$$

Lastly,

$$\begin{aligned} \sum_s u_{\mathbf{k},s}^A \bar{u}_{\mathbf{k},s,B} &= \frac{1}{2|k|} [k_\mu \gamma^\mu]_B^A \\ \sum_s v_{\mathbf{k},s}^A \bar{v}_{\mathbf{k},s,B} &= \frac{1}{2|k|} [k_\mu \gamma^\mu]_B^A . \end{aligned} \quad (\text{A57})$$

b. Elements of canonical quantization

Canonical quantization of the free spinor field results in the mode expansion

$$\Psi(t, \mathbf{x}) = \sum_{\mathbf{k},s} a_{\mathbf{k},s} \tilde{\psi}_{\mathbf{k},s,+}(t, \mathbf{x}) + b_{\mathbf{k},s}^\dagger \tilde{\psi}_{\mathbf{k},s,-}(t, \mathbf{x}) \quad (\text{A58})$$

in the Heisenberg picture, or

$$\Psi(\mathbf{x}) = \sum_{\mathbf{k},s} a_{\mathbf{k},s} \psi_{\mathbf{k},s,+}(\mathbf{x}) + b_{\mathbf{k},s}^\dagger \psi_{\mathbf{k},s,-}(\mathbf{x}) \quad (\text{A59})$$

in the Schrödinger picture. Here, $a_{\mathbf{k},s}$ and $b_{\mathbf{k},s}$ are particle and antiparticle ladder operators. They satisfy the canonical anticommutation relations

$$\{a_{\mathbf{k},s}, a_{\mathbf{p},r}^\dagger\} = \delta_{\mathbf{k},\mathbf{p}} \delta_{s,r} , \quad \{b_{\mathbf{k},s}, b_{\mathbf{p},r}^\dagger\} = \delta_{\mathbf{k},\mathbf{p}} \delta_{s,r} , \quad (\text{A60})$$

and all yet undetermined relations vanish. Again after renormalizing the vacuum energy, the Hamiltonian of the free spinor field is

$$H_\Psi = \sum_{\mathbf{k},s} \omega_{\mathbf{k}} \left(a_{\mathbf{k},s}^\dagger a_{\mathbf{k},s} + b_{\mathbf{k},s}^\dagger b_{\mathbf{k},s} \right) . \quad (\text{A61})$$

As before, particle number eigenstates are generated from the vacuum by application of creation operators. However, the order of the creation operators is now relevant, because they anticommute.

Appendix B: On the normalization of field modes

We briefly sketch why the mode functions of the scalar field are normalized with respect to Eq. (96), and those of the spinor field according to Eq. (97).

The underlying reason is that the Lagrange density of the free scalar field Φ given in Eq. (A3) contains a double time derivative of the field, which leads to the conjugate momentum $\Pi = \partial_0 \Phi$. The Lagrange density Eq. (A23) for spinor fields Ψ , on the other hand, only contains a single time derivative of the field, and leads to the conjugate momentum $\Pi = i\Psi^\dagger$. This in turn makes said normalization conditions necessary to ensure that the canonical (anti)commutation relations of the ladder operators are met. To make the connection evident, assume the modified relations

$$[a_{\mathbf{k}}, a_{\mathbf{p}}^\dagger] = \alpha \delta_{\mathbf{k},\mathbf{p}} , \quad \{a_{\mathbf{k},s}, a_{\mathbf{p},r}^\dagger\} = \alpha \delta_{\mathbf{k},\mathbf{p}} \delta_{s,r} , \quad (\text{B1})$$

and so on.

1. Scalar field

To see how the normalization arises naturally, quantize the scalar field directly in the Heisenberg picture. The task is to find a linear operator $\Phi(x)$ which (a) solves the Klein-Gordon equation

$$(\square + m^2)\Phi(x) = 0 \quad (\text{B2})$$

as an operator equation, (b) satisfies the usual commutation relations with its canonical conjugate field $\Pi = \partial_0 \Phi$, namely

$$[\Phi(x), \Pi(y)]|_{x_0=y_0} = i\delta(\mathbf{x} - \mathbf{y}) , \quad (\text{B3})$$

and (c) is self-adjoint:

$$\Phi^\dagger(x) = \Phi(x) , \quad \Pi^\dagger(x) = \Pi(x) . \quad (\text{B4})$$

In the first step, assume that Φ can be expanded in a Fourier series using the mode functions Eq. (A10):

$$\Phi(x) = \sum_{\mathbf{k}} \Phi_{\mathbf{k}}(t) \varphi_{\mathbf{k}}(\mathbf{x}) , \quad \Pi(x) = \sum_{\mathbf{k}} \Pi_{\mathbf{k}}(t) \varphi_{\mathbf{k}}(\mathbf{x}) , \quad (\text{B5})$$

where $\Pi_{\mathbf{k}}(t) = \partial_0 \Phi_{\mathbf{k}}(t)$. In the Fourier domain, the Klein-Gordon equation becomes

$$(\partial_0^2 + \omega_{\mathbf{k}}^2) \Phi_{\mathbf{k}}(t) \quad (\text{B6})$$

and the canonical commutation relations imply

$$[\Phi_{\mathbf{k}}(t), \Pi_{\mathbf{p}}^\dagger(t)] = i\delta_{\mathbf{k},\mathbf{p}} , \quad (\text{B7})$$

where we have already exploited that

$$\Phi_{\mathbf{k}}^\dagger(t) = \Phi_{-\mathbf{k}}(t) , \quad \Pi_{\mathbf{k}}^\dagger(t) = \Pi_{-\mathbf{k}}(t) . \quad (\text{B8})$$

Solving the problem now amounts to finding $\Phi_{\mathbf{k}}(t)$.

The next step is to make an ansatz for $\Phi_{\mathbf{k}}$:

$$\Phi_{\mathbf{k}}(t) = u_{\mathbf{k}}(t) a_{\mathbf{k}} + u_{-\mathbf{k}}^*(t) a_{-\mathbf{k}}^\dagger . \quad (\text{B9})$$

The $u_{\mathbf{k}}(t)$ are simply functions, while $a_{\mathbf{k}}$ are linear operators. The Klein-Gordon equation reduces to

$$(\partial_0^2 + \omega_{\mathbf{k}}^2) u_{\mathbf{k}}(t) = 0 , \quad (\text{B10})$$

which means that $u_{\mathbf{k}}$ is a linear combination of $e^{\pm i\omega_{\mathbf{k}}t}$. Requiring the commutation relations Eq. (B1) for the ladder operators, the commutation relations Eq. (B7) for the field lead to the condition

$$-i\alpha [u_{\mathbf{k}}(t)\partial_0 u_{\mathbf{k}}^*(t) - u_{\mathbf{k}}^*(t)\partial_0 u_{\mathbf{k}}(t)] = 1 . \quad (\text{B11})$$

In combination with $\langle \varphi_{\mathbf{p}} , \varphi_{\mathbf{k}} \rangle = \delta_{\mathbf{k},\mathbf{p}}$, we obtain

$$(\tilde{\varphi}_{\mathbf{k}} , \tilde{\varphi}_{\mathbf{p}}) = \frac{1}{\alpha} \delta_{\mathbf{k},\mathbf{p}} , \quad (\text{B12})$$

which, in case of the canonical commutation relations of the ladder operators $\alpha = 1$, is indeed the normalization condition Eq. (96).

2. Spinor field

A very similar analysis for spinor fields leads to the normalization Eq. (97) for spinor mode functions. This time, the task is to find a linear operators $\Psi(x)$ which (a) solves the Dirac equation

$$(i\gamma^\mu \partial_\mu - m)\Psi(x) = 0 \quad (\text{B13})$$

as an operator equation, and (b) satisfies the canonical anticommutation relations with its conjugate field $\Pi = i\Psi^\dagger$:

$$\{\Psi^A(x), \Pi_B(y)\}_{|_{x^0=y^0}} = i\delta(\mathbf{x} - \mathbf{y}) \delta_B^A . \quad (\text{B14})$$

The Hermitian conjugate of the field is automatically $\Psi_B^\dagger(x) = -i\Pi_B(x)$ by definition of Π .

Now assume once again that the operator can be expanded in a Fourier series

$$\begin{aligned} \Psi^A(x) &= \sum_{\mathbf{k}} \Psi_{\mathbf{k}}^A(t) \varphi_{\mathbf{k}}(\mathbf{x}) \\ \Pi_B(x) &= \sum_{\mathbf{k}} \Pi_{\mathbf{k},B}(t) \varphi_{\mathbf{k}}(\mathbf{x}) , \end{aligned} \quad (\text{B15})$$

where $\Pi_{\mathbf{k},B}(t) = i\Psi_{-\mathbf{k},B}^\dagger(t)$. Translated to the Fourier domain, the problem becomes the following: find a linear operator $\Psi_{\mathbf{k}}^A(t)$ that solves the differential equation

$$(i\gamma^0 \partial_0 + \gamma^i k_i - m)\Psi_{\mathbf{k}}^A(t) = 0 \quad (\text{B16})$$

and satisfies

$$\{\Psi_{\mathbf{k}}^A(t), \Pi_{-\mathbf{p},B}(t)\} = i\delta_{\mathbf{k},\mathbf{p}} \delta_B^A . \quad (\text{B17})$$

In the next step, make an ansatz that again separates the functional part from the operator part:

$$\begin{aligned} \Psi_{\mathbf{k}}^A(t) &= \sum_s u_{\mathbf{k},s}^A(t) a_{\mathbf{k},s} + v_{-\mathbf{k},s}^A(t) b_{-\mathbf{k},s}^\dagger \\ \Pi_{\mathbf{k},B}(t) &= i \sum_s v_{\mathbf{k},s,B}^\dagger(t) b_{\mathbf{k},s} + u_{-\mathbf{k},s,B}^\dagger(t) a_{-\mathbf{k},s}^\dagger . \end{aligned} \quad (\text{B18})$$

The Dirac equation then reduces to

$$\begin{aligned} (i\gamma^0 \partial_0 + \gamma^i k_i - m) u_{\mathbf{k},s}^A(t) &= 0 \\ (i\gamma^0 \partial_0 - \gamma^i k_i - m) v_{\mathbf{k},s}^A(t) &= 0 . \end{aligned} \quad (\text{B19})$$

The spinors Eq. (A29) that solve the classical Dirac equation satisfy

$$\begin{aligned} (\gamma^\mu k_\mu - m) u_{\mathbf{k},s} &= 0 \\ (\gamma^\mu k_\mu + m) v_{\mathbf{k},s} &= 0 , \end{aligned} \quad (\text{B20})$$

so it is easy to see that the above equations are solved by

$$\begin{aligned} u_{\mathbf{k},s}^A(t) &= C_s u_{\mathbf{k},s} e^{-i\omega_{\mathbf{k}}t} \\ v_{\mathbf{k},s}^A(t) &= D_s v_{\mathbf{k},s} e^{+i\omega_{\mathbf{k}}t} , \end{aligned} \quad (\text{B21})$$

where $C_s, D_s \in \mathbb{C}$. Our ansatz thus reads

$$\begin{aligned} \Psi_{\mathbf{k}}^A(t) &= \\ \sum_s C_s u_{\mathbf{k},s}^A e^{-i\omega_{\mathbf{k}}t} a_{\mathbf{k},s} &+ D_s v_{-\mathbf{k},s}^A e^{+i\omega_{\mathbf{k}}t} b_{-\mathbf{k},s}^\dagger . \end{aligned} \quad (\text{B22})$$

The anticommutation relations Eq. (B17), together with those for the ladder operators Eq. (B1), then lead to the condition

$$\alpha \sum_s C_s^2 u_{\mathbf{k},s}^A u_{\mathbf{k},r,B}^\dagger + D_s^2 v_{-\mathbf{k},s}^A v_{-\mathbf{k},r,B}^\dagger = \delta_B^A . \quad (\text{B23})$$

Direct computation shows that this condition is met for $C_s = D_s = \sqrt{m(\alpha\omega_{\mathbf{k}})^{-1}}$. The field operator thus enjoys the mode expansion

$$\Psi^A(x) = \sum_{\mathbf{k},s} \tilde{\psi}_{\mathbf{k},s,+}(x) a_{\mathbf{k},s} + \tilde{\psi}_{\mathbf{k},s,-}(x) b_{\mathbf{k},s}^\dagger \quad (\text{B24})$$

with mode functions

$$\begin{aligned}\tilde{\psi}_{\mathbf{k},s,+}(x) &= \sqrt{\frac{m}{\alpha\omega_{\mathbf{k}}L^n}} u_{\mathbf{k},s} e^{-ik\cdot x} \\ \tilde{\psi}_{\mathbf{k},s,-}(x) &= \sqrt{\frac{m}{\alpha\omega_{\mathbf{k}}L^n}} v_{\mathbf{k},s} e^{+ik\cdot x}.\end{aligned}\quad (\text{B25})$$

These satisfy

$$\langle \tilde{\psi}_{\mathbf{k},s,\epsilon}, \tilde{\psi}_{\mathbf{p},r,\delta} \rangle = \frac{1}{\alpha} \delta_{\mathbf{k},\mathbf{p}} \delta_{s,r} \delta_{\epsilon,\delta}, \quad (\text{B26})$$

and, choosing $\alpha = 1$, we finally obtain Eq. (97).

Appendix C: Proofs of Wick normal-ordering

1. Quantized scalar field

In this section, theorem VI.2 is proven on the basis of theorem VI.1. We already know from theorem VI.1 how to rewrite the time-ordered product of fields as a sum of normal-ordered products with more and more contractions. To normal-order the entire product and obtain the expression stated in the theorem, we therefore merely need to commute all creation operators from right to the very left, and all annihilation operators from the left to the very right. In doing so, we will pick up commutators, between ladder operators and fields as well as between the different ladder operators themselves. By theorem VI.1, the full product

$$(a_{\mathbf{p}})_{\mathbf{p}} (b_{\bar{\mathbf{p}}})_{\bar{\mathbf{p}}} [T\Phi^{\epsilon_1}(x_1) \cdots \Phi^{\epsilon_n}(x_n)] (a_{\mathbf{k}}^\dagger)_{\mathbf{k}} (b_{\bar{\mathbf{k}}}^\dagger)_{\bar{\mathbf{k}}}$$

can be reduced to a sum of products of the form

$$(a_{\mathbf{p}})_{\mathbf{p}} (b_{\bar{\mathbf{p}}})_{\bar{\mathbf{p}}} : \Phi^{\epsilon_1}(x_1) \cdots \Phi^{\epsilon_n}(x_n) : (a_{\mathbf{k}}^\dagger)_{\mathbf{k}} (b_{\bar{\mathbf{k}}}^\dagger)_{\bar{\mathbf{k}}}.$$

For these holds

Lemma C.1. *Using the notation of theorem VI.2, the following identity holds:*

$$\begin{aligned}(a_{\mathbf{p}})_{\mathbf{p}} (b_{\bar{\mathbf{p}}})_{\bar{\mathbf{p}}} : \Phi^{\epsilon_1}(x_1) \cdots \Phi^{\epsilon_n}(x_n) : (a_{\mathbf{k}}^\dagger)_{\mathbf{k}} (b_{\bar{\mathbf{k}}}^\dagger)_{\bar{\mathbf{k}}} \\ = : (a_{\mathbf{p}})_{\mathbf{p}} (b_{\bar{\mathbf{p}}})_{\bar{\mathbf{p}}} \Phi^{\epsilon_1}(x_1) \cdots \Phi^{\epsilon_n}(x_n) (a_{\mathbf{k}}^\dagger)_{\mathbf{k}} (b_{\bar{\mathbf{k}}}^\dagger)_{\bar{\mathbf{k}}} : \\ + \sum_{\substack{\text{single} \\ \text{contractions}}} : a_{\mathbf{p}_1} \cdots a_{\mathbf{p}_i} \cdots \overbrace{\Phi^{\epsilon_j}(x_j)} \cdots b_{\bar{\mathbf{k}}_N}^\dagger : \\ + \sum_{\substack{\text{double} \\ \text{contractions}}} \cdots.\end{aligned}\quad (\text{C1})$$

where contractions are only allowed between two ladder operators, and between a ladder operator and a field (not between two fields).

Proof of Lemma C.1. To achieve normal-ordering, the annihilation operators have to be moved past the field operators as well as the creation operators to the very right of

the expression. Then, the creation operators have to be commuted past the field operators to the very left. Recall the commutation relations of the ladder operators of the quantized complex field Eq. (A14), with all other pairings vanishing. In the first step, we need the resulting commutation relations between annihilation operators and the field parts. The four possible commutators are

$$\begin{aligned}[a_{\mathbf{k}}, \Phi(x)] &= 0, & [a_{\mathbf{k}}, \Phi^\dagger(x)] &= \mathbf{1} \varphi_{\mathbf{k}}^*(x), \\ [b_{\mathbf{k}}, \Phi(x)] &= \mathbf{1} \varphi_{\mathbf{k}}^*(x), & [b_{\mathbf{k}}, \Phi^\dagger(x)] &= 0.\end{aligned}\quad (\text{C2})$$

Consider the simplest case, when there is only one annihilation operator $a_{\mathbf{k}}$ on the left, and no annihilation operators on the right. To move $a_{\mathbf{k}}$ to the right, it has to be commuted with each and every field $\Phi^{\epsilon_i}(x_i)$ operator sooner or later—or more precisely with their constituent ladder operators. Each field operator decomposes into two part, one containing the annihilation operators, and the other the creation operators:

$$\begin{aligned}a_{\mathbf{k}} : \Phi^{\epsilon_1}(x_1) \cdots \Phi^{\epsilon_n}(x_n) : \\ = a_{\mathbf{k}} : \Phi^{\epsilon_1}(x_1) \cdots [\Phi_a^{\epsilon_i}(x_i) + \Phi_b^{\dagger\epsilon_i}(x_i)] \cdots \Phi^{\epsilon_n}(x_n) :.\end{aligned}\quad (\text{C3})$$

This decomposition can be done for all the other $n - 1$ field operators as well. The result are 2^{n-1} summands containing $\Phi_a^{\epsilon_i}$ as a factor (and all possible combinations of the parts of the other fields), and another set of 2^{n-1} summands containing $\Phi_b^{\dagger\epsilon_i}$ multiplied with the same set of combinations of parts of the other fields. Let us pick one such set and call it S for brevity. For example, S might be

$$S = \Phi_a^{\epsilon_1}(x_1) \cdots \Phi_a^{\epsilon_{i-1}}(x_{i-1}) \widehat{\Phi_a^{\epsilon_i}(x_i)} \Phi_a^{\epsilon_{i+1}}(x_{i+1}) \cdots \Phi_a^{\epsilon_n}(x_n).$$

Note that

$$\sum_S S = : \Phi^{\epsilon_1}(x_1) \cdots \widehat{\Phi^{\epsilon_i}(x_i)} \cdots \Phi^{\epsilon_n}(x_n) : , \quad (\text{C4})$$

where the term with hat is omitted. Since the entire product is normal-ordered at the end, $\Phi_a^{\epsilon_i}$ and $\Phi_b^{\dagger\epsilon_i}$ will end up at different positions inside S :

$$\begin{aligned}: \Phi^{\epsilon_1}(x_1) \cdots \Phi^{\epsilon_n}(x_n) : \\ = \sum_S \left[S_1 \Psi_a^{\epsilon_i}(x_i) S_2 + S_1^* \Psi_b^{\dagger\epsilon_i}(x_i) S_2^* \right],\end{aligned}\quad (\text{C5})$$

where S_i, S_i^* are two different partitions of S : $S_1 S_2 = S$ and $S_1^* S_2^* = S$. Thus,

$$\begin{aligned}a_{\mathbf{k}} : \Phi^{\epsilon_1}(x_1) \cdots \Phi^{\epsilon_n}(x_n) : \\ = \cdots + a_{\mathbf{k}} S_1 \Phi^{\epsilon_i}(x_i) S_2 + a_{\mathbf{k}} S_1^* \Phi_b^{\dagger\epsilon_i}(x_i) S_2^* + \cdots.\end{aligned}\quad (\text{C6})$$

We now start moving $a_{\mathbf{k}}$ to the right, and the contribution from $\Phi(x_i)$ will be the following: $a_{\mathbf{k}}$ is commuted through S_1 (creating an additional term containing the commutator with other field parts in each step), and will

eventually end up next to $\Phi^{\epsilon_i}(x_i)$. Commuting $a_{\mathbf{k}}$ and $\Phi^{\epsilon_i}(x_i)$ gives two terms

$$S_1 a_{\mathbf{k}} \Phi^{\epsilon_i}(x_i) S_2 = [a_{\mathbf{k}}, \Phi^{\epsilon_i}(x_i)] S + S_1 a_{\mathbf{k}} \Phi^{\epsilon_i}(x_i) S_2, \quad (\text{C7})$$

where we have used that the commutator is proportional to the identity operator $\mathbf{1}$ in any case. The same is true for the second term containing $\Phi_b^{\dagger \epsilon_i}$:

$$\begin{aligned} S_1^* a_{\mathbf{k}} \Phi_b^{\dagger \epsilon_i}(x_i) S_2^* \\ = [a_{\mathbf{k}}, \Phi_b^{\dagger \epsilon_i}(x_i)] S + S_1^* a_{\mathbf{k}} \Phi_b^{\dagger \epsilon_i}(x_i) S_2^*. \end{aligned} \quad (\text{C8})$$

After combining the two commutators one obtains

$$\begin{aligned} a_{\mathbf{k}} : \Phi^{\epsilon_1}(x_1) \cdots \Phi^{\epsilon_n}(x_n) : \\ = \cdots + [a_{\mathbf{k}}, \Phi^{\epsilon_i}(x_i)] S + S_1 \Phi^{\epsilon_i}(x_i) a_{\mathbf{k}} S_2 \\ + S_1^* \Phi_b^{\dagger \epsilon_i}(x_i) a_{\mathbf{k}} S_2^* + \cdots. \end{aligned} \quad (\text{C9})$$

All the terms containing commutators with the other fields have not been made explicit. Since this works for any combination S of the ladder operators of the other fields, the sum of all these will just give

$$[a_{\mathbf{k}}, \Phi^{\epsilon_i}(x_i)] : \Phi^{\epsilon_1}(x_1) \cdots \widehat{\Phi^{\epsilon_i}(x_i)} \cdots \Phi^{\epsilon_n}(x_n) : \quad (\text{C10})$$

from the first term according to Eq. (C4). The other two terms need to be processed further, giving rise to commutators with the other fields. In the end, after commuting $a_{\mathbf{k}}$ all the way through S there will be a commutator term like the above for every field, and a term which yields

$$\begin{aligned} \sum_S \left[S_1 \Psi_a^{\epsilon_i}(x_i) S_2 + S_1^* \Psi_b^{\dagger \epsilon_i}(x_i) S_2^* \right] a_{\mathbf{k}} \\ = : \Phi^{\epsilon_1}(x_1) \cdots \Phi^{\epsilon_n}(x_n) : a_{\mathbf{k}} \\ = : a_{\mathbf{k}} \Phi^{\epsilon_1}(x_1) \cdots \Phi^{\epsilon_n}(x_n) : \end{aligned} \quad (\text{C11})$$

according to Eq. (C5). By virtue of the commutators Eq. (C2) and the definition Eq. (162) of the contractions, we finally obtain

$$\begin{aligned} a_{\mathbf{k}} : \Phi^{\epsilon_1}(x_1) \cdots \Phi^{\epsilon_n}(x_n) : = : a_{\mathbf{k}} \Phi^{\epsilon_1}(x_1) \cdots \Phi^{\epsilon_n}(x_n) : \\ + \sum_{i=1}^n : \overbrace{a_{\mathbf{k}} \Phi^{\epsilon_1}(x_1) \cdots \Phi^{\epsilon_i}(x_i) \cdots \Phi^{\epsilon_n}(x_n)} : . \end{aligned} \quad (\text{C12})$$

Since it was nowhere used that a is a particle annihilation operator, the same relation holds for antiparticle annihilation operators b .

Now, if there is a single creation operator on the right instead, the relevant commutation relations are:

$$\begin{aligned} [\Phi(x), a_{\mathbf{k}}^\dagger] = \mathbf{1} \varphi_{\mathbf{k}}(x), \quad [\Phi^\dagger(x), a_{\mathbf{k}}^\dagger] = 0, \\ [\Phi(x), b_{\mathbf{k}}^\dagger] = 0, \quad [\Phi^\dagger(x), b_{\mathbf{k}}^\dagger] = \mathbf{1} \varphi_{\mathbf{k}}(x), \end{aligned} \quad (\text{C13})$$

and a similar reasoning eventually gives

$$\begin{aligned} : \Phi^{\epsilon_1}(x_1) \cdots \Phi^{\epsilon_n}(x_n) : a_{\mathbf{p}}^\dagger = : \Phi^{\epsilon_1}(x_1) \cdots \Phi^{\epsilon_n}(x_n) a_{\mathbf{p}}^\dagger : \\ + \sum_{i=1}^n : \Phi^{\epsilon_1}(x_1) \cdots \overbrace{\Phi^{\epsilon_i}(x_i) \cdots \Phi^{\epsilon_n}(x_n)} : a_{\mathbf{p}}^\dagger \end{aligned} \quad (\text{C14})$$

in terms of the contractions Eq. (162).

If both types are present, Eq. (C12) immediately allows to write:

$$\begin{aligned} a_{\mathbf{k}} : \Phi^{\epsilon_1}(x_1) \cdots \Phi^{\epsilon_n}(x_n) : a_{\mathbf{p}}^\dagger \\ = : \Phi^{\epsilon_1}(x_1) \cdots \Phi^{\epsilon_n}(x_n) : a_{\mathbf{k}} a_{\mathbf{p}}^\dagger \\ + \sum_{i=1}^n : \overbrace{a_{\mathbf{k}} \Phi^{\epsilon_1}(x_1) \cdots \Phi^{\epsilon_i}(x_i) \cdots \Phi^{\epsilon_n}(x_n)} : a_{\mathbf{p}}^\dagger. \end{aligned} \quad (\text{C15})$$

The first term on the right-hand side evaluates to

$$\begin{aligned} : \Phi^{\epsilon_1}(x_1) \cdots \Phi^{\epsilon_n}(x_n) : a_{\mathbf{p}}^\dagger a_{\mathbf{k}} : \\ + : \overbrace{a_{\mathbf{k}} \Phi^{\epsilon_1}(x_1) \cdots \Phi^{\epsilon_n}(x_n)} : a_{\mathbf{p}}^\dagger \end{aligned} \quad (\text{C16})$$

using the contractions Eq. (161). The second term in Eq. (C15), as well as the first term in Eq. (C16) can then be evaluated using Eq. (C14). In total, one obtains

$$\begin{aligned} a_{\mathbf{k}} : \Phi^{\epsilon_1}(x_1) \cdots \Phi^{\epsilon_n}(x_n) : a_{\mathbf{p}}^\dagger = : a_{\mathbf{k}} \Phi^{\epsilon_1}(x_1) \cdots \Phi^{\epsilon_n}(x_n) a_{\mathbf{p}}^\dagger : \\ + \sum_{i=1}^n : \overbrace{a_{\mathbf{k}} \Phi^{\epsilon_1}(x_1) \cdots \Phi^{\epsilon_i}(x_i) \cdots \Phi^{\epsilon_n}(x_n)} : a_{\mathbf{p}}^\dagger : \\ + : \overbrace{a_{\mathbf{k}} \Phi^{\epsilon_1}(x_1) \cdots \Phi^{\epsilon_n}(x_n)} : a_{\mathbf{p}}^\dagger : \\ + \sum_{i=1}^n : a_{\mathbf{k}} \Phi^{\epsilon_1}(x_1) \cdots \overbrace{\Phi^{\epsilon_i}(x_i) \Phi^{\epsilon_n}(x_n)} \cdots : a_{\mathbf{p}}^\dagger : \\ + \sum_{i=1}^n \sum_{\substack{j=1 \\ j \neq i}}^n : \overbrace{a_{\mathbf{k}} \Phi^{\epsilon_1}(x_1) \cdots \Phi^{\epsilon_j}(x_j) \cdots \Phi^{\epsilon_i}(x_i) \cdots \Phi^{\epsilon_n}(x_n)} : a_{\mathbf{p}}^\dagger : . \end{aligned} \quad (\text{C17})$$

Repeated application of Eqs. (C12) and (C14) finally yields Eq. (C1) in the general case. \square

Proof of Theorem VI.2. Combining theorem VI.1 and lemma C.1 directly allows one to express

$$(a_{\mathbf{p}})_{\mathbf{p}} (b_{\bar{\mathbf{p}}})_{\bar{\mathbf{p}}} [T \Phi^{\epsilon_1}(x_1) \cdots \Phi^{\epsilon_n}(x_n)] (a_{\mathbf{k}}^\dagger)_{\mathbf{k}} (b_{\bar{\mathbf{k}}}^\dagger)_{\bar{\mathbf{k}}}$$

as normal-ordered, plus sums of the same normal-ordered products with all the contractions (single, double, ... fully contracted), defined in Eqs. (155), (161) and (162). If the vacuum expectation value is taken, all terms which still contain uncontracted normal-ordered operators vanish. If the total number of operators (ladder operators and field operators) is odd, there will be at least one normal-ordered operator remaining and all terms vanish. Only if the number of operators is even, the terms where all operators are contracted survives since all the contractions are proportional to the identity operator. Note that some or all of these surviving terms can still be zero, since many of the contractions also vanish. \square

2. Quantized spinor field

We now prove theorem VI.5. Analogous to the proof of theorem VI.2, we first prove the following

Lemma C.2. *Using the notation of theorem VI.5, the following identity holds:*

$$\begin{aligned}
& (a_{\mathbf{p},r})_{\mathbf{p},r} (b_{\bar{\mathbf{p}},\bar{r}})_{\bar{\mathbf{p}},\bar{r}} : \Psi^{\epsilon_1}(x_1) \cdots \\
& \cdots \Psi^{\epsilon_n}(x_n) : (a_{\mathbf{k},s}^\dagger)_{\mathbf{k},s} (b_{\bar{\mathbf{k}},\bar{s}}^\dagger)_{\bar{\mathbf{k}},\bar{s}} \\
& = : (a_{\mathbf{p},r})_{\mathbf{p},r} (b_{\bar{\mathbf{p}},\bar{r}})_{\bar{\mathbf{p}},\bar{r}} \Psi^{\epsilon_1}(x_1) \cdots \\
& \cdots \Psi^{\epsilon_n}(x_n) (a_{\mathbf{k},s}^\dagger)_{\mathbf{k},s} (b_{\bar{\mathbf{k}},\bar{s}}^\dagger)_{\bar{\mathbf{k}},\bar{s}} : \\
& + \sum_{\substack{\text{single} \\ \text{contractions}}} : a_{(\mathbf{p},r)_1} \cdots a_{(\mathbf{p},r)_i} \cdots \overbrace{\Psi^{\epsilon_j}(x_j)} \cdots b_{(\bar{\mathbf{k}},\bar{s})_{\bar{N}}}^\dagger : \\
& + \sum_{\substack{\text{double} \\ \text{contractions}}} \cdots . \tag{C18}
\end{aligned}$$

where contractions are only allowed between two ladder operators, and between a ladder operator and a field (not between two fields).

The proof is very similar to the proof of lemma C.1, but with the additional complexity that one has to keep track of signs introduced by anticommuting the involved operators.

Proof of Lemma C.2. To achieve normal-ordering, the annihilation operators have to be moved past the field operators and the creation operators to the right, and the creation operators subsequently past the fields to the left. Recall the anticommutation relations between the ladder operators Eq. (A60), with all remaining anticommutators vanishing. For the first step, we need to know how the annihilation operators anticommute with the fields. From the above relations and the separation of the spinor field according to Eqs. (173) and (174) one obtains:

$$\begin{aligned}
\{a_{\mathbf{k},s}, \Psi(x)\} &= 0, \quad \{a_{\mathbf{k},s}, \bar{\Psi}(x)\} = \mathbf{1} \bar{\psi}_{\mathbf{k},s,+}(x), \\
\{b_{\mathbf{k},s}, \bar{\Psi}(x)\} &= 0, \quad \{b_{\mathbf{k},s}, \Psi(x)\} = \mathbf{1} \psi_{\mathbf{k},s,-}(x). \tag{C19}
\end{aligned}$$

Let us begin with one annihilation operator on the left: to move it to the right, it has to be anticommutated with any field operator $\Psi^{\epsilon_i}(x_i)$ at some point, picking up an anticommutator in the process. Each field operator decomposes into two parts, one containing the creation operators, one the annihilation operators

$$\begin{aligned}
a_{\mathbf{k},s} : \Psi^{\epsilon_1}(x_1) \cdots \Psi^{\epsilon_i}(x_i) \cdots \Psi^{\epsilon_n}(x_n) : \\
= a_{\mathbf{k},s} : \Psi^{\epsilon_1}(x_1) \cdots [\Psi_a^{\epsilon_i}(x_i) + \Psi_b^{\epsilon_i}(x_i)] \cdots \Psi^{\epsilon_n}(x_n) : . \tag{C20}
\end{aligned}$$

The same can be done for the other fields, and we essentially end up with sums of products of ladder operators (with sums in front, and multiplied mode functions), where each term contains one ladder operator per field. Let us

pick out one of these products of ladder operators from the field $\Psi^{\epsilon_1}(x_1), \dots, \Psi^{\epsilon_n}(x_n)$ without $\Psi^{\epsilon_i}(x_i)$ and denote it S for brevity. Both parts of $\Psi^{\epsilon_i}(x_i)$ are multiplied with S , but since the entire product of field operators is then normal-ordered, the position where they are inserted into S will be different. Through normal-ordering, $\Psi_a^{\epsilon_i}(x_i)$ will be shifted from position i to some position $i+m$, picking up a sign $(-1)^m$, and $\Psi_b^{\epsilon_i}(x_i)$ will be shifted from position i to some other position $i+l$, picking up a sign $(-1)^l$. Therefore,

$$\begin{aligned}
a_{\mathbf{k},s} : \Psi^{\epsilon_1}(x_1) \cdots \Psi^{\epsilon_i}(x_i) \cdots \Psi^{\epsilon_n}(x_n) : \\
= \cdots + a_{\mathbf{k},s} (-1)^m S_1 \Psi_a^{\epsilon_i}(x_i) S_2 \\
+ a_{\mathbf{k},s} (-1)^l S_1^* \Psi_b^{\epsilon_i}(x_i) S_2^* + \dots, \tag{C21}
\end{aligned}$$

where $S_1 S_2 = S = S_1^* S_2^*$. Consider the first term, containing $\Psi_a^{\epsilon_i}(x_i)$: the ladder operator $a_{\mathbf{k},s}$ is successively anticommutated through the operators of S_1 , creating an additional term containing the anticommutator, and picking up a sign for $a_{\mathbf{k},s}$ in each step. By the time $a_{\mathbf{k},s}$ reaches $\Psi_a^{\epsilon_i}(x_i)$, it already had to be anticommutated through the $(i+m-1)$ normal-ordered ladder operators in S_1 and has therefore picked up a sign $(-1)^{i+m-1}$, which leaves us with an overall sign $(-1)^{i+2m-1} = (-1)^{i-1}$. Anticommuting $a_{\mathbf{k},s}$ and $\Psi_a^{\epsilon_i}(x_i)$, we get two terms:

$$\begin{aligned}
(-1)^{i-1} S_1 a_{\mathbf{k},s} \Psi_a^{\epsilon_i}(x_i) S_2 \\
= (-1)^{i-1} \{a_{\mathbf{k},s}, \Psi_a^{\epsilon_i}(x_i)\} S - \\
(-1)^{i-1} S_1 \Psi_a^{\epsilon_i}(x_i) a_{\mathbf{k},s} S_2, \tag{C22}
\end{aligned}$$

where we have used the fact that the anticommutator is proportional to the identity operator in any case, and can therefore be pulled in front of the product $S_1 S_2 = S$. The same argumentation works on the second term, $\Psi_b^{\epsilon_i}(x_i)$, and we obtain

$$\begin{aligned}
(-1)^{i-1} S_1^* a_{\mathbf{k},s} \Psi_b^{\epsilon_i}(x_i) S_2^* \\
= (-1)^{i-1} \{a_{\mathbf{k},s}, \Psi_b^{\epsilon_i}(x_i)\} S \\
- (-1)^{i-1} S_1^* \Psi_b^{\epsilon_i}(x_i) a_{\mathbf{k},s} S_2^*. \tag{C23}
\end{aligned}$$

The two anticommutators can be combined to

$$\{a_{\mathbf{k},s}, \Psi_a^{\epsilon_i}(x_i)\} + \{a_{\mathbf{k},s}, \Psi_b^{\epsilon_i}(x_i)\} = \{a_{\mathbf{k},s}, \Psi^{\epsilon_i}(x_i)\} \tag{C24}$$

such that Eq. (C21) becomes

$$\begin{aligned}
a_{\mathbf{k},s} : \Psi^{\epsilon_1}(x_1) \cdots \Psi^{\epsilon_i}(x_i) \cdots \Psi^{\epsilon_n}(x_n) : \\
= \cdots + (-1)^i S_1 \Psi_a^{\epsilon_i}(x_i) a_{\mathbf{k},s} S_2 + (-1)^i S_1^* \Psi_b^{\epsilon_i}(x_i) a_{\mathbf{k},s} S_2^* \\
+ (-1)^{i-1} \{a_{\mathbf{k},s}, \Psi^{\epsilon_i}(x_i)\} S + \dots. \tag{C25}
\end{aligned}$$

We have not written out the anticommutators $a_{\mathbf{k},s}$ has picked up with the operators in S_1 and S_1^* . Since this needs to be done for any of the field operators, we end

up with

$$\begin{aligned}
a_{\mathbf{k},s} : \Psi^{\epsilon_1}(x_1) \cdots \Psi^{\epsilon_n}(x_n) : \\
&= (-1)^n : \Psi^{\epsilon_1}(x_1) \cdots \Psi^{\epsilon_n}(x_n) : a_{\mathbf{k},s} \\
&+ \sum_{i=1}^n (-1)^{i-1} \{a_{\mathbf{k},s}, \Psi^{\epsilon_i}(x_i)\} : \Psi^{\epsilon_1}(x_1) \cdots \\
&\quad \cdots \widehat{\Psi^{\epsilon_i}(x_i)} \cdots \Psi^{\epsilon_n}(x_n) : . \quad (\text{C26})
\end{aligned}$$

The first term on the right-hand side is normal-ordered, and the sign can be absorbed into anticommuting the annihilation operator back to the beginning of the product. The second term can be rewritten by taking into account the anticommutation relations Eq. (C19) and defining contractions like in Eq. (186)

$$\begin{aligned}
a_{\mathbf{k},s} : \Psi^{\epsilon_1}(x_1) \cdots \Psi^{\epsilon_n}(x_n) : &=: a_{\mathbf{k},s} \Psi^{\epsilon_1}(x_1) \cdots \Psi^{\epsilon_n}(x_n) : \\
&+ \sum_{i=1}^n : \overbrace{a_{\mathbf{k},s} \Psi^{\epsilon_1}(x_1) \cdots \Psi^{\epsilon_i}(x_i)} : \cdots \Psi^{\epsilon_n}(x_n) : . \quad (\text{C27})
\end{aligned}$$

Note in particular that the sign is absorbed into the definition of the contraction. Since we have nowhere used that a is a particle annihilation operator, the same identity holds for antiparticle annihilation operators b .

Now consider what happens if a creation operator is added at the right. Using the last two equations, we can immediately write

$$\begin{aligned}
a_{\mathbf{k},s} : \Psi^{\epsilon_1}(x_1) \cdots \Psi^{\epsilon_n}(x_n) : a_{\mathbf{p},r}^\dagger \\
&= (-1)^n : \Psi^{\epsilon_1}(x_1) \cdots \Psi^{\epsilon_n}(x_n) : a_{\mathbf{k},s} a_{\mathbf{p},r}^\dagger \\
&+ \sum_{i=1}^n : \overbrace{a_{\mathbf{k},s} \Psi^{\epsilon_1}(x_1) \cdots \Psi^{\epsilon_i}(x_i)} a_{\mathbf{p},r}^\dagger \Psi^{\epsilon_n}(x_n) : a_{\mathbf{p},r}^\dagger . \quad (\text{C28})
\end{aligned}$$

Taking into account the anticommutation relations between the ladder operators and defining contractions Eq. (185), the first term on the right-hand side can be expressed as

$$\begin{aligned}
&: \overbrace{a_{\mathbf{k},s} \Psi^{\epsilon_1}(x_1) \cdots \Psi^{\epsilon_n}(x_n)} a_{\mathbf{p},r}^\dagger : \\
&+ (-1)^{n+1} : \Psi^{\epsilon_1}(x_1) + \cdots \Psi^{\epsilon_n}(x_n) : a_{\mathbf{p},r}^\dagger a_{\mathbf{k},s} . \quad (\text{C29})
\end{aligned}$$

To handle the remaining terms, we need to evaluate expressions of the form

$$: \Psi^{\epsilon_1}(x_1) \cdots \Psi^{\epsilon_i}(x_i) \cdots \Psi^{\epsilon_n}(x_n) : a_{\mathbf{p},r}^\dagger . \quad (\text{C30})$$

The relevant anticommutation relations are

$$\begin{aligned}
\{\bar{\Psi}(x), a_{\mathbf{k},s}^\dagger\} = 0, \quad \{\Psi(x), a_{\mathbf{k},s}^\dagger\} = \mathbf{1} \psi_{\mathbf{k},s,+}(x), \\
\{\Psi(x), b_{\mathbf{k},s}^\dagger\} = 0, \quad \{\bar{\Psi}(x), b_{\mathbf{k},s}^\dagger\} = \mathbf{1} \bar{\psi}_{\mathbf{k},s,-}(x), \quad (\text{C31})
\end{aligned}$$

and a reasoning analogous to the one that led to Eq. (C27) eventually yields

$$\begin{aligned}
&: \Psi^{\epsilon_1}(x_1) \cdots \Psi^{\epsilon_n}(x_n) : a_{\mathbf{p},r}^\dagger \\
&= : \Psi^{\epsilon_1}(x_1) \cdots \Psi^{\epsilon_n}(x_n) a_{\mathbf{p},r}^\dagger : \\
&+ \sum_{i=1}^n : \Psi^{\epsilon_1}(x_1) \cdots \overbrace{\Psi^{\epsilon_i}(x_i) \Psi^{\epsilon_n}(x_n)} : \cdots a_{\mathbf{p},r}^\dagger : . \quad (\text{C32})
\end{aligned}$$

Using this in Eqs. (C28) and (C29), one obtains

$$\begin{aligned}
a_{\mathbf{k},s} : \Psi^{\epsilon_1}(x_1) \cdots \Psi^{\epsilon_n}(x_n) : a_{\mathbf{p},r}^\dagger &=: a_{\mathbf{k},s} \Psi^{\epsilon_1}(x_1) \cdots \Psi^{\epsilon_n}(x_n) a_{\mathbf{p},r}^\dagger : + \sum_{i=1}^n : \overbrace{a_{\mathbf{k},s} \Psi^{\epsilon_1}(x_1) \cdots \Psi^{\epsilon_i}(x_i)} \Psi^{\epsilon_n}(x_n) a_{\mathbf{p},r}^\dagger : \\
&+ : \overbrace{a_{\mathbf{k},s} \Psi^{\epsilon_1}(x_1) \cdots \Psi^{\epsilon_n}(x_n)} a_{\mathbf{p},r}^\dagger : + \sum_{i=1}^n : a_{\mathbf{k},s} \Psi^{\epsilon_1}(x_1) \cdots \overbrace{\Psi^{\epsilon_i}(x_i) \Psi^{\epsilon_n}(x_n)} : \cdots a_{\mathbf{p},r}^\dagger : \\
&+ \sum_{i=1}^n \sum_{\substack{j=1 \\ j \neq i}}^n : a_{\mathbf{k},s} \Psi^{\epsilon_1}(x_1) \cdots \overbrace{\Psi^{\epsilon_j}(x_j) \cdots \Psi^{\epsilon_i}(x_i)} \Psi^{\epsilon_n}(x_n) a_{\mathbf{p},r}^\dagger : . \quad (\text{C33})
\end{aligned}$$

Iterative application of Eqs. (C27) and (C32) then yields Eq. (C18) in the general case. \square

Proof of Theorem VI.5. Similar to the proof of theorem VI.2, combining theorem VI.4 with lemma C.2 yields theorem VI.5: at first, one obtains a completely normal

ordered term plus all normal-ordered terms with single contractions (between two fields, between two ladder operators and between ladder operator and field) plus all normal-ordered term with two contractions and so on. Taking the vacuum expectation value, all terms vanish due to the normal-ordering, with the exception of those

terms that are fully contracted and therefore proportional to the identity $\mathbf{1}$. Full contraction is only possible for an even number of operators, such that products containing an odd number of operators vanish. \square

3. UDW-type detector

Theorem VI.7 is essentially a simplification of the theorem VI.5 proven in the previous section. Again, first consider

Lemma C.3. *Using the notation of theorem VI.7, the*

following identity holds:

$$\begin{aligned}
& [\sigma^-]^a : \mu(t_1) \cdots \mu(t_n) : [\sigma^+]^b \\
& = : [\sigma^-]^a \mu(t_1) \cdots \mu(t_n) [\sigma^+]^b : \\
& + \sum_{\text{single contractions}} : \overbrace{\sigma^- \cdots \mu(t_1) \cdots \mu(t_i)} \cdots \mu(t_n) \cdots \sigma^+ : \\
& + \sum_{\text{double contractions}} : \overbrace{\sigma^- \cdots \mu(t_1) \cdots \mu(t_j) \cdots \mu(t_i) \cdots \mu(t_n)} \cdots \sigma^+ : .
\end{aligned} \tag{C34}$$

Proof of Lemma C.3. The proof runs analogous to the proof of lemma C.2, but is somewhat simpler since there is only one type of ladder operator (σ) instead of two (a, b), and the monopole operator is self-adjoint, unlike the spinor field. This time, the relevant anticommutation relations are Eq. (124), and

$$\{\sigma^-, \mu(t)\} = \mathbf{1} e^{+i\Omega t}, \quad \{\mu(t), \sigma^+\} = \mathbf{1} e^{-i\Omega t} \tag{C35}$$

instead of Eq. (C19) and Eq. (C31). This gives rise to the contractions defined in Eqs. (198) and (199). Beyond that, the proof follows the exact same steps as before. \square

Proof of Theorem VI.7. The theorem follows directly from theorem VI.6 and lemma C.3, analogous to the proof of theorem VI.5. \square

-
- [1] D. R. Terno, Phys. Rev. A **89**, 042111 (2014).
[2] W. G. Unruh, Phys. Rev. D **14**, 870 (1976).
[3] B. Seligman DeWitt, in *General Relativity: An Einstein Centenary Survey*, edited by S. W. Hawking and W. Israel (Cambridge University Press, Cambridge, 1979) p. 680.
[4] R. H. Jonsson, E. Martín-Martínez, and A. Kempf, Phys. Rev. Lett. **114**, 110505 (2015).
[5] R. H. Jonsson, E. Martín-Martínez, and A. Kempf, Phys. Rev. A **89**, 022330 (2014).
[6] S. J. Summers and R. F. Werner, Phys. Lett. A **110**, 257 (1985).
[7] A. Valentini, Phys. Lett. A **153**, 321 (1991).
[8] B. Reznik, Found. Phys. **33**, 167 (2003).
[9] G. V. Steeg and N. C. Menicucci, Phys. Rev. D **79**, 044027 (2009).
[10] E. Martín-Martínez, E. G. Brown, W. Donnelly, and A. Kempf, Phys. Rev. A **88**, 052310 (2013).
[11] S. A. Fulling, Phys. Rev. D **7**, 2850 (1973).
[12] P. C. W. Davies, J. Phys. A **8**, 609 (1975).
[13] P. G. Grove and A. C. Ottewill, J. Phys. A **16**, 3905 (1983).
[14] N. D. Birrell and P. C. W. Davies, *Quantum Fields in Curved Space* (Cambridge University Press, Cambridge, 1984).
[15] L. C. B. Crispino, A. Higuchi, and G. E. A. Matsas, Rev. Mod. Phys. **80**, 787 (2008).
[16] K. J. Hinton, J. Phys. A **16**, 1937 (1983).
[17] K. J. Hinton, Class. Quantum Grav. **1**, 27 (1984).
[18] L. Sriramkumar, “On the response of non-linearly coupled, accelerated detectors in odd-dimensional flat spacetimes,” (2001), arXiv:gr-qc/0106054.
[19] P. Candelas and D. W. Sciama, Phys. Rev. Lett. **38**, 1372 (1977).
[20] S. Takagi, Prog. Theor. Phys. Suppl. **88**, 1 (1986).
[21] B. Reznik, A. Retzker, and J. Silman, Phys. Rev. A **71**, 042104 (2005).
[22] M. Cliche and A. Kempf, Phys. Rev. D **83**, 045019 (2011).
[23] E. Martín-Martínez, E. G. Brown, W. Donnelly, and A. Kempf, Phys. Rev. A **88**, 052310 (2013).
[24] S.-Y. Lin and B. L. Hu, Phys. Rev. D **81**, 045019 (2010).
[25] S. J. Olson and T. C. Ralph, Phys. Rev. Lett. **106**, 110404 (2011).
[26] M. Cliche and A. Kempf, Phys. Rev. A **81**, 012330 (2010).
[27] E. Martín-Martínez, M. Montero, and M. del Rey, Phys. Rev. D **87**, 064038 (2013).
[28] A. M. Alhambra, A. Kempf, and E. Martín-Martínez, Phys. Rev. A **89**, 033835 (2014).
[29] M. Soffel, B. Müller, and W. Greiner, Phys. Rev. D **22**, 1935 (1980).
[30] S. W. Hawking, Commun. Math. Phys. **43**, 199 (1975).
[31] M. Montero and E. Martín-Martínez, Phys. Rev. A **83**, 062323 (2011).
[32] B. R. Iyer and A. Kumar, J. Phys. A **13**, 469 (1980).
[33] S. Takagi, Prog. Theor. Phys. **74**, 501 (1985).
[34] L. Sriramkumar and T. Padmanabhan, Class. Quantum Grav. **13**, 2061 (1996).

- [35] J. Louko and A. Satz, *Class. Quantum Grav.* **25**, 055012 (2008).
- [36] D. E. Diaz and J. Stephany, *Rev. Mex. Fis.* **49S3**, 120 (2003).
- [37] P. Langlois, *Ann. Phys. (Amsterdam)* **321**, 2027 (2006).
- [38] C. H. G. Bessa, J. G. Dueñas, and N. F. Svaiter, *Class. Quantum Grav.* **29**, 215011 (2012).
- [39] E. Harikumar and R. Verma, *Mod. Phys. Lett. A* **28**, 1350063 (2013).
- [40] E. Martín-Martínez and J. Louko, *Phys. Rev. D* **90**, 024015 (2014).
- [41] V. Alonso, S. D. Vincenzo, and L. Mondino, *Eur. J. Phys.* **18**, 315 (1997).
- [42] J. J. Sakurai and J. Napolitano, *Modern Quantum Mechanics*, 2nd ed. (Addison-Wesley, New York, 2011).
- [43] J. D. Bjorken and S. D. Drell, *Relativistic Quantum Fields* (McGraw-Hill, New York, 1965).
- [44] B. F. Svaiter and N. F. Svaiter, *Phys. Rev. D* **46**, 5267 (1992).
- [45] W. Greiner and J. Reinhardt, *Quantum Electrodynamics* (Springer, New York, 2008).
- [46] W. G. Brenna, E. G. Brown, R. B. Mann, and E. Martín-Martínez, *Phys. Rev. D* **88**, 064031 (2013).
- [47] M. E. Peskin and D. V. Schroeder, *An Introduction To Quantum Field Theory* (Addison-Wesley, New York, 1995).
- [48] K. Brádler and R. Jáuregui, *Phys. Rev. A* **85**, 016301 (2012).
- [49] M. Montero and E. Martín-Martínez, *Phys. Rev. A* **85**, 016302 (2012).
- [50] L. Hodgkinson, J. Louko, and A. C. Ottewill, *Phys. Rev. D* **89**, 104002 (2014).
- [51] K. K. Ng, L. Hodgkinson, J. Louko, R. B. Mann, and E. Martín-Martínez, *Phys. Rev. D* **90**, 064003 (2014).
- [52] B. A. Juárez-Aubry and J. Louko, *Class. Quantum Grav.* **31**, 245007 (2014).
- [53] W. G. Brenna, R. B. Mann, and E. Martín-Martínez, “Anti-Unruh Phenomena.” arXiv:1504.02468 [quant-ph].